

Preliminary Definition Study
 The Ultra High Resolution XUV Spectroheliograph
 An Attached Payload for the Space Station "Freedom"
 NASA Contract NAS 8-38666
 Final Report

(NASA-CR-184156) THE ULTRA HIGH RESOLUTION
 XUV SPECTROHELIOGRAPH: AN ATTACHED PAYLOAD
 FOR THE SPACE STATION FREEDOM Final Report
 (Stanford Univ.) 61 p CSCL 22B

N91-22365

Unclas
0012372

G3/19

Report No. UHRXS 90-2

Principal Investigator	Arthur B.C. Walker, Jr.	CSSA, Stanford University,
Principal Scientist	Richard B. Hoover	SSL, Marshall Space Flight Center, NASA
Senior Co-Investigators	Troy W. Barbee, Jr.	Lawrence Livermore National Laboratory
	Einar Tandberg-Hanssen	SSL, Marshall Space Flight Center, NASA
	J. Gethyn Timothy	CSSA, Stanford University
Project Scientist	Joakim F. Lindblom	CSSA, Stanford University

October 1990



TABLE OF CONTENTS

I. Statement of Work	1
II. Scientific and Instrumental Requirements and Expected Performance.....	2
1.0 Scientific Overview	2
2.0 Mechanical Envelope and Optical Branch.....	4
2.1 Mechanical Envelope	4
2.2 Internal Architecture.....	4
3.0 Imaging Telescopes	6
3.1 Multilayer Optics	6
3.2 Filters.....	6
3.3 Optical Bench.....	8
3.4 Ritchey-Chrétien Telescope Assembly and Alignment.....	9
3.5 Choice of Mirror Substrates	9
3.6 The Herschellian Telescopes.....	9
3.7 Photographic Emulsions.....	11
3.8 Telescope Focal Properties.....	11
3.9 Active Mirrors Servo	12
3.10 Image Quality.....	12
3.11 Discussion.....	12
4.0 XUV, EUV and FUV Spectroscopic Systems.....	14
4.1 The Telescopes	14
4.2 Optical Configurations of the Spectrographs.....	14
4.3 Slits	14
4.4 The Gratings	14
5.0 The Soft X-Ray Spectroscopic Systems	15
5.1 The Objective Double Crystal Spectrometer	15
5.2 The Wolter Sector Telescopes.....	15
6.0 The MAMA Detectors	16
6.1 MAMA Detector Systems.....	16
6.2 Performance Characteristics.....	22
6.3 Future Developments.....	26
7.0 Experiment Electronics Logic and Data Formats	28
7.1 Experiment Control.....	28
7.2 Data Formats and Data Handling	28
8.0 Film Cameras	30
9.0 Expected Performance	31
9.1 Imaging Telescopes	31
9.2 The Soft X-Ray Spectroheliographs.....	31
9.3 Spectroscopic Systems.....	31
10.0 Environmental Effects.....	34
10.1 Thermal Control	34
10.2 External Environment	34
10.3 Internal Environment	34
11.0 Preflight and Inflight Calibration	34



12.0	Pointing Accuracy and Stability.....	34
13.0	Ground Operations	34
14.0	Launch Enclosure.....	34
15.0	Flight Operation.....	34
16.0	Observing Programs, Data Reduction and Analysis.....	35
17.0	Utilization of <i>UHRXS</i> on Space Station	36
18.0	Future Evolution of <i>UHRXS</i>	36
III.	Work Breakdown Structure.....	37
1.0	Program Development and Control.....	37
2.0	Systems Engineering.....	37
3.0	Engineering Model.....	38
4.0	Flight Unit.....	39
5.0	Ground Support Equipment.....	48
6.0	Flight Operations.....	48
7.0	Data Handling and Analysis	49
8.0	Science Programs.....	49
9.0	The <i>UHRXS</i> Organization and the Work Breakdown Structure.....	49
IV.	The <i>UHRXS</i> Program.....	50
1.0	<i>UHRXS</i> Development Approach.....	50
2.0	Organization of the <i>UHRXS</i> Team.....	50
3.0	Instrument Procurement Strategy	53
4.0	Instrument Procurement and Operations Plan.....	55

LIST OF FIGURES

1.	Configuration of the <i>UHRXS</i>	5
2.	Configuration of the <i>MSSTA</i> Ritchey-Chrétien Herschellian Telescope	7
3.	Optical Performance of the <i>MSSTA</i> Telescopes.....	10
4.	Focal Spot Diagrams for the <i>MSSTA</i> Telescopes	11
5.	The Active Mirror Servo.....	12
6.	The Corona at $\lambda\lambda$ 171 Å - 175 Å.....	13
7.	FUV Beam Splitter.....	15
8.	Configuration of the Grating Spectrographs.....	15
9.	Configurations of the Soft XUV Spectroheliograph	15
10.	Properties of the Soft X-Ray Image	16
11.	The MAMA Detector.....	17
12.	MAMA Anode Array Encoding Geometries.....	18
13.	Operation of MAMA Encoding Geometry	19
14.	MAMA Fine-Fine Address Circuit.....	20
15.	MAMA Photo Cathode Configurations	21
16.	MAMA Anode Configurations.....	22
17.	224 x 960 Pixel Fine-Fine MAMA Detector Components	23
18.	MAMA Images of a USAF Test Target.....	24
19.	MAMA Performance Data.....	24
20.	MAMA Images.....	25
21.	MAMA Demountable Tubes	26
22.	Configuration of the Film Cameras	27
23.	<i>UHRXS</i> Electronics Diagram	29
24.	Configuration of the Film Cameras	30
25.	Response of the <i>UHRXS</i> Imaging Telescopes.....	32
26.	Response of the <i>UHRXS</i> Spectroscopic Telescopes	33
27.	Coverage of the Isoelectronic Sequences of H, He, C, Ne, Mg, Si and Fe.....	35
28.	<i>UHRXS</i> Management Structure	51

LIST OF TABLES

1.	Characteristics of the <i>UHRXS</i> Imaging Systems.....	3
2.	Characteristics of the <i>UHRXS</i> Spectroscopic Systems.....	3
3.	<i>UHRXS</i> Mass Properties.....	4
4.	<i>UHRXS</i> Electrical Properties.....	4
5.	Efficiencies and Bandpasses of the <i>MSSTA</i> Ritchey-Chrétien Telescopes.....	6
6.	Properties of the <i>MSSTA</i> Ritchey-Chrétien and Cassegrain Filters.....	8
7.	Overview of <i>UHRXS</i> Filter Component Material.....	8
8.	On Axis Image Point Spread Allocation at λ 173 Å.....	12
9.	Predicted Performance of the <i>UHRXS</i> Imaging System.....	13
10.	XUV, EUV and FUV Spectroheliograph Performance.....	14
11.	Properties of the Objective Bragg Crystal Spectrometers and Wolter Telescopes.....	16
12.	Characteristics of the MAMA Encoding-Electrode Geometries.....	20
13.	Soft X-Ray Spectroheliograph Performance.....	32



I. STATEMENT OF WORK

The contractor shall commence a definition effort at Stanford in coordination with Marshall Space Flight Center, and Lawrence Livermore National Laboratory on the Ultra-High Resolution XUV Spectroheliograph described in proposal CSSA 88-17. The following tasks will be performed:

1. Refine the scientific instrument requirements, and support the planned Space Station meeting in September, 1990. The following issues will be addressed:
 - a. Experiment Mechanical Observation and Optical Bench.
 - b. Experiment internal architecture.
 - c. Requirements for the film cameras.
 - d. Telescope optical properties resulting from offset pointing.
 - e. Properties of telescope multilayer coatings.
 - f. Properties of gratings.
 - g. Configuration of MAMA detectors.
 - h. Telescope filters.
 - i. Effect of natural and artificial environments on critical materials, including filters and optics.
 - j. Internal environment and experiment.
2. Respond to specific issues, such as experiment hardware classification, safety requirements, and hardware redundancy, as required.
3. Develop a preliminary plan for the life cycle of the *UHRXS* experiment, including refurbishment and upgrading.
4. Develop a preliminary plan for film replacement by robotics.



II. SCIENTIFIC AND INSTRUMENTAL REQUIREMENTS AND EXPECTED PERFORMANCE

1.0 Scientific Overview: The principal goal of the *UHRXS*¹ is to improve our ability to identify and to understand the fundamental physical processes which shape the structure and dynamics of the solar chromosphere and corona; the ability of the *UHRXS* imaging telescopes and spectrographs to resolve fine scale structures over a broad wavelength (and hence temperature) range is critical to this mission. We review the scientific objectives and instrumental capabilities of the *UHRXS* investigation, before proceeding to a discussion of the expected performance of the *UHRXS* observatory.

Objectives: The phenomena which are the principal focus of the *UHRXS* investigation include:

- The morphology and energetics of the fine structure of the solar chromosphere/corona interface, including the "chromospheric network", spicules, prominences, cool loops, and the magnetic field.
- The structure, energetics and evolution of high temperature coronal loops.
- The large scale structure and dynamics of the corona, including the solar wind interface (represented by phenomena such as polar plumes), the magnetic field, and coronal mass ejections.
- Solar flares, especially the evolution of the pre-flare state, the nature of the impulsive energy release, and the evolution of post-flare loops.

Among the principal issues we plan to address are:

- The nature of the mechanisms responsible for heating and cooling the various structures (spicules, loops, polar plumes, prominences) which control the flow of mass and energy in the solar atmosphere.
- The source of the material found in coronal structures and the solar wind, and the mechanisms responsible for transporting this material and establishing the various abundance anomalies observed.
- The source of the energy responsible for transient phenomena, including coronal mass ejections, particle acceleration, and the mechanisms responsible for the impulsive release of energy.

Collectively, these objectives require: (i) observations with very high angular resolution, because the fundamental processes in the solar atmosphere operate on very small scales [typically several hundred kilometers or less (100 km corresponds to ~ 0.15 arc-second resolution from earth)], (ii) observations encompassing wide fields of view, because many phenomena of interest (such as prominences) involve very large scale structures, and the precise location and timing of dynamic phenomena such as flares, prominences, and coronal mass ejections, are difficult to predict, (iii) observations covering a wide range of temperatures, since the solar atmosphere is a strongly coupled system involving interrelated phenomena occurring over four decades of temperature (10,000 °K to 100,000,000 °K), and (iv) the ability to directly measure the fundamental parameters of the solar plasma, temperature, density, non-thermal motions, abundances, microscopic conditions governing the excitation of radiation, and the solar magnetic field, on very small scales. *UHRXS* is able to satisfy these very demanding requirements by utilizing a variety of instrumental techniques.

Instrumentation: The *UHRXS* instrumentation consists of:

- eight XUV Ritchey-Chrétien multilayer telescopes, each able to image the chromosphere and corona to $1 R_{\odot}$ above the limb in a narrow wavelength band, between $\sim 70 \text{ \AA}$ and $\sim 300 \text{ \AA}$, that is dominated by a line multiplet excited over a narrow temperature range. Two Herschellian multilayer telescopes provide high resolution narrow band soft x-ray ($40 \text{ \AA} < \lambda < 70 \text{ \AA}$) images. Collectively, these telescopes allow detailed observations of solar structures in the temperature range $50,000 \text{ K} < T < 30,000,000 \text{ K}$, with 0.1 arc-sec resolution.
- a multilayer coronagraph, able to image the corona to $>10 R_{\odot}$ with ~ 0.3 arc-second resolution in a band at $\sim 173 \text{ \AA}$, which is dominated by the emission of Fe IX and Fe X ($\sim 800,000 \text{ K}$ to $1,300,000 \text{ K}$).

- an FUV Telescope ($\lambda\lambda$ 1150 Å - 1600 Å), able to image the chromosphere and corona to $1 R_{\odot}$ above the limb in ~ 15 Å bands at 1216 Å [H I Ly α ($7,000 < T < 30,000$)], and 1550 Å [C IV ($T \sim 100,000$ K)], permitting observations of solar structures in the temperature range $7,000 \text{ K} < T < 100,000 \text{ K}$ with 0.1 arc-sec resolution.
- three soft x-ray telescopes, each able to form spectroheliograms with angular resolution ~ 2.0 arc-sec over a field of view ~ 8 arc min \times 8 arc min in the wavelength range $\lambda\lambda$ 1.7 Å - 45 Å, thereby investigating the morphology of the coronal plasma in the temperature range between $\sim 1,000,000 \text{ K}$ and $100,000,000 \text{ K}$.
- five high resolution grating spectrographs covering XUV ($\lambda\lambda$ 170 Å - 215 Å), EUV ($\lambda\lambda$ 450 Å - 1100 Å), and FUV ($\lambda\lambda$ 1150 Å - 1600 Å) bands which include strong lines of H I; He I, He II; C III, C V; O V, O VI; Ne VII; Mg X; Fe VIII - Fe XIV, and Fe XXIV. The field of view of the spectrographs is ~ 4 arc min \times 4 arc min, angular resolution $\sim 0.5''$; spectral resolution as high as $\lambda/\Delta\lambda \sim 30,000$ can be attained.

The characteristics of the *UHRXS* instruments are given in Tables 1 and 2. Observations from the Imaging Systems are recorded on high resolution photographic emulsions; Observations from the Spectroscopic Systems are recorded using the MAMA photoelectric array detector.

Table 1. Characteristics of the *UHRXS* Imaging Systems

System	λ_0^* (Å)	Ion	Temperature (°K)	Telescope Parameters					Resolution	
				Aperture (mm)	Focal Lgt (mm)	Plate Scale ($\mu\text{m}/\text{arc-sec}$)	f ratio	Airy Radius (arc-sec)	Angular (arc-sec)	Spectral $\lambda/\Delta\lambda$
A	1215.60/	H I	20,000	305	3500	17.5	11.5	0.10	0.10	80
	1548.00	C IV	100,000							
B	304.00	He II	50,000	190	3500	17.5	18.3	0.04	0.10	20
C	143.30	Ne V	400,000	190	3500	17.5	18.3	0.02	0.10	32
	or 150.1	O VI	300,000							
D	88.10	Ne VIII	650,000	190	3500	17.5	18.3	0.01	0.10	60
A 1	69.70	Si VIII	850,000	100	2500	12.5	25.0	0.02	0.15	60
E	173.00	Fe IX/X	1,000,000	190	3500	17.5	18.3	0.02	0.10	30
F**	195.14	Fe XII	1,500,000	190	3500	17.5	18.3	0.03	0.10	25
G	211.00	Fe XIV	2,500,000	190	3500	17.5	18.3	0.03	0.10	23
A 2	54.7	Fe XVI	4,000,000	100	2500	12.5	25.0	0.02	0.15	100
H	93.93	Fe XVIII	6,500,000	190	3500	17.5	18.3	0.02	0.10	40
I	132.80	Fe XX/XXIII	11,000,000	190	3500	17.5	18.3	0.02	0.10	33
F**	192.00	Fe XXIV	20,000,000	190	3500	17.5	18.3	0.03	0.10	25
N	173.00	Fe IX/X	1,000,000	190	1000	5.0	5.2	0.02	0.30	30

* Central wavelength, λ_0 , of telescope bandpass; ** The bandpass of system F includes lines of both Fe XII and Fe XXIV; *** Note that these bandpasses are determined by FUV multilayer interference filters.¹

Table 2. Characteristics of the *UHRXS* Spectroscopic Systems

System	λ_p (Å)	Telescope Parameters		Resolution		Ions Observed	Temperature Range (°K)
		Aperture (mm)	Focal Length (mm)	Angular (arc-sec)	Spectral ($\lambda/\Delta\lambda$)		
$\alpha 1/\alpha 2$	1150-1600	305	10,000	0.1/0.5*	30,000	H I, Fe II, C I, C II, O I, O IV, C IV, Si II	7,000-100,000
β	540-1150	190	10,000	0.1/0.5*	14,000	He I, He II, C III, O V, O VI, Mg X	50,000-1,000,000
Γ	170-190	190	10,000	0.1/0.5*	12,000	O V, O VI, Fe VIII, Fe IX, Fe X, Fe XI	200,000-1,250,000
$\Sigma 1a$	40.0-44.1	75	2,500	2.0	200	C V, Si XII	800,000-2,000,000
Δ^{**}	190-215	190	10,000	0.1/0.5*	8,000	Fe XII, Fe XIII, Fe XIV	1,500,000-3,000,000
$\Sigma 1b$	18.5-22.5	75	2,500	2.0	300	O VII, O VIII	1,500,000-4,000,000
$\Sigma 2a$	13.0-15.5	75	2,500	2.0	750	Ne IX, Fe XVII, Fe XVIII	3,000,000-8,000,000
$\Sigma 3a$	8.4-9.2	75	2,500	2.0	850	Mg IX, Mg XII	6,000,000-12,000,000
$\Sigma 3b$	6.1-6.8	75	2,500	2.0	8,000	Si XIII, Si XIV	8,000,000-16,000,000
Δ^{**}	190-215	190	10,000	0.1/0.5*	8,000	Fe XXIV	16,000,000-30,000,000
$\Sigma 2b$	1.7-1.9	75	2,500	2.0	10,000	Fe XXV, Fe XXVI	25,000,000-100,000,000

* See discussion in Section II:4.0; ** The bandpass of System Δ includes lines of Fe XII - XIV, as well as Fe XXIV.

2.0 Mechanical Envelope and Optical Branch: The *UHRXS* mechanical configuration is shown in Figure 1a.

2.1 Mechanical Envelope: The *UHRXS* outer envelope is a vacuum tight enclosure ~1.5 meter in diameter and ~3.0 meters long. Our present design calls for a separate aperture door for each telescope, however this philosophy will be re-examined during our design phase.

A major question, which cannot be fully resolved until the configuration of the pointing system is determined, is how the camera modules will be mounted, and accessed for film replacement. If the pointer utilized is a center of mass configuration, then the cameras will be accessible from the rear, as shown in Figure 24b (Section II: 8.0). If the experiment is end mounted to the pointer, then the cameras will be accessible from the side, as shown in Figure 24b. This will, in turn, affect where the electronics modules are placed. Tables 3 and 4 present our preliminary estimates of the *UHRXS* mass and electrical properties.

Several designs are under consideration for the fabrication of the mechanical envelope. One option is to machine the envelope from a cylindrical aluminum forging (Figure 1b). A second option is to weld an polygonal structure from machined aluminum plates (Figure 1c). In either design, a vacuum-tight enclosure will be formed by fore and aft bulkheads mounted with viton o-rings.

2.2 Internal Architecture: The major interior structure of the *UHRXS* is an optical bench consisting of three bulkheads connected by a truss structure, on which the main experiment components are mounted. The eight XUV imaging telescopes will be mounted on the main bulkhead (Figure 1d). The coronagraph and objective crystal spectrometers will be mounted on a forward bulkhead, and the EUV, XUV and FUV grating spectrographs and their telescopes will be mounted on a rear bulkhead.

Table 3. Mass *UHRXS* Properties

Solar Aspect Sensor	1 kg
R.C. XUV Telescope Modules Typical	(5 kg)
Dual Camera Module Typical	(12 kg)
XUV Telescopes	
Total 8 Modules	88 kg
Ultraviolet Telescope/Spectrograph	18 kg
Soft X-Ray Herschellian Telescope	
Module and Camera	10 kg
XUV Coronagraph and Camera	10 kg
XUV/EUV Spectrograph Typical	(10 kg)
XUV/EUV Spectrographs	
Total 3 Modules	30 kg
Objective Crystal Spectrographs	20 kg
MAMA Detector and HVPS Typical	(3 kg)
MAMA Detectors (7 systems)	21 kg
System Electronics	15 kg
Optical Bench and Mechanical Envelope	75 kg
Baseplates	(10 kg)
Mechanical Envelope	(45 kg)
Optical Bench	(20 kg)
Contingency and miscellaneous	45 kg
Total	333 kg

Table 4. Electrical *UHRXS* Properties

MAMA Amplifiers and HVPS	50 watts
MAMA Encoders	20 watts
Central Electronics	40 watts
Solar Sensor and Correlation Tracking	5 watts
Active Mirror Servos	30 watts
Cameras	20 watts
Thermal Control	25 watts
Contingency	<u>25 watts</u>
Total	215 watts

Additional Specifications:

TM Rate:	10 Mbs
Volume:	5 cubic meters

Command Requirements: see Section II:15

3.0 Imaging Telescopes: The principal technology on which the *UHRXS* is based is that of normal incidence multilayer optics. Barbee² has described the development of multilayer optics technology, and Walker *et al.*³ have described the development and application of multilayer mirrors for astronomical imaging. The design of the *UHRXS* imaging systems, which are figured as conventional Ritchey-Chrétien⁴ or Herschellian optical systems, is based directly on our successful rocket flight of October 1987,⁵ which obtained the first high resolution astronomical XUV images with both types of optical systems. (A high resolution single reflection multilayer image has also recently been reported by Golub *et al.*⁶). Subsequently, we have developed and successfully tested a new rocket payload⁷, the "*Multi Spectral Solar Telescope Array (MSSTA)*", which is scheduled for its initial flight in December 1990. This new payload incorporates seven Ritchey-Chrétien multilayer telescopes (Figure 2a) which are similar (with, however, smaller apertures) to those planned for *UHRXS*. Recently completed performance tests⁸ have shown that the *MSSTA* telescopes have multilayer coatings of very high efficiency, and optical figures of high quality, providing us with great confidence that we will be able to meet, or exceed, the performance specifications we have set for *UHRXS*. Each *UHRXS* telescope consists of five basic elements: the multilayer mirrors, an active servo to stabilize the image, a fiber epoxy optical bench, a thin metallic filter, and an image recording device. We discuss the anticipated performance of the *UHRXS* telescopes below.

3.1 Multilayer Optics: The physics of multilayer structures for x-ray optics is a rapidly developing field. Barbee⁹ has discussed the current status of multilayer optics. A number of factors influence multilayer performance, including the materials chosen to form the alternating "scattering" and "spacer" layers of the multilayer, the nature of the interfaces and the relative thickness of the two dissimilar layers in a layer pair, and the RMS micro-roughness of the interfaces (which is strongly influenced by the micro-roughness of the substrates on which the multilayers are formed). In his discussion, Barbee emphasizes two multilayer systems, Mo/Si and Rh/C, which will be used for the majority of the multilayer telescopes which are included in *UHRXS*. The principle characteristics of the multilayer mirrors which determine *UHRXS* performance are mirror reflectivity and bandpass. We have already carried out extensive measurements (Table 5^{8,10}) on the Mo/Si mirrors which were fabricated by one of us (TWB) for the *MSSTA* payload. The improvements in multilayer technology which have occurred over the past few years are made apparent by comparing the efficiency of system VI-a, which was fabricated in 1987, and System XII-E, which was fabricated in 1990.¹⁰ Considerable flexibility in multilayer resolving power is possible¹¹ (for example at $\sim 173 \text{ \AA}$; resolutions over the range $15 < \lambda/\Delta\lambda < 75$ appear to be possible), however high resolution comes at the expense of efficiency. We have assumed the values of reflectivity given in Table 9 and the wavelength bandpasses given in Table 1 for *UHRXS*.

Table 5. Efficiencies and Bandpasses of the *MSSTA* Ritchey-Chrétien Telescopes

System	Mirror Coating	Central Wavelength (Å)	$\epsilon^N(\lambda_0)^*$	$\epsilon^s(\lambda_0)^{**}$	$\epsilon^a_{p,s}(\lambda_0)^+$	$\lambda_{(p,s)}fwhm$	$\epsilon^2(\lambda_0)$	$\lambda fwhh$
VI-a	Mo/Si	173	.25	.26	.26	17	.063	12
VI-b	Mo/Si	211	.30	.32	.32	19	.09	14
XII-D	Mo/Si	150	.45	.43	.44	12	.20	8
XII-E	Mo/Si	173	.43	.41	.41	17	.19	10
XII-F	Mo/Si	193	.32	.39	.36	22	.10	15
XII-C	Mo/Mg ₂ Si	304	.25	.25	.25	26	.063	18
XII-G	Mo/Mg ₂ Si	335	.20	--	.20	34	.04	23
XII-A/B	Al/MgF ₂ /Os	1216/1550	--	--	.51/.78 ⁺⁺	150/300	.26/.62	100/200

* Measurements at NIST

** Measurements at SSRL

+ Adopted values

++ Measured by Acton Research

3.2 Filters: Thin metallic filters which suppress visible and ultraviolet radiation by a factor of 10^{10} are a critical component of a multilayer telescope. In addition to suppressing visible and ultraviolet light, filters must also reduce "contamination" from XUV radiation (especially from strong lines such as He I λ 304 Å) outside the bandpass of each telescope. The successful fabrication of filters for the *MSSTA* payload^{8,12} by Lúxel Corporation has given us confidence that filters can be fabricated for *UHRXS* with the desired properties. Based on the characteristics of the *MSSTA* filters (Table 6), we have developed the preliminary *UHRXS* filter designs in Table 7. As Table 6 demonstrates, we have been able to develop filter designs which can reduce off-band contamination to less than 1% for most of the *MSSTA* XUV band passes, and to no more than 10% for any bandpass. The *MSSTA* filter materials are divided between 2 filters of equal thickness placed near the focal plane (Figure 2a), to minimize the possibility of light leaks due to pinholes.

FOLDOUT FRAME

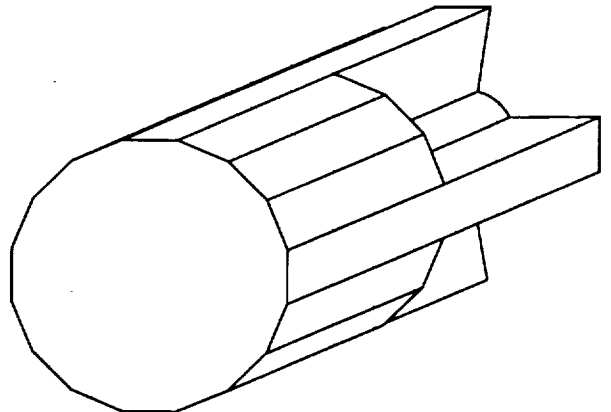
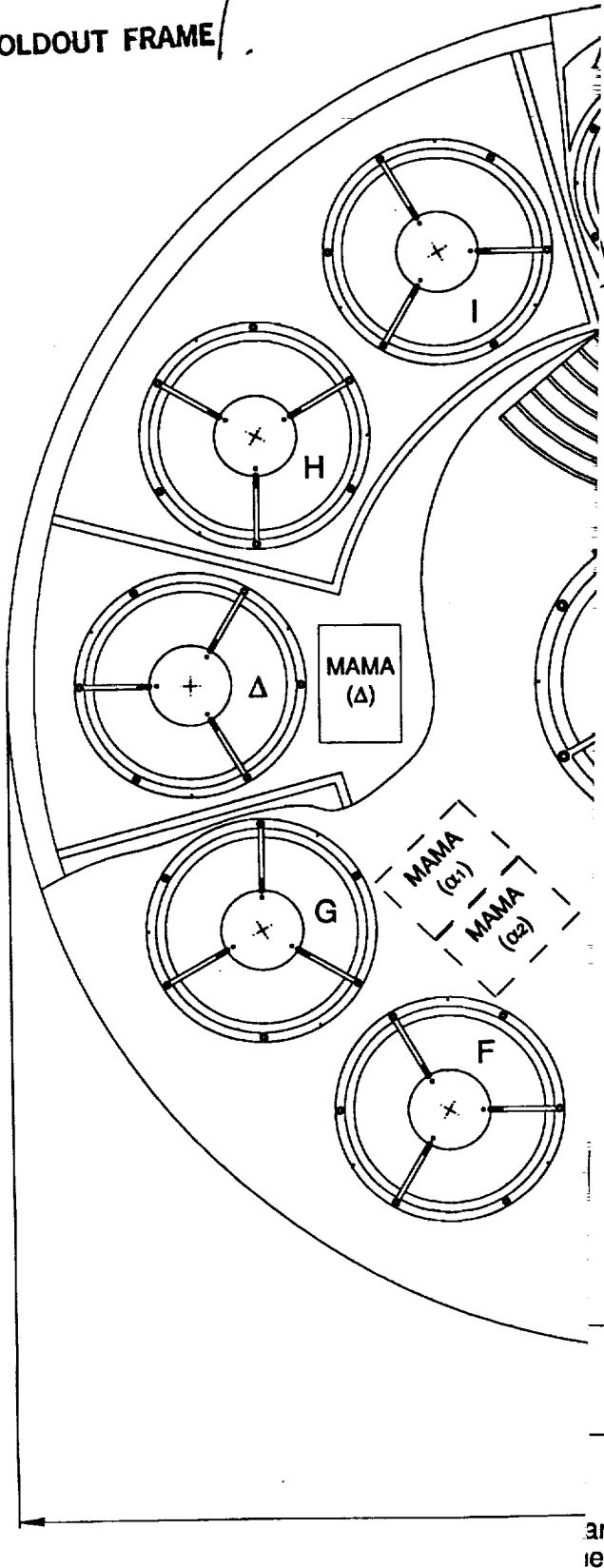


Figure 1d. UHRXS mechanical envelope fabricated by welding plates into a polygonal structure.

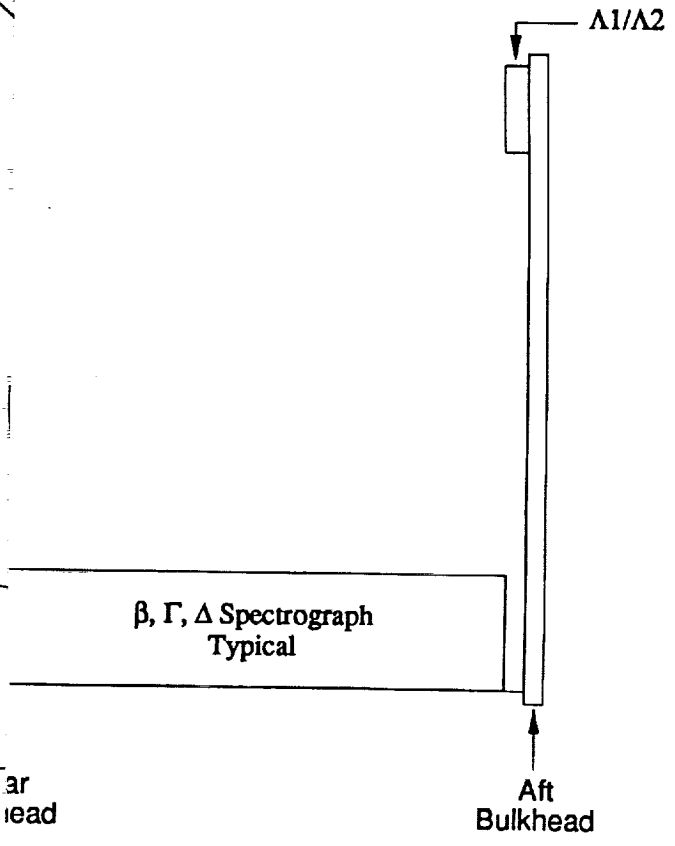


Figure 1a. Front View of the UHRXS observatory structure, showing the location of the various telescopes and spectrographs. The location of the coronagraph (M), spectroheliographs (β, Γ, Δ), and the soft X-ray detectors is also shown.



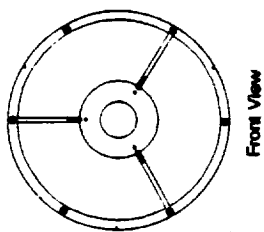
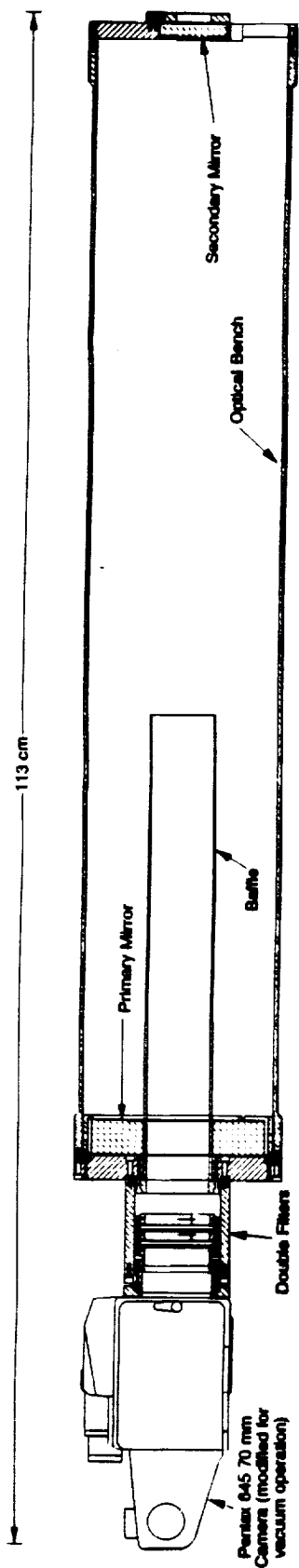


Figure 2a. Configuration of the MSSTA Ritchey-Chretien Telescope.

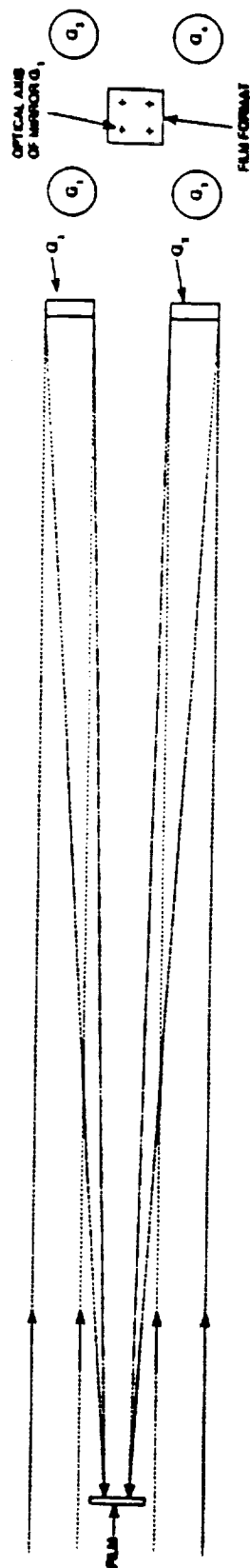


Figure 2b. Configuration of the Herschellian Telescopes. Our original baseline configuration included 4 Herschellian telescopes. Currently, we are considering the replacement of two of these telescopes by the soft x-ray spectrographs described in section II.5.

UHRXS will also use two main filters. However, thermal control considerations (see section II:10.1) make it highly desirable to have a full aperture filter at the telescope entrance. We are studying two alternatives to enhance the telescope thermal properties: (i) the use of a third thin prefilter at the enhance aperture of each *UHRXS* Ritchey Chrétien Telescope, or (ii) placing one of the two main filters at the entrance aperture. *The fabrication of prefilters, if their use is deemed essential, is a complex issue.*

Table 6. Properties of the MSSTA Ritchey-Chrétien and Cassegrain Filters

System	Wavelength λ_0 (Å)	Filter Composition Microns	Transmission at λ_0	Flux at λ /Flux at λ_0		
				λ_{304} Å	$\lambda_{400-900}$ Å	$\lambda_{171-193}$ Å
XII-A	1216	Mg ₂ F/Al	0.013	-	-	-
XII-B	1548	Mg ₂ F/Al	0.013	-	-	-
XII-C	304	Al(.28)/C(.0125)	0.139	1.000	0.005	0.0005
XII-D	150	Be(.60)	0.212	0.006	0.0001	0.076
XII-E	173	Al(.28)C(.04)	0.208	0.003	0.0003	-
XII-F	193	Al(.28)KBr(.16)H ₂ O(.01)	0.155	0.002	0.0000	-
XII-G	335	Al(.18)/C(.008)/Te(.14)	0.070	0.040	0.088	0.0001
VI-a	173	Al(.28)/C(.04)	0.208	0.005	0.0005	-
VI-b	211	Al(.28)/KBr(.16)H ₂ O(.01)	0.143	0.026	0.0000	0.085

Table 7. Overview of UHRXS XUV Filter Component Material

Bandpass (Å)	Aluminum	Alum Ox.	Carbon	KBr	Tellurium	Beryllium	Molybd.	Rhodium	Phthal*
173	2845 Å	60 Å	382 Å						
304	2950 Å	60 Å	152 Å						
193, 211	2914 Å	60 Å	154 Å	1746 Å					
335	1706 Å	60 Å	110 Å		1288 Å				
150						6000 Å			
132.8, 143.3						3000 Å	2800 Å		
88.1, 93.9			275 Å				2800 Å	800 Å	384 Å
54.7, 69.7			3638 Å					1600 Å	2358 Å

* Phthalocyanene

3.3 Optical Bench: Our baseline optical bench design utilizes a fiber epoxy optical bench. This design is based on the optical benches developed for the *MSSTA* payload.⁷ The *MSSTA* optical benches (Figure 2a) were fabricated from ASA-12k graphite fiber, and an HBRF55A epoxy resin matrix was used. The use of longitudinal fibers increases stiffness, and yields benches with a very low coefficient of thermal expansion. The telescope tubes are coated to minimize the effects of length changes due to moisture. We have tested the sensitivity of the location of the focal plane of the λ_0 335 Å telescope to changes in temperature [over a range of 20° F (from 65° F - 85° F)] and humidity. No variation in the location of the focal plane was found as a result of either temperature or humidity variations. However, in order to maintain the image quality required, the Ritchey-Chrétien telescope optical bench length must be maintained to an accuracy of 0.05 mm (50 microns). We are concerned that this accuracy may be attainable only by very stringent control of the moisture content of the fiber epoxy bench. We propose to study two alternative approaches to maintaining the proper separation between the primary and secondary mirrors.

- the use of an invar optical bench, coupled with very precise control of the temperature of the bench.

- the use of a graphite epoxy optical bench, which incorporates the ability to measure the value of the primary/secondary mirror separation by using a set of reference invar rods, and to control that separation with an active system of piezo-electric actuators.

We are confident that one of the above approaches, or a combination of both, will prove effective.

3.4 Ritchey-Chrétien Telescope Assembly and Alignment: During the fabrication of the *MSSTA* telescopes, we developed procedures for assembly, alignment and testing which are directly applicable to *UHRXS*. For example, the use of a low outgassing elastomer to mount the primary mirror has proven to be a highly successful approach.⁸

We have described the interferometric tests carried out on the *MSSTA* telescopes in a recent paper.¹³ The procedure used to test the figure quality and optical alignment of the *MSSTA* telescopes is shown in Figure 3a. The interferometer and wedge provide two beams which after propagation through the telescope produce a set of fringes that may be analyzed to determine the quality of the optics, and verify telescope alignment. Analysis of the fringes produced when the optical flat is translated through the position of best focus was carried out using the code Micro-Fringe 3.1. Figure 3b represents the predicted energy distribution of a point source imaged in the focal plane in the absence of diffraction for the *MSSTA* λ_0 335 Å telescope. The same information is conveyed in a different form in Figure 3c in which the geometrical zonal spot diagram is presented. In Figure 3d, the point spread function, as computed from the analysis of the interferometric fringes, is presented. *The performance predicted for the telescope is essentially diffraction limited!* The results presented for the λ_0 335 Å telescope in Figure 3 are typical of the performance found for all of the *MSSTA* Ritchey-Chrétien telescopes.

3.5 Choice of Mirror Substrates: The diffraction limited performance predicted by the measured geometrical perfection of the *MSSTA* telescopes provides a strong indication that our resolution goals can be achieved for *UHRXS*. However, the critical technology that will determine the performance of the *UHRXS* telescopes at their operational wavelengths is the surface finish of the mirror substrates on which the multilayer coatings have been applied. Harvey, Zmek and Ftacis¹⁴ have examined the effect of surface finish on the performance of multilayer mirrors. Since the multilayer coating tends to smooth high frequency surface imperfections, it is the substrate mid-frequency surface imperfections which will determine image quality (the high frequency imperfections affect multilayer reflectivity most strongly). The analysis of Harvey *et al.* indicates that for a primary aperture of 10 inches (the aperture of the *UHRXS* telescopes is 7.5") a 5 Å RMS substrate microroughness should result in an image with, respectively, 40% at 44 Å, 75% at 125 Å, and 90% at 304 Å of the energy in a 0.1 arc-second diameter circle for a point source. Baker Consulting, Inc. has polished the Zerodur mirrors for the *MSSTA* telescopes using an advanced flow polishing technique to a smoothness of ~ 1-2 Å RMS.¹⁵ We may be able to achieve sub-Angstrom smoothness for *UHRXS* with the use of sapphire substrates. *The selection of the substrate material for the multilayer mirrors is a key decision.*

Performance of the Ritchey-Chrétien Telescopes: Laser interferometric measurements on the assembled *MSSTA* telescopes indicate that their optical performance implies a system accuracy of $\sim \lambda/100$ for 6328 Å light. These results, coupled with the theoretical analysis of Harvey *et al.*, results suggest that the optical quality achieved for the *MSSTA* telescopes is sufficient to exceed 0.1 arc-second resolution. In section II:3.10, we discuss the combined impact of optical quality and of other factors such as spacecraft jitter and film resolution on overall *UHRXS* system performance.

3.6 The Herschellian Telescopes: At wavelengths shorter than 70 Å, the lower efficiency of multilayer mirrors and the weakness of the solar flux combine to make a single off-axis parabolic Herschellian mirror⁷ a more effective configuration than the double reflection Ritchey-Chrétien. However, the preceding discussion on multilayer fabrication and telescope assembly, and performance of the imaging Ritchey-Chrétien telescopes applies, with few exceptions, to the Herschellian telescopes as well. The properties and performance of the Herschellian Telescopes (A 1 and A 2), multilayer coatings, and filters are given in Table 1 and 9. The configuration of the Herschellian telescopes is shown in Figure 2b.

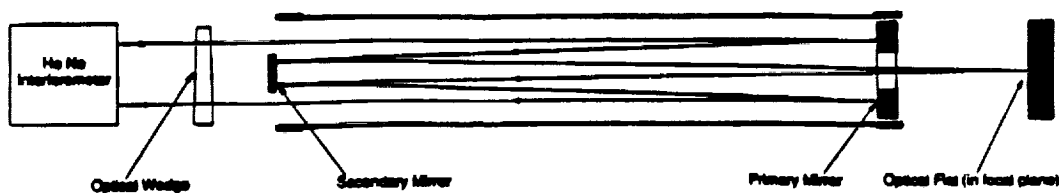


Figure 3a. Arrangement of the He/Ne Laser (λ 6328 Å) interferometer, optical wedge, optical flat, and telescope during alignment tests. The interferometer used was the Zygo PTI. The angle of the wedge is greatly exaggerated.

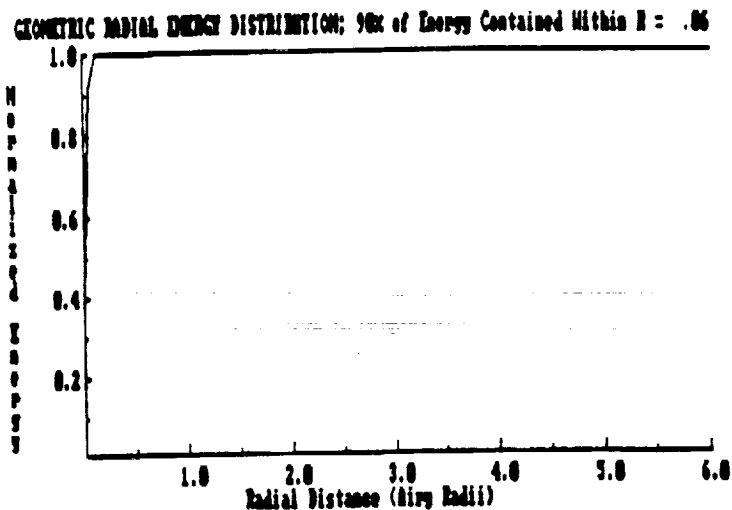


Figure 3b. Radial Energy distribution for a point source imaged by the λ_0 335 Å in the absence of diffraction. The very high quality mirrors place 90% of the energy in a circle of radius 0.06 Airy Radii ($R_s = 0.066''$) or 0.004".

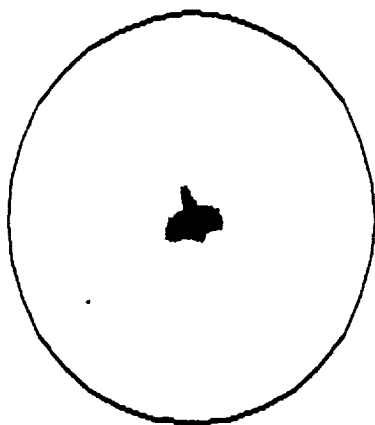


Figure 3c. Calculated Geometrical Zonal Spot Diagram for the λ_0 335 Å telescope based on interferometric measurements. The circle represents the Airy Disk radius (0.066").

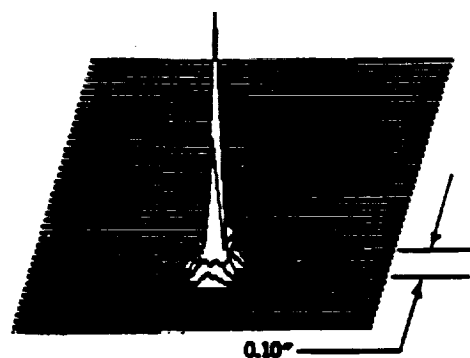


Figure 3d. Calculated point spread function (PSF) of the λ_0 335 Å telescope based on interferometric measurements. The PSF is dominated by diffraction effects.

3.7 Photographic Emulsions: We plan to use photographic films in 70 mm format to record the observations from the imaging telescopes (A-I, M, $\Lambda 1$, $\Lambda 2$). To reach the resolution that we have set as our goal, 0.1 arc-sec, will require an emulsion with a resolution exceeding ~ 1 microns (500 lines pairs/ μm). We have successfully used Kodak XUV 100 emulsion with a resolution of 200 l/mm in our October 1987 flight.⁵ We are currently testing the Kodak XUV sensitive 649 emulsion, which has resolving power as high as 2000 l/mm.¹⁶ We do not anticipate that obtaining XUV film with adequate sensitivity and resolving power will be an insurmountable problem. The skill, and supportive policy of the Research Division of Kodak has been an important part of the success we have achieved in obtaining high resolution XUV images of the sun. However, we are concerned about FUV films because, presently, Schumann emulsions¹⁷ are no longer available, and we have not yet found a FUV film with sufficient sensitivity and resolving power to replace Schumann emulsions such as 101-07.

3.8 Telescope Focal Properties: We have studied two element optical systems,¹⁸ including Cassegrain (parabola/Hyperbola), pseudo Cassegrain (sphere/sphere), Dall-Kirkham (ellipsoid/sphere) and Ritchey-Chrétien (hyperboloid/hyperboloid) during the design of the MSSTA telescope. It is well known that improved performance over a wide field of view can be achieved with aplanatic telescopes for which (to third order at least) coma is zero and spherical aberration is absent. The Ritchey-Chrétien telescope,⁴ which is an aplanatic form of the Cassegrain configuration, utilizes hyperboidal primary and secondary mirrors. The conic constant for the Ritchey-Chrétien secondary mirror is more negative than for the classical Cassegrain, which has a concave paraboloidal primary and a convex hyperboidal secondary. Consequently, the Ritchey-Chrétien design was selected as the optical configuration for all the UHRXS telescopes except the Herschellians. This provides an aplanatic system with excellent performances over a wide field of view. Our theoretical studies revealed that the MSSTA Ritchey-Chrétien telescopes are optically capable of yielding spatial resolution better than 0.3 arc-seconds over a 48 arc-minute field of view, which corresponds to 200 line pairs/mm spatial resolution at the film plane. It further established that spatial resolution of 0.03 arc-sec (2000 line pair/mm) resolution is theoretically possible near the optical axis at a wavelength of 173 Å, with resolution of the order of 0.1 arc-seconds out to 10 arc-minutes off axis. Figure 4 shows the effect of moving a flat detector plane along the optical axis in increments of 0.3 mm (300 microns). Based on these results, we plan to control the location of the focal plane to 0.05 mm (50 microns). This will be accomplished by controlling the primary/secondary mirror separation.

We note that since these Ritchey-Chrétien telescopes are aplanats; the primary image degradation arises from curvature of field and astigmatism. At the edge of the usable field of aplanatic telescopes the distortion is usually only a few hundredths of an arc-second. Image blur due to astigmatism is symmetric and therefore the center of the point spread function can be very precisely located.

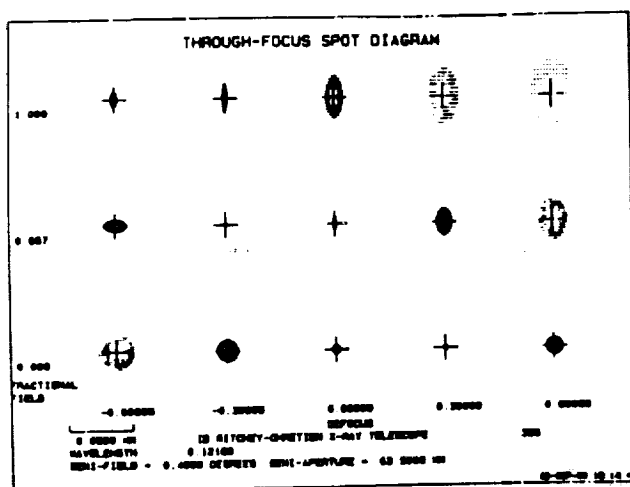


Figure 4a. Through-focus spotlight diagrams for the MSSTA Ritchey-Chrétien design. For the focal length of 3500 mm, the scale of 50 shown above corresponds to 3 arc-seconds.

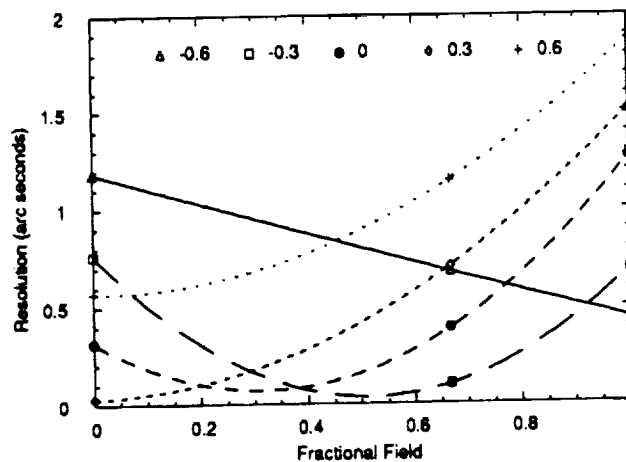
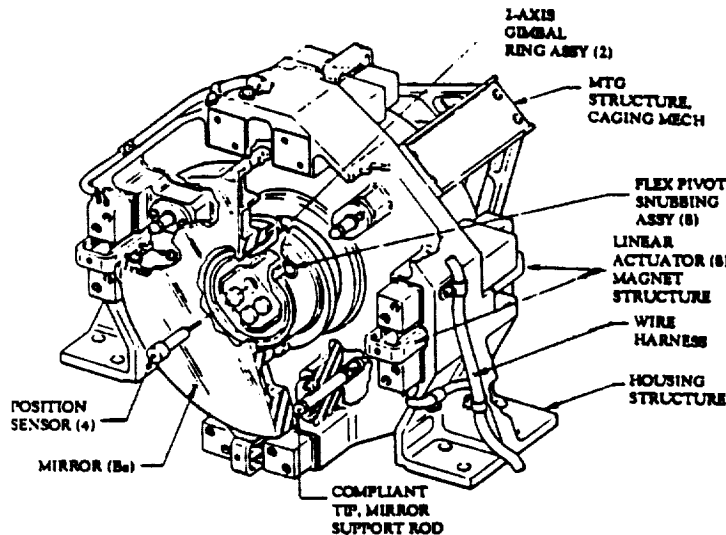


Figure 4b. Dependence of the MSSTA Ritchey-Chrétien resolution on field angle.



3.9 Active Mirror Servo: The pointing stability and accuracy required for the high resolution *UHRXS* observations will be achieved by active control of the secondary mirrors of the *UHRXS* telescopes (primary mirrors for the Herschellian Telescopes). The mirror articulation system we plan to use, the Active Mirror Servo (AMS), has been developed by Ball Aerospace Systems Division (Figure 5); the AMS has already achieved stabilization of a 6 inch aperture mirror to the level of 0.08 arc-sec with a 600 Hz bandwidth, using an error signal derived from a Lockheed Intermediate Sun Sensor (LISS). The range of the AMS, $\sim \pm 15$ arc min, is adequate to compensate for pointing errors and jitter introduced by either the proposed PIP, or the IPS.

Figure 5 (left). The Ball Aerospace Active Mirror Servo.

3.10 Image Quality: The quality of the image recorded on the *UHRXS* films is determined by the following factors:

- i. Telescope aberrations (for a perfect optical system) including diffraction (δ_a)
- ii. Aberrations due to (a) mirror tilt and (b) decentration (δ_t)
- iii. The widening of the point spread function due to surface imperfections and slope errors (δ_e)
- iv. Defocussing due to errors in primary/secondary separation (δ_s)
- v. Image blurring due to spacecraft and pointer jitter and tracking errors (δ_j)
- vi. Image blurring due to target motion (δ_m)
- vii. Image blurring due to finite film resolution (δ_d)
- viii. Scattering due to the various filters used (δ_f)

The net resolution, δ , is given by

$$\delta = [\delta_f^2(r, \lambda) + \delta_a^2(r, \lambda) + \delta_t^2(r, \lambda) + \delta_e^2(r, \lambda) + \delta_s^2(r, \lambda) + \delta_j^2(r, \lambda) + \delta_m^2(r, \lambda) + \delta_d^2(r, \lambda)]^{1/2}$$

where r is the field position from the optical axis. For large field angles (Figure 4), and in the FUV, $\delta_a(r, \lambda)$ will dominate the resolution. At small field angles and at XUV wavelengths, δ_a can be held at 0.03". We list a preliminary allocation of the error budget below. The net point spread function projected by Table 8 is 0.075 arc-seconds.

Table 8. On Axis Image Point Spread Allocation at λ 173 Å

Term	Allocation	δ^2	Term	Allocation	δ^2
$\delta_f(0)$	0.02"	0.0004	$\delta_s(0)$	0.03	0.0009
$\delta_a(0)$	0.03	0.0009	$\delta_j(0)$	0.02	0.0004
$\delta_t(0)$	0.03	0.0009	$\delta_m(0)$	0.02	0.0004
$\delta_e(0)$	0.03	0.0009	$\delta_d(0)$	0.03	0.0009

3.11 Discussion: Although there are significant issues to be resolved during the fabrication of the *UHRXS* telescopes (i.e., retaining proper focus may require the use of an invar optical bench and/or active sensing and control of primary/secondary mirror separation), we are confident that the primary *UHRXS* instruments, the imaging telescopes A-I, will meet or exceed their goal of achieving 0.1 arc-second resolution. We note that in order to achieve the highest possible resolution on-axis with the Ritchey-Chrétien optical design, we must place the film plane at the optimum focal position. This will cause the resolution at for example 173 Å to degrade from 0.03" on-axis to 0.05 at 8' off-axis, 0.33 arc-sec 16' off-axis, and 0.75 arc-sec at 24' off-axis. We plan to investigate the effects of defocussing, which in general will slightly degrade on-axis resolution, but improve resolution off-axis. (This point is discussed by Hadaway *et al.*¹⁸).

We also intend to investigate the possibility of slightly curving the focal plane, which will provide a larger field at the highest resolution. In any event, in operation it will be necessary to point the *UHRXS* telescopes directly at a structure on the limb, in order to image that structure with the highest resolution. We note that the sensitivity of the *UHRXS* telescopes (Table 9) is more than adequate for all of the scientific goals that we have established. We can judge this by noting that the brightness of the *UHRXS* 173 Å images, E and **N**, exceeds that of the 173 Å telescope (VIa) which obtained the images shown in Figure 6 by factors of ~ 12 and 350, respectively!

Table 9. Predicted Performance of the *UHRXS* Imaging Systems

	Telescope Parameters			Solar Line Intensity(a)				Flux In Focal Plane (b)			
	λ_0 (Å)	$\epsilon(\lambda)$ (§)	$t_f(\lambda)^*$	Full Disk	Network	Active Region	Flare	Full Disk	Network Region	Active Region	Flare
A	1215.60/ 1548.00	0.8/0.8	0.05	--	85.67	220.27	--	--	9,300	24,000	--
B	304.00	0.25/0.25	0.17	7.60 (d)	10.99	73.00 (c)	--	160	1,500	8,000	--
C	143.30	0.60/0.60	0.20	0.04 (e)	0.03 (f)	0.10 (f)	--	5.6	230	1,500	--
D	88.10	0.50/0.50	0.20	.044	0.03 (f)	0.200 (f)	--	4.3	3.0	20	--
A 1	69.70	0.30	0.15	0.10	0.05 (f)	0.500 (f)	--	6.5	3.2	32	--
E	173.00	0.55/0.55	0.20	1.60	1.00	8.00	--	190	120	950	--
F	195.40	0.40/0.40	0.22	1.52	0.70	7.50	--	104	48	516	--
G	211.00	0.35/0.35	0.22	0.60	0.15	3.00	--	32	8	160	--
A 2	54.7	.15	0.15	0.13	--	2.60 (g)	--	2	--	40	--
H	93.90	0.60/0.40	0.15	0.03	--	1.50 (h)	--	2.1	--	105	--
I	132.80	0.60/0.35	0.15	--	--	--	5.0 (j)	--	--	--	500 (j)
F	192.0	0.40/0.40	0.22	--	--	--	2.5 (j)	--	--	--	180 (j)
N	173.00	0.55/0.55	0.50	1.60	1.00	8.00	--	5,792	NA (l)	NA (l)	--
VIa (k)	173.00	0.25/0.25	0.30	1.60	1.00	8.00	--	17.6	10.5	88	--

(§) Reflectivity of primary and secondary mirrors; (*) Filter Transmission; (a) Solar line intensity given in 10^3 ergs/(cm²-sec-str.). Network and active region fluxes from Vernazz and Reeves.³³ Full disk flux from Malinovsky and Heroux³⁴ except as noted; (b) Focal Plane Flux given in milli-ergs/(cm²-sec); (c) Cohen;³⁵ (d) Freeman and Jones;³⁶ (e) Estimated from calculations of Doeschek and Cowan;³⁷ (f) From ratios of Ne VIII λ 780 Å; (g) Flux assumed to be in 5% of disk; (h) Flux assumed to be in 2% of disk; (j) Estimated from Feldman *et al.*³⁸ and Doeschek and Cowan³⁷; (k) Included for comparison; not part of *UHRXS*; (l) Disk will be occulted.

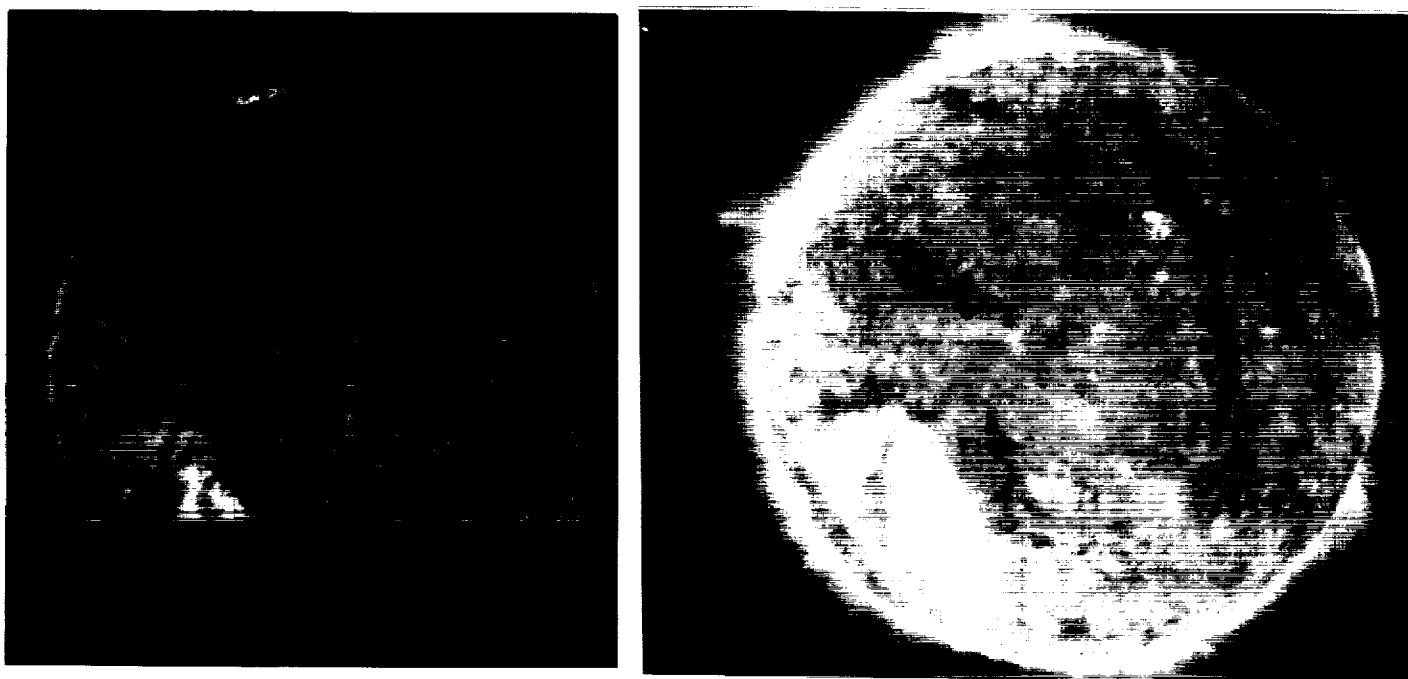


Figure 6. The corona at $\lambda\lambda$ 171 Å-175 Å (Fe IX/Fe X) as photographed with Telescope VI-a (see Tables 5 and 9) on October 23, 1987. The exposure times were 8 seconds (left) and 200 seconds (right). Kodak XUV-100 film was used.



4.0 XUV, EUV and FUV Spectroscopic Systems: The baseline *UHRXS* Spectroscopic systems (Table 10) cover bands in the XUV (170 Å - 215 Å), EUV (450 Å - 1100 Å) and FUV (1150 Å - 1600 Å). Each system consists of a telescope similar to the primary imaging telescopes (Sec. 3.0), a slit which defines the size of the solar region being analyzed, a grating, a thin metallic filter, and a MAMA detector. The grating spectrographs provide very high angular resolution (0.1 x 0.5 arc-seconds) combined with spectral resolution high enough to study line profiles over the temperature range $10,000 \text{ K} < T < 30,000,000 \text{ K}$.

4.1 The Telescopes: The telescopes for the XUV and EUV spectrographs are identical to the imaging telescopes, A-K, except that the focal length is 10,000 mm rather than 3,500 mm., which permits 0.25 arc-sec pixels with the baselined MAMA detector. Each telescope is coated with a suitable reflecting surface (Mo/Si multilayers for the XUV, Os for the EUV, Al/MgF₂/Os interference films for the FUV). The FUV spectrographs are fed by Telescope A (Tables 1, 2) using a magnifying beamsplitter (Figure 7).

4.2 Optical Configuration of the Spectrographs: If the size of an image in the direction of dispersion in the focal plane is limited by the use of a slit, a Rowland Geometry grating spectrometer can produce stigmatic images of line profiles at several discrete wavelengths, provided the source spectrum consists of strong emission lines which dominate a weak continuum. The solar coronal spectrum satisfies this criteria. The properties of the image of the entrance slit will be determined by the configuration of the grating. Sampson¹⁹ discusses the focusing properties of a number of grating configurations. If a spherical grating is used at near normal incidence, astigmatism is small, and a high-quality image results. If the grating is used away from normal incidence, then a toroidal or ellipsoidal grating allows astigmatism to be eliminated for two wavelengths, and at wavelengths adjoining these wavelengths. For a toroidal grating¹⁹ in the special case where the angle of incidence, and the diffraction angle of the spectral line of interest are equal, the horizontal and vertical radii of the Grating must be related by $r = R \cos^2\alpha$. If the grating is ellipsoidal, then the condition for a stigmatic image are given by $c^2 = b^2 \cos\beta \cos\alpha$, and $R = b^2/a$, where a, b, and c are the radii of the grating in the x, y and z axes.

We plan to use an ellipsoidal Rowland Geometry grating spectrometer with $R = 1000 \text{ mm}$ at near normal incidence in the focal plane of the Ritchey-Chrétien telescopes as shown in Figure 8, to provide a dispersed spectrum which will be recorded by a MAMA detector. The plate scale will be 50 microns/arc second, allowing a field 250 arc-sec (4 arc min) along the direction of the slit to be observed. The size of the field observed in the direction of the dispersion will, of course, be determined by the width of the slit.

4.3 Slits: The grating spectrographs can utilize slits with either a width equivalent to 0.1" or to 0.5". Since the telescopes are capable of resolution which approaches or exceeds 0.1", we can achieve 0.1" resolution across the slit, and 0.5" along the slit (limited by the MAMA pixel size) or 0.5" x 0.5" resolution respectively in the two slit configurations.

Table 10. XUV, EUV, and FUV Spectroheliograph Performance

Wavelength (Å)	Grating Parameters					Plate Scales Resolution				Count Rate ^e		
	A _{eff} ^a	Freq(F ^a)	Effic.	α	β	μ/arcsec	μ/Å	Δθ	Δλ	Line(Å)	Phot/(arcsec) ² -sec	
α1 1210-1245	6.7	1400	0.1	5°	5°	50	400	0.5"	.035	HI	20,700/53,000	b/c
α2 1530-1565	6.7	1400	0.1	6.23°	6.23°	50	400	0.5"	.035	C IV	6,900/35,000	b/c
β 450-1100	11.5	1400	0.01	~3°	~3°	50	400	0.5"	.035	HeI(λ584)	700/4,620	b/c
	6.5		0.05							HeII(λ304) ^d	2,600/17,341	b/c
Γ 170-195	22	3600	0.15	2°	2°	50	1000	0.5"	.014	FeIX(λ171)	830/9,000	b/c
Δ 190-215	15	3600	0.10	2°	2°	50	1000	0.5"	.014	FeXII(λ192)	3,200	c

^a lines/mm, ^b in the chromospheric network, ^c in active regions, ^d second order, ^e solar fluxes taken from Table 9.

* Telescope effective area $(\pi/4) (A^2 - a^2) \epsilon_p \epsilon_s \epsilon_f \epsilon_b$ in cm².

4.4 The Gratings: Two gratings will use multilayer coatings to operate in the XUV; one will be coated with Osmium to operate in the EUV, and two will operate in the FUV by utilizing multilayer interference coatings. Barbee *et al.*²⁰ have recently reviewed the status of multilayer gratings. Based on the discussion by Barbee *et al.*, we have estimated the performance given in Table 10 for the multilayer gratings Δ and Γ. The performance assumed for the FUV (α1, α2) and EUV (β) gratings is based on the literature (see for example Hutley *et al.*,²¹ Huber *et al.*,²¹ and Morgan *et al.*²¹).

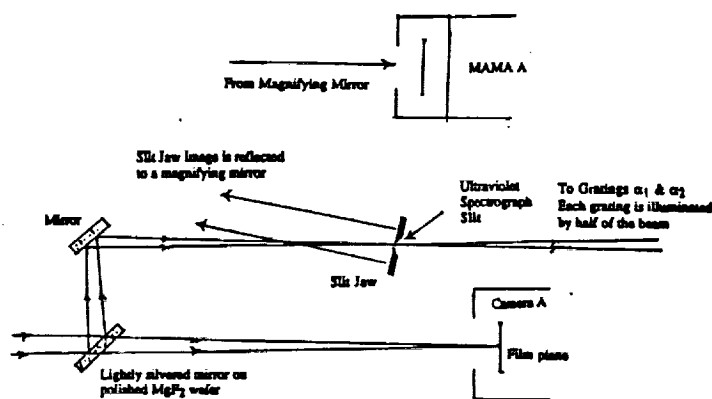


Figure 7. FUV Beam Splitter. Note that the splitter will appear as a dark line in the image recorded by MAMA A.

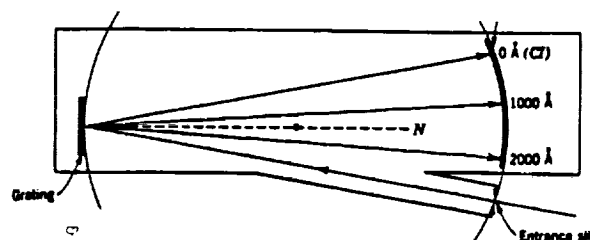


Figure 8. Configuration of the ellipsoidal grating spectrometer.

5.0 The Soft X-Ray Spectroscopic Systems: As we pointed out in Paper I¹, the original *UHRXS* concept incorporated four Herschellian telescopes. We plan to explore, for the initial *UHRXS* configuration, the replacement of two of the Herschellian telescopes with three spectroheliographs which use sectored Wolter telescopes ($\Sigma 1$ – $\Sigma 3$). (The two remaining Herschellian telescopes are described in Section 3.5) The configuration of the spectroheliographs is shown in Figure 9. Each spectroheliograph consists of four components, an objective double Bragg crystal spectrometer, a Wolter I mirror segment, a thin metallic filter, and a MAMA detector, which is shared by all three telescopes.

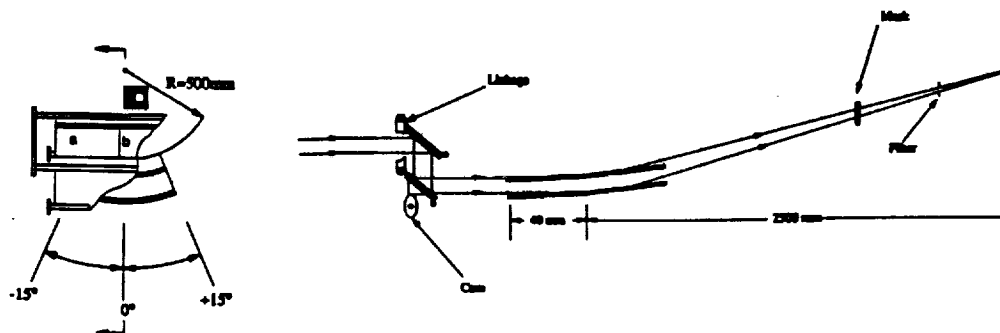


Figure 9. Configuration of the soft x-ray spectroheliographs. The objective crystal spectrometer is divided into two sections (a, b) which select different wavelengths. The mask determines the wavelength range which reaches the detector.

5.1 The Objective Double Crystal Spectrometer: The objective crystal spectrometer acts as a narrow bandpass filter, with a bandpass centered at $\lambda_0 = 2d \sin \theta$ (where θ is the Bragg angle and d the crystal lattice spacing) for sources along a locus parallel to the crystal rotation axis. The center of the bandpass varies for a source which is at an angle α from the optical axis of the telescope according to the equation, $\lambda = \lambda_0 (1 + \alpha \cot \theta)$, as illustrated in Figure 10. The bandwidth of the filter is determined by the rocking curve of the crystals. Burek²² has presented a comprehensive review of the properties of natural Bragg crystals. Table 11 summarizes the properties of a representative set of Bragg crystals that might be used for the soft x-ray spectroheliographs $\Sigma 1$ - $\Sigma 3$. Each double crystal spectrometer is designed to observe line multiplets in two bands (in 4 cases the H-like and He-like line multiplets of O, Mg, Si, and Fe). The line multiplet to be observed is selected by a cam, which scans the Bragg angle to allow the crystal to scan over the appropriate wavelength range. Note that scanning the Bragg angle generates a line profile for each point in the image field.

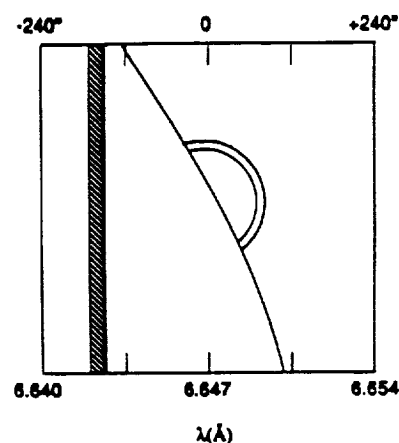
5.2 The Wolter Sector Telescopes: The monochromatic radiation from each objective crystal spectrometer is imaged by a nested Wolter I sector telescope²³ Details of the Wolter sector telescopes are given in Figure 9 and Table 11. In order to use a larger angle of incidence (and hence achieve greater collecting area for a mirror of a given length) the 1.79 - 1.85 Å telescope is coated with W/C multilayers.

Table 11. Properties of Objective Bragg Crystal Spectrometers and Wolter Telescopes

System	λ (Å)	Ion	Crystal Properties				Telescope Properties			Filter	
			Crystal	2d (Å)	θ	R_p	$\lambda/\Delta\lambda$	Angle	Coating		Reflectivity
Σ 1a	40.2-41.6	C V	Rb/C	57.00	45.0	.25	200	3.0°	Nickel	.60	Rh/C/Ph ⁷
	44.02	Si XII			50.5	.22					
Σ 1b	21.6-22.1	O VII	Rb/C	40.00	32.0	.20	300	3.0°	Nickel	.50	C/Al
	18.97	O VIII			28.0	.30					
Σ 2a	15.00	Fe XVII	TIAP	25.76	36.0	.15	750	2.5°	Gold	.40	C/Al
	13.4-13.8	Ne IX			31.5	.40					
Σ 3a	9.1-9.3	Mg XI	ADP	10.642	59.5	.60	8,200	1.5°	Nickel	.60	Al
	8.42	Mg XII			52.5	.65					
Σ 3b	6.6-6.8	Si XIII	EDDT	8.81	49.0	.80	8,000	1.5°	Nickel	.60	Be
	6.18	Si XIV			44.5	.80					
Σ 2b	1.85-1.87	Fe XXV	Topaz	2.71	43.1	.60	10,000	2.5°	W/C	.60	Be
	1.79	Fe XXVI			41.3	.60					

Discussion: The soft x-ray spectroheliographs provide high resolution imaging and spectroscopy over the spectral range λ 1.7 Å - 45 Å, which is essential to studies of the high temperature ($T > 3,000,000$ K) solar plasma. These observations will be unique in this wavelength interval, because they combine both high angular (2") and high spectral ($\lambda/\Delta\lambda \lesssim 1000$) resolution. We note that image stabilization for all the soft x-ray spectrographs will be achieved by image motion compensation within the MAMA logic system.²⁴

Figure 10 (at right). Wavelength dependence of the image of a loop on the solar limb observed at 6.647 Å (Si XIII $1s^2 1S - 1s2p^1P$). The shaded area indicates the resolution, $\Delta\lambda$, of the spectroheliograph. At 10^7 K, the line profile fwhm is $\sim 6 \Delta\lambda$.



6.0 The MAMA Detectors: The current status of the MAMA array detector has been described by Timothy *et al.*²⁵ The MAMA is well suited to the requirements of our program; it has the following advantages, compared to competing technologies. (i) It is flight proven, and the developments required for *UHRXS* are currently on-going. (ii) The MAMA can have extremely fast (in principle sub-microsecond) response time, which is well matched to the dynamics of solar phenomena. (iii) The MAMA does not suffer from bias levels which vary across the array (i.e., non "flat field") as does the CCD. (iv) The nature of the MAMA (event detection by coincidence with orthogonal anode arrays) allows compensation for image motion to be achieved, at the microsecond level, within the detector, with virtually no compromise to the quality of the image.²⁴ (v) The MAMA can be made with a photocathode that is blind to the visible, greatly simplifying the problem of suppression of scattered light in UV, EUV, and XUV instruments. (vi) The detector format (i.e. array size) can be electronically controlled.

The *UHRXS* MAMA Configuration: The MAMA array that we plan to use will have a 1000 x 1000 pixel format with 12-14 micron pixels. This will allow 2.0 arc-second resolution (1.0 arc-second pixels) over a field of view of ~ 16 arc-min x 16 arc-min for each of the x-ray spectroheliographs, and 0.5 arc-second resolution (0.25 arc-second pixels) over a field of view of ~ 4 arc-min x 4 arc-min for the XUV, EUV and FUV spectrographs. We review the current status of the MAMA technology below.

6.1 MAMA Detector Systems: The components of a MAMA detector consist of the tube assembly, which can be sealed with a window or used in the open-structure configuration, containing a single, high-gain, curved-channel microchannel plate (MCP) electron multiplier with the photocathode material deposited on, or mounted in proximity focus with the front surface. To detect and measure the positions of the electron clouds generated by single photon events, the MAMA detector employs two layers of precision electrodes which are mounted in proximity focus with the output surface of the MCP (see Figures 11a and b).

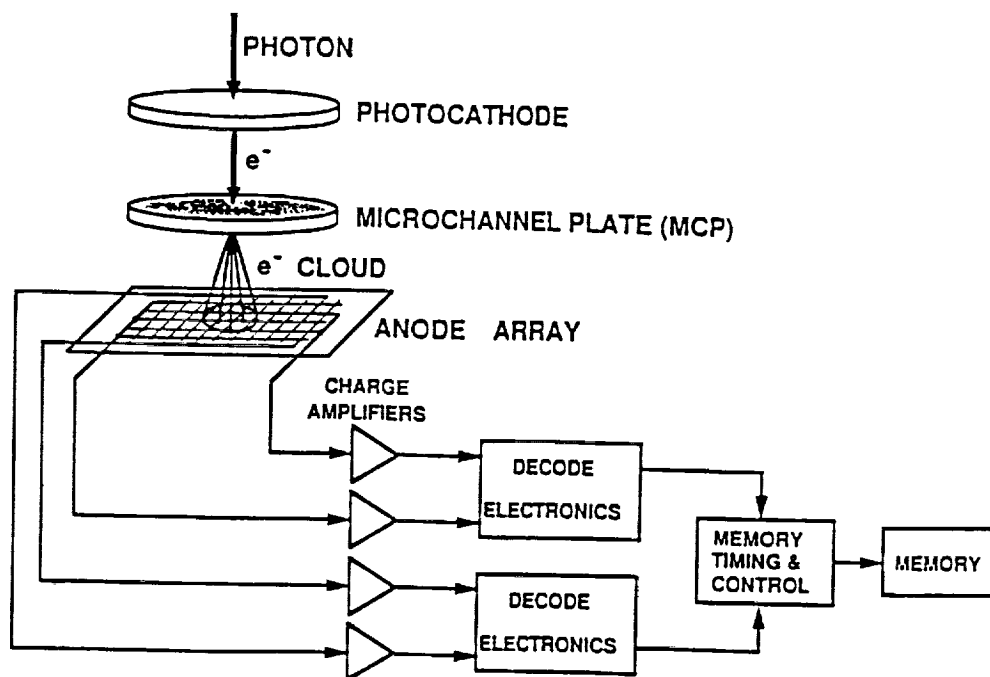


Figure 11a. Schematic of the imaging MAMA detector system.

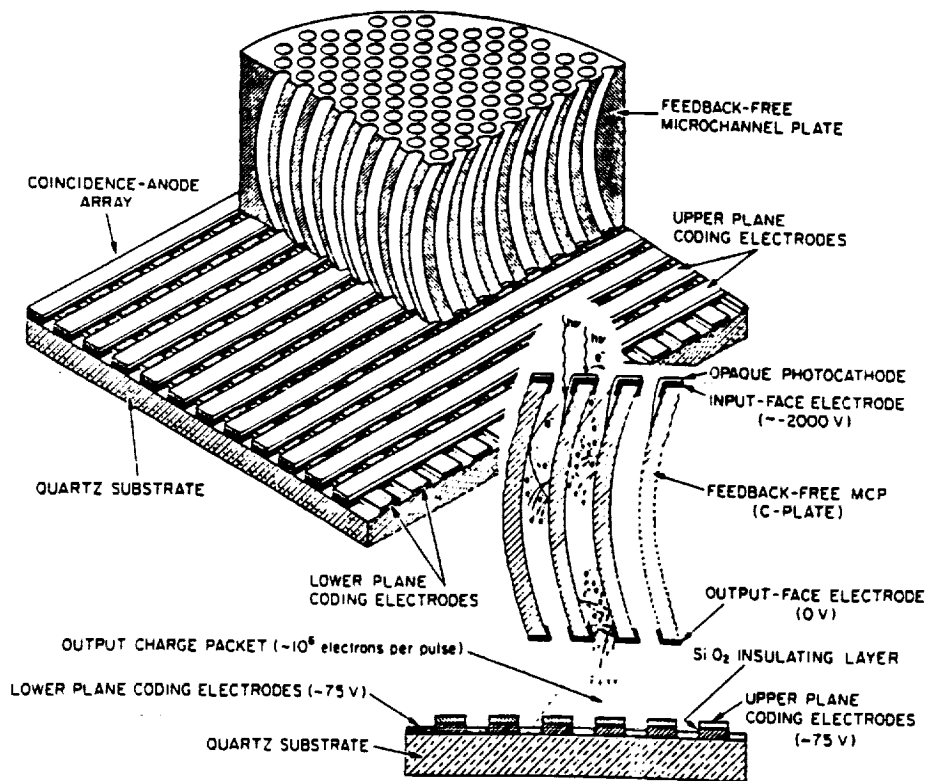


Figure 11b. Schematic showing details of the curved-channel MCP and the imaging multi-layer anode array used in the MAMA detector tubes.

Digital logic circuits respond to the simultaneous arrivals of signals from several of these electrodes in each axis, which are arranged in groups to uniquely identify a $x \times b$ pixels in one dimension with only $a + b$ amplifier and discriminator circuits. For example, a total of 32×32 , i.e. 1024, pixels in one dimension can be uniquely identified with $32 + 32$, i.e. 64, amplifier and discriminator circuits. In the imaging MAMA detector tube, the arrays are mounted in tandem with orthogonal orientations, so that positions can be sensed in two dimensions. In this configuration $(a \times b)^2$ pixels can be uniquely identified with only $2 \times (a + b)$ amplifier and discriminator circuits. The (1024×1024) -pixel array thus requires a total of only 128 amplifier and discriminator circuits. The two layers of anode electrodes in the imaging arrays are insulated from each other by a SiO_2 dielectric layer. This dielectric between the upper layer electrodes is etched away to allow the low energy (~ 30 eV) electrons in the charge cloud from the MCP to be collected simultaneously on both arrays.

The encoding-electrode geometry has been refined as the MAMA technology has become more mature. Three different encoding-electrode geometries are currently under evaluation, as shown in the schematics in Figure 12. These are, in order of development, the coarse-fine, balanced coarse-fine and fine-fine configurations. All the configurations encode the position of the detected photon in a similar manner. A charge pulse detected on a fine-encoding electrode (e.g. output F1 in Figure 12a or b) could have originated on one of a number of pixel electrodes connected to this output electrode along one axis of the array. This positional ambiguity is removed by the detection of a simultaneous output pulse on one of the coarse-encoding electrodes (e.g. output C1 in Figure 12a or b). There is only one position along the array where a particular pair of fine- and coarse-encoding electrodes are adjacent. The fine-fine configuration (Figure 12c) operates in an identical manner with the simultaneous detection of pulses on the odd and even sets of electrodes. In the imaging arrays, this position-encoding technique is implemented simultaneously in the two axes.

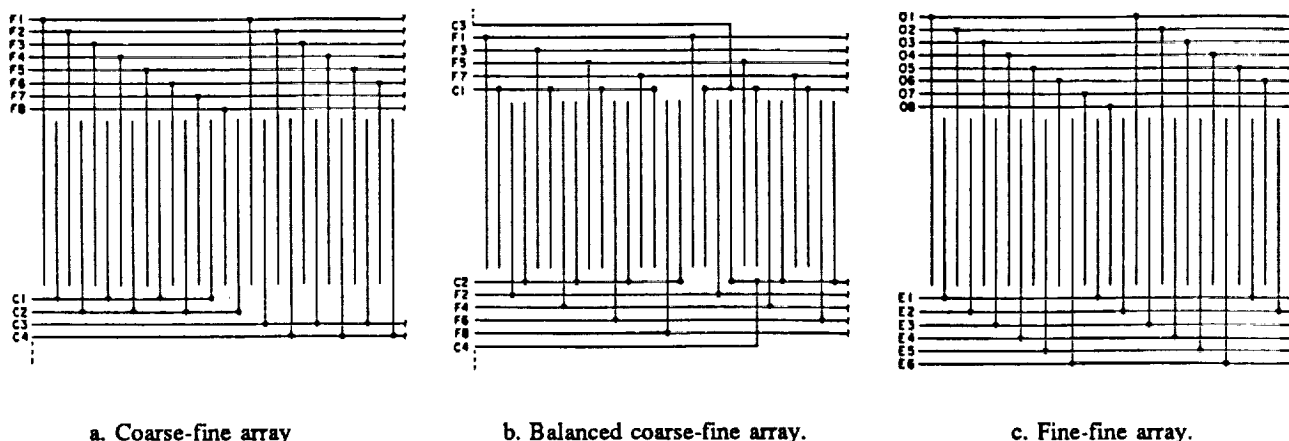


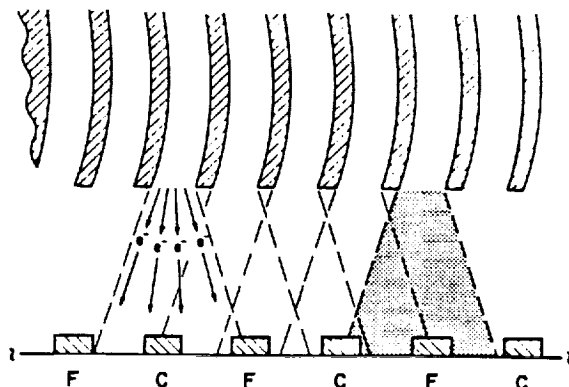
Figure 12. Configurations of the different MAMA anode array encoding geometries.

In practice, it is not possible to exactly align a channel in the MCP with a particular pair of pixel electrodes. Also, in order to obtain a uniform response across the active area, the dimensions of the channels are smaller than the separation between the pixel electrodes. Typically, 10- or 12-micron-diameter channels on 12- or 15-micron centers are used in the MAMA detectors with 25×25 microns² pixels. Furthermore, the high-gain MCP produces a space-charge saturated electron cloud which expands rapidly when leaving the channel (see Figure 13a.)

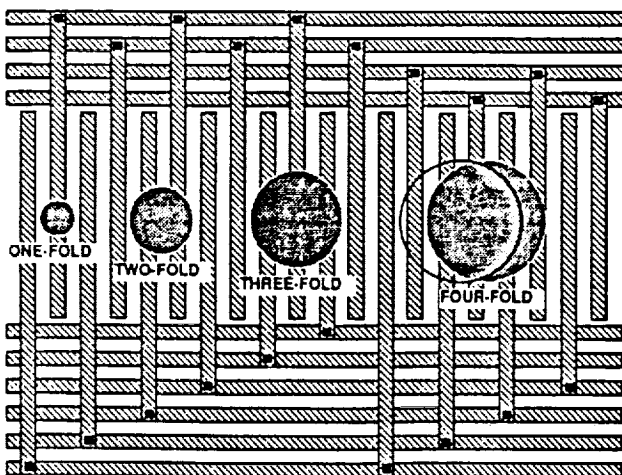
In order to maintain the inherent high spatial resolution of the MAMA readout array, the spreading of the charge cloud is controlled by keeping the distance from the output surface of the MCP to the anode array as small as possible (typically of the order of 50 to 100 microns) and by applying an accelerating potential of the order of +50 to +150 V between the output surface of the MCP and the anode electrodes. A small differential voltage in the range 1 to 5 V is applied between the upper and lower sets of electrodes in order to ensure that the charge cloud divides uniformly between the electrodes in the two layers.

In the coarse-fine and balanced coarse-fine arrays, the position of a charge cloud collected on two or three adjacent electrodes in each axis is uniquely encoded. The positions of adjacent two-fold and three-fold events in each axis are determined by the digital address-decode circuits. Since the nominal pixel size in the MAMA is determined by the center-to-center spacing of the anode electrodes, the positions of adjacent two-fold and three-fold events differ by about one half

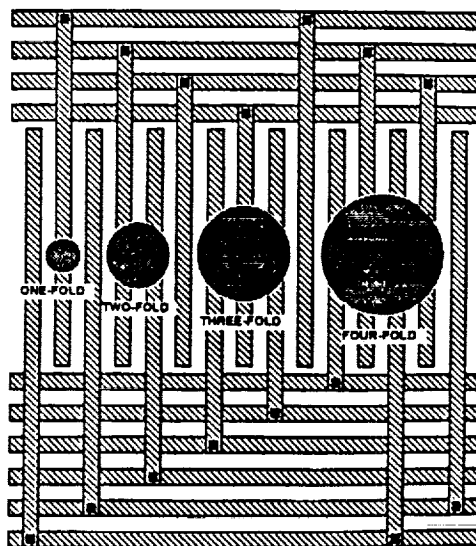
of a pixel i.e. about 12.5 microns in the arrays with 25×25 microns² pixels. In the present MAMA systems adjacent two-fold and three-fold events are co-added to produce the nominal pixel resolution with a good uniformity of response. However, in these two array configurations a charge cloud collected on four or more electrodes produces a positional ambiguity (see Figure 13b). Furthermore, we have determined that the imbalance in the inter-electrode capacitance between the different groups of encoding electrodes in the coarse-fine array produces a fixed pattern in the flat field response and slightly degrades the point spread function²⁶. These effects are significantly reduced by interlacing the coarse- and fine-encoding electrodes in the balanced coarse-fine array; however, inductive coupling caused by the very fast (< 500 ps) charge pulses from the MCP still affects the pixel-to-pixel uniformity of response. For these reasons the fine-fine array, in which the electrodes are capacitively balanced and inductively decoupled, is now the configuration of choice. In addition, as shown in Figure 13c, four-fold and higher-fold events can be encoded without positional ambiguity. The present systems of decode electronics fabricated at Stanford University are designed to accept up to six-fold events in each axis. The key characteristics of the different encoding-electrode geometries are summarized in Table 12.



a. Schematic showing the spreading of the space-charge saturated electron cloud from the high-gain MCP.



b. Schematic showing the positional ambiguity introduced when the charge cloud is collected on four or more electrodes in one axis of a coarse-fine array.



c. Schematic showing the unique position encoding when the charge cloud is collected on more than three electrodes in one axis of the fine-fine array.

Figure 13. Modes-of-operation of the different MAMA encoding-electrode geometries.

Table 12. Characteristics of the MAMA Encoding-Electrode Geometries**Coarse-fine array -**

- $n + m$ outputs encode $n \times m$ pixels in one-dimensional array
- $2(n + m)$ outputs encode $(n \times m)^2$ pixels in two-dimensional array
- position ambiguity for four-fold and higher-fold events in each axis
- imbalance in capacitive coupling between coarse- and fine-encoding electrodes
- inductive coupling between different groups of electrodes

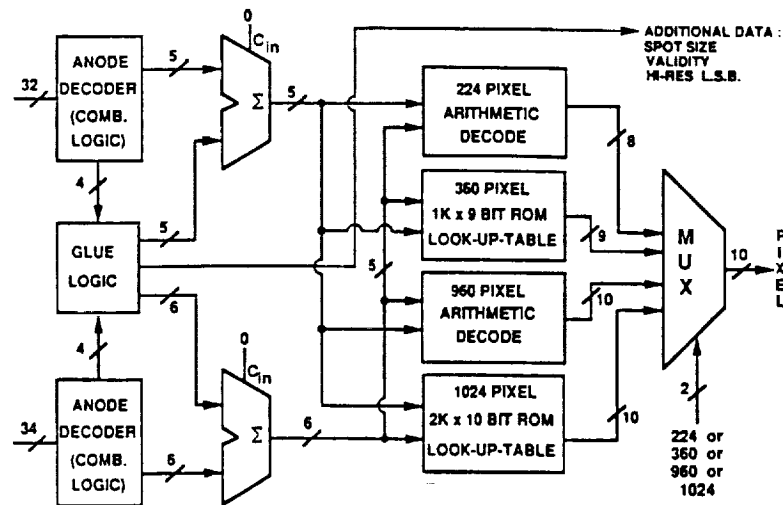
Balanced coarse-fine array -

- $n + m$ outputs encode $n \times m$ pixels in one-dimensional array
- $2(n + m)$ outputs encode $(n \times m)^2$ pixels in two dimensional array
- position ambiguity for four-fold and higher-fold events in each axis
- coarse- and fine-encoding electrodes capacitively balanced
- inductive coupling between different groups of electrodes

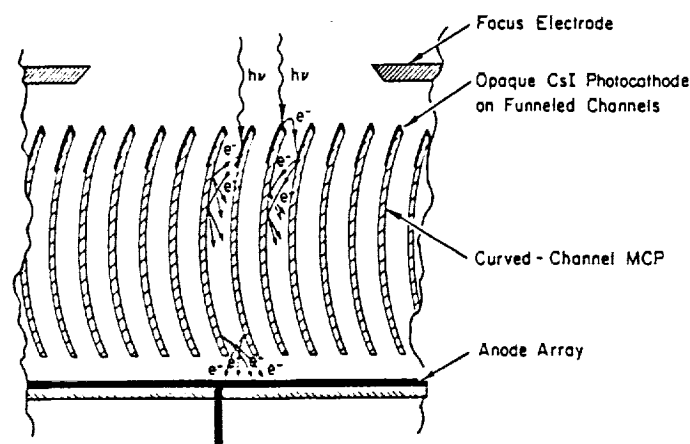
Fine-fine array -

- $2(n + 1)$ outputs encode $n \times (n + 2)$ pixels in one-dimensional array
- $4(n + 1)$ outputs encode $[n \times (n + 2)]^2$ pixels in two-dimensional array
- no position ambiguity for up to (~ six fold events in each axis)
- n must be even to avoid position ambiguities in last group of electrodes in each axis
- capacitively balanced
- inductively decoupled

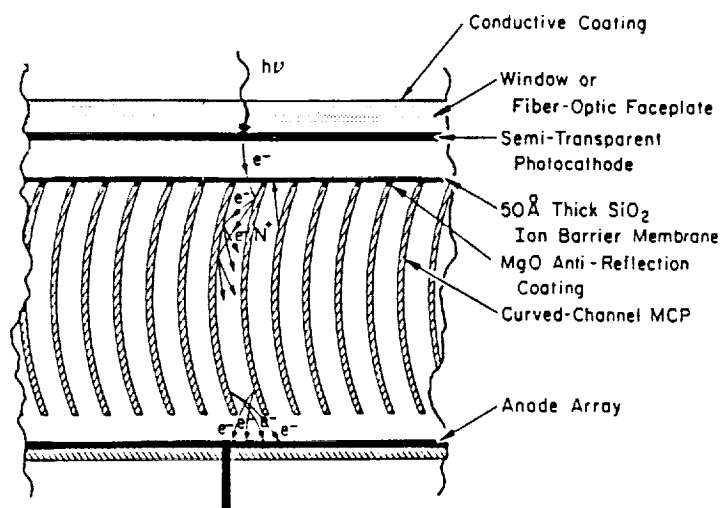
It is of importance to note that the simultaneous arrival of pulses on non-adjacent electrodes in each axis is declared a non-valid event and rejected by the address-decode circuits. The spatial resolution and geometric fidelity of the MAMA detector is accordingly independent of position on the array or of signal level, a unique characteristic which has been verified in a number of laboratory and ground-based telescope tests. A schematic of one of the decode circuits is shown in Figure 14 and described in detail by Kastle.²⁷

**Figure 14. Schematic of the MAMA fine-fine address-decode circuit.**

A number of different photocathodes are currently being utilized in the MAMA detector tubes. At FUV and EUV wavelengths below about 1500 Å opaque alkali-halide photocathodes deposited directly on the front surface of the MCP provide the best detective quantum efficiencies (DQEs). In this configuration, photoelectrons produced in the photocathode on the web area between the channels can be collected by means of appropriate focusing potentials, as shown in Figure 15a. The pulse-counting DQE can accordingly be greater than 80% of the intrinsic photocathode quantum efficiency. However, the lateral drift of the photoelectrons will be energy dependent and the focusing voltage required to maintain the desired point spread function will depend on both the photocathode material and on the wavelength.²⁸ The best photocathode materials available at this time are CsI, KBr and MgF₂.²⁹ All can be used in the open-structure configuration at soft x-ray, XUV and EUV wavelengths, but CsI, and to a lesser extent, KBr will degrade rapidly if exposed to humidity. Our present baseline configuration utilizes MgF₂ photocathodes. However, for the soft x-ray spectrograph in particular, CsI may offer significant advantages. *The use of a CsI cathode would require that the microchannel plate and cathode be sealed in a small vacuum enclosure with a motor driven door.*



a. Opaque photocathode for use at FUV and EUV wavelengths.



b. Semi-transparent, proximity-focused photocathode for use at ultraviolet and visible wavelengths.

Figure 15. Schematics of MAMA photocathode configurations.

At ultraviolet and visible wavelengths, where activated photocathodes such as Cs_2Te , K_2CsSb , and $(\text{Cs})\text{Na}_2\text{KCsSb}$ must be employed, the MAMAs utilize the semi-transparent, proximity-focused photocathode structure shown in Figure 15b. In this configuration, the input surface of the MCP is typically covered with a thin (of the order of 50 to 100 Å thick) SiO_2 film which inhibits photocathode degradation caused by backbombardment with positive ions produced within the channels. Since the SiO_2 film prevents photoelectrons landing on the web area from reaching the MCP channels the pulse-counting DQE is reduced by a factor proportional to the channel open-area ratio of the MCP (typically 50 to 65%). This reduction in the DQE is highly undesirable and we are currently investigating techniques to eliminate the film while at the same time ensuring the long-term stability of the photocathode quantum efficiency.

6.2 Performance Characteristics: The configurations of representative imaging MAMA detector systems now under evaluation are shown in Figure 16. All of the imaging MAMA anode arrays have been fabricated by Ball Aerospace Systems Group (BASG), Boulder CO and units of all arrays have been fabricated with zero defects.

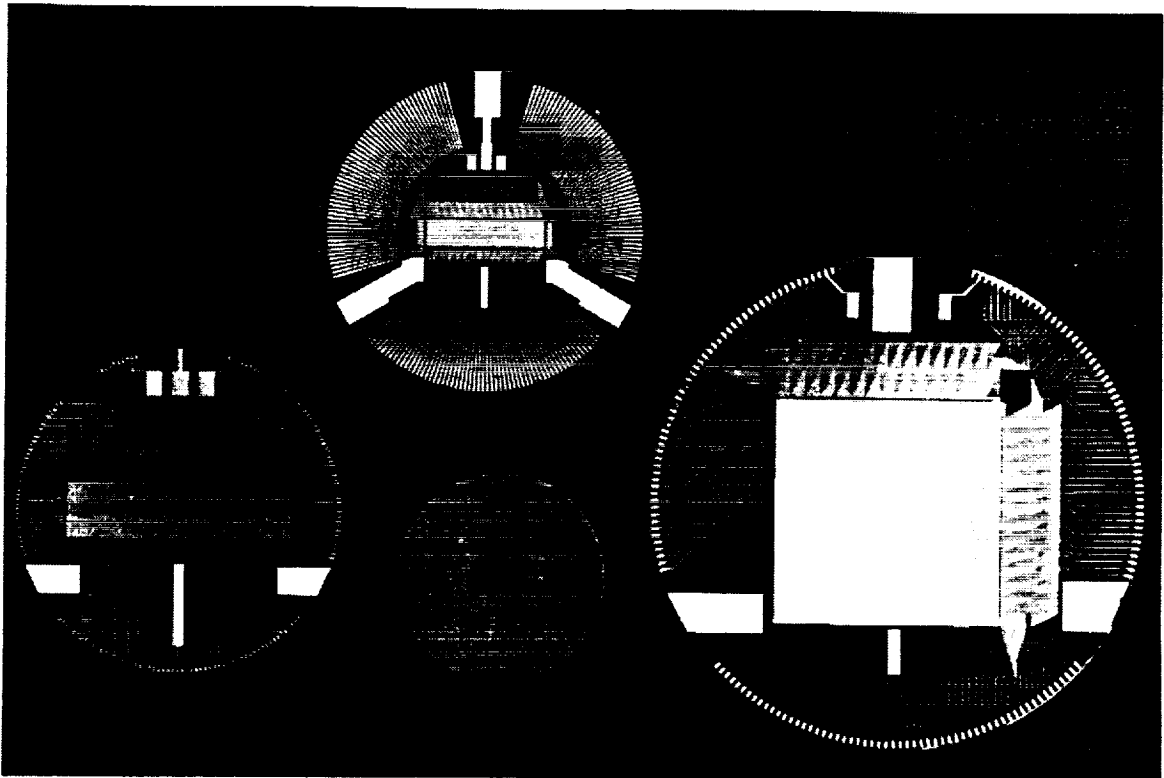


Figure 16. Configurations of representative imaging MAMA arrays.
 Left: (256 x 1024)-pixel balanced coarse-fine array with 25×25 microns² pixels.
 Center: (224 x 960)-pixel fine-fine array with 14×14 microns² pixels.
 Right: (1024 x 1024)-pixel fine-fine array with 25×25 microns² pixels.

The (256 x 1024)-pixel balanced coarse-fine detector system with 25×25 microns² pixels (left array in Figure 16) was flown successfully on the NASA Goddard astronomy sounding rocket on 26 June 1989. The detector was used in the time-tag imaging mode and recorded ultraviolet images of the galaxy NGC 6240. The timetagged data stream is being used to correct the image blurs caused by drifts in the rocket pointing system. Analyses of these data are currently being carried out by Dr. Andrew Smith at the NASA Goddard Space Flight Center.

The (224 x 960)-pixel fine-fine detector system with 14×14 microns² pixels (center array in Figure 16) is being used in the laboratory to verify the capability of the MAMA to provide the spatial resolution required for the prime spectrograph of the *Lyman* FUSE mission. This detector utilizes a curved-channel MCP with 8 micron-diameter channels fabricated by Galileo Electro-Optics Corp., Sturbridge, MA (see Figure 17).

In the initial imaging tests, the first (224 x 960)-pixel detector, which is defect free, has demonstrated the theoretical imaging performance at 2537 Å. The images of positive and negative USAF test targets recorded at this wavelength are shown in Figure 18. A cut through the image of a 20-micron-diameter spot of light and a row from a rectified flat-field image are shown in Figure 19. The spot image has the expected profile, and the deviations in the flat field are in perfect agreement with the Poisson statistics of the original exposure.

The (1024 x 1024)-pixel fine-fine array with 25 x 25 microns² pixels (right array in Figure 16) has been configured with the encoding electrodes on only two sides of the active area. This permits four of these arrays to be fabricated on a single substrate to produce a (2048 x 2048)-pixel array with a dead space between the four quadrants of three pixels or less. An array with this configuration is currently being fabricated for the Space Telescope Imaging Spectrometer (STIS). Imaging tests of the (1024 x 1024)-pixel detector system (i.e. one quadrant of the STIS detector) are currently being carried out at both ultraviolet and visible wavelengths. The arrays currently installed in both the 40-mm-format ultraviolet demountable tube and the 40-mm-format sealed visible-light tube are defect free. As examples of the type of data currently being recorded with these detectors, an image of a test mask and a rectified flat field recorded at 2537 Å are shown in Figure 20. One of us (J. Gethyn Timothy) plans to fly the ultraviolet version of this detector on the NASA Goddard astronomy sounding rocket late in 1990.

Detailed studies of the performance characteristics of all of the detector systems are now in progress.

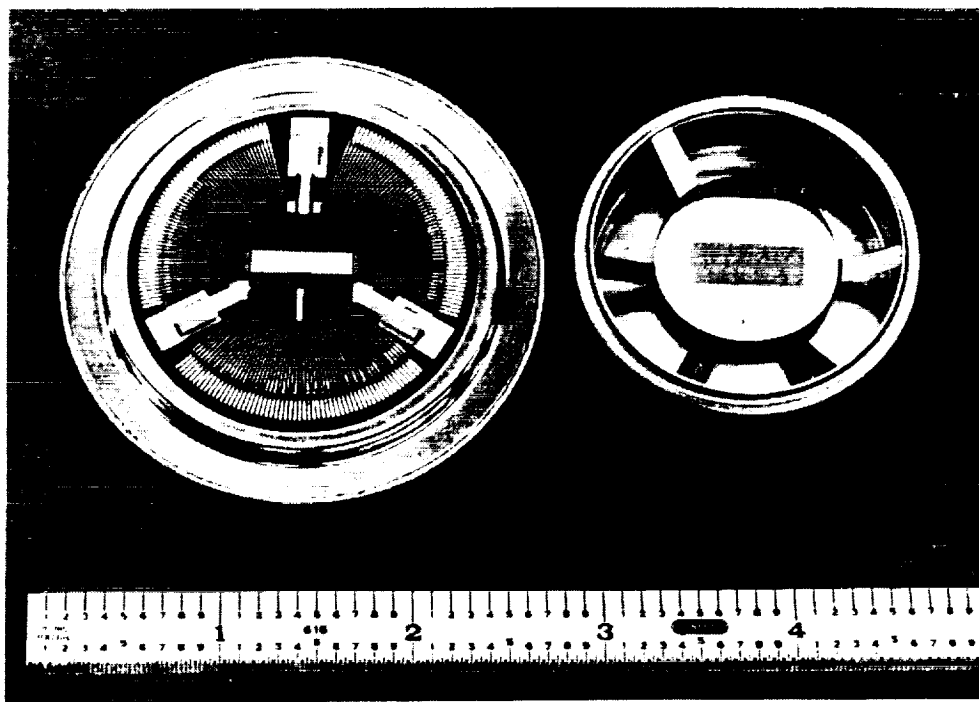


Figure 17. (224 x 960)-pixel fine-fine MAMA detector components.
 Left: anode array mounted on the ceramic header.
 Right: curved-channel MCP with 8-micron-diameter channels.

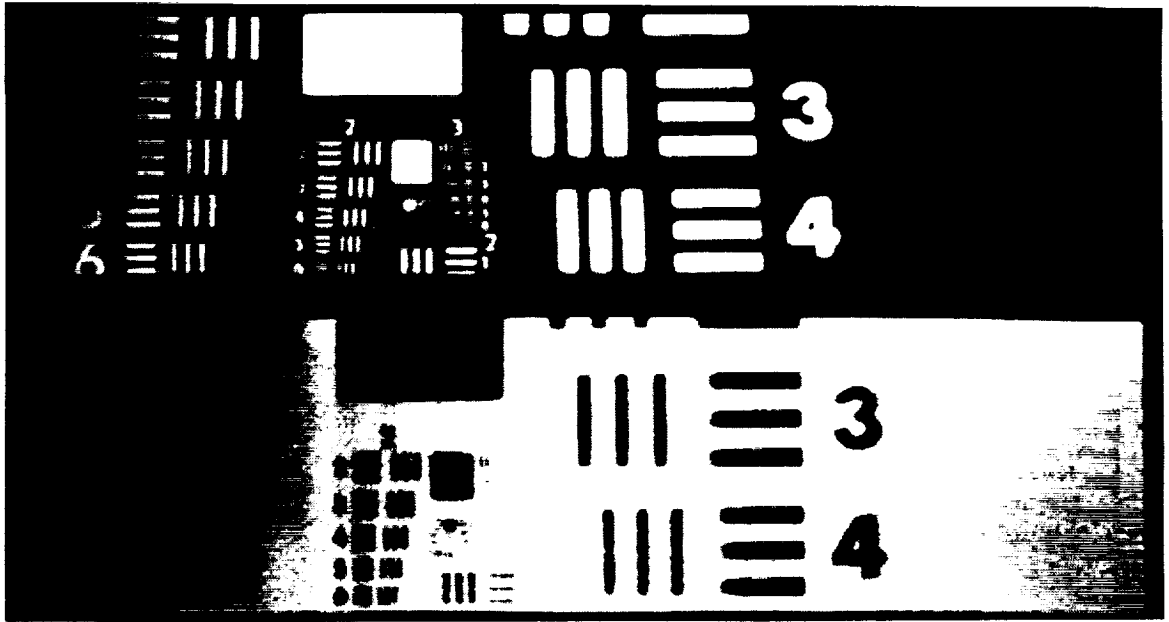


Figure 18. Positive and negative images of a USAF test target taken at ultraviolet wavelengths with a (224 x 960)-pixel fine-fine array with 14×14 microns² pixels and a curved channel MCP with 8-micron-diameter channels. The sequence of bars in these images starts with a resolution of 2.51 line-pairs mm^{-1} (Group 0, element 3 on the right side of the images). The closest bars in the image have a resolution of 113.6 line-pairs mm^{-1} (Group 5, element 6 to the left of the image centers).

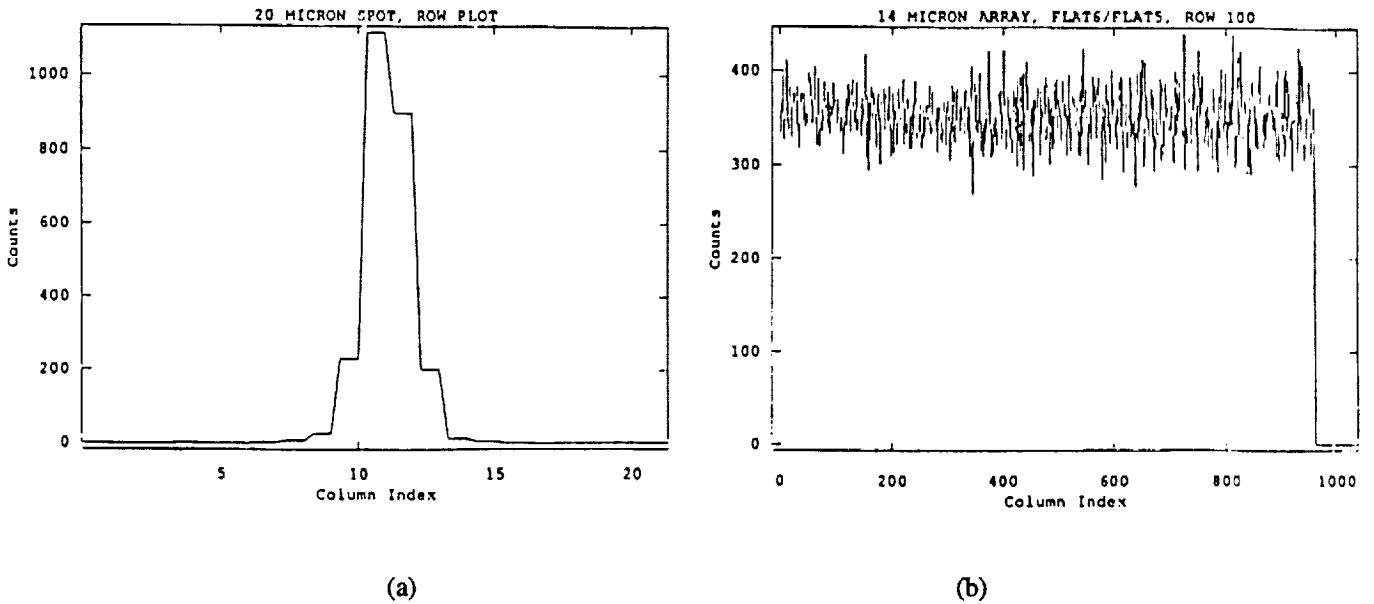
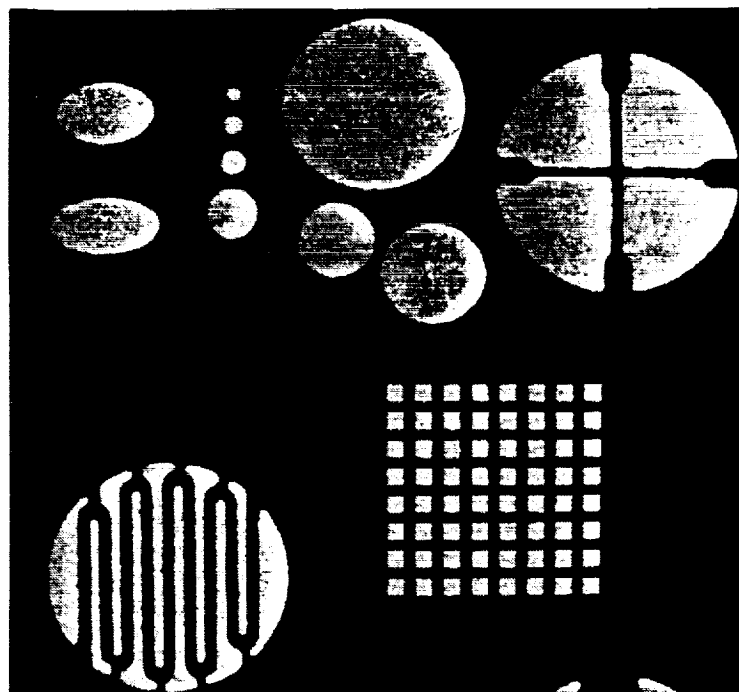
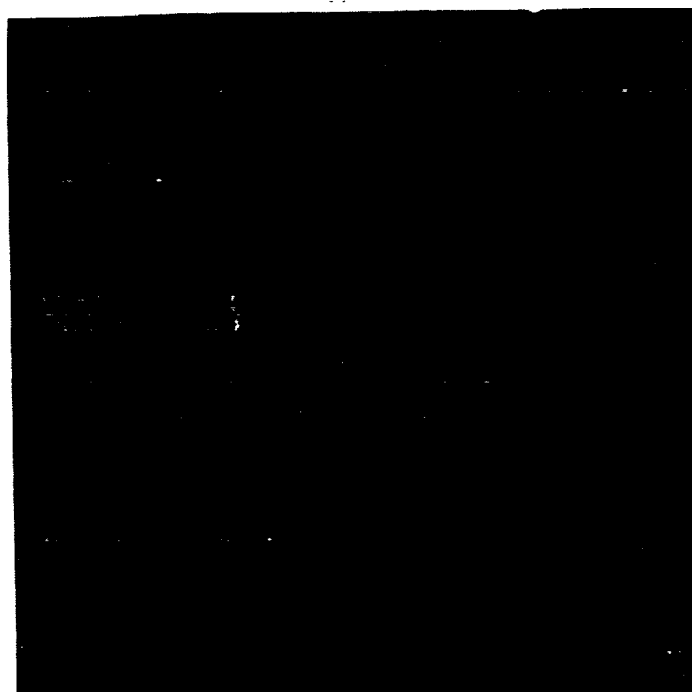


Figure 19. Data recorded with the 14-micron-pixel MAMA detector. a. A cut through an ultraviolet image of a 20-micron spot of light at 2537 \AA . b. A row from a rectified flat field image. Here one flat field image has been rectified by another and then renormalized to its original count rate. The data illustrated show deviations which are in perfect agreement with the Poisson statistics of the original exposures (7.6%).



a. Test mask.



b. Rectified flat field.

Figure 20. Images recorded with the (1024 x 1024)-pixel MAMA detector at 2537 Å.

6.3 Future Developments: A number of breadboard units of the SOHO detectors are now in fabrication. The detectors will operate in different scientific instruments over the wavelength range from about 400 to 1600 Å. Open detector tubes, sealed detector tubes and sealed detector tubes with openable covers will be employed. All will be based on the standard 25-mm-format demountable tube body fabricated by EMR Photoelectric, Princeton, NJ (see Figure 21).

In addition to the laboratory evaluations, the primary tasks of the MAMA program at this time are the detailed design and fabrication of the (360 x 1024)-pixel flight detectors for the SOHO mission and the fabrication of the prototype (2048 x 2048)-pixel detectors for STIS (Figure 22).

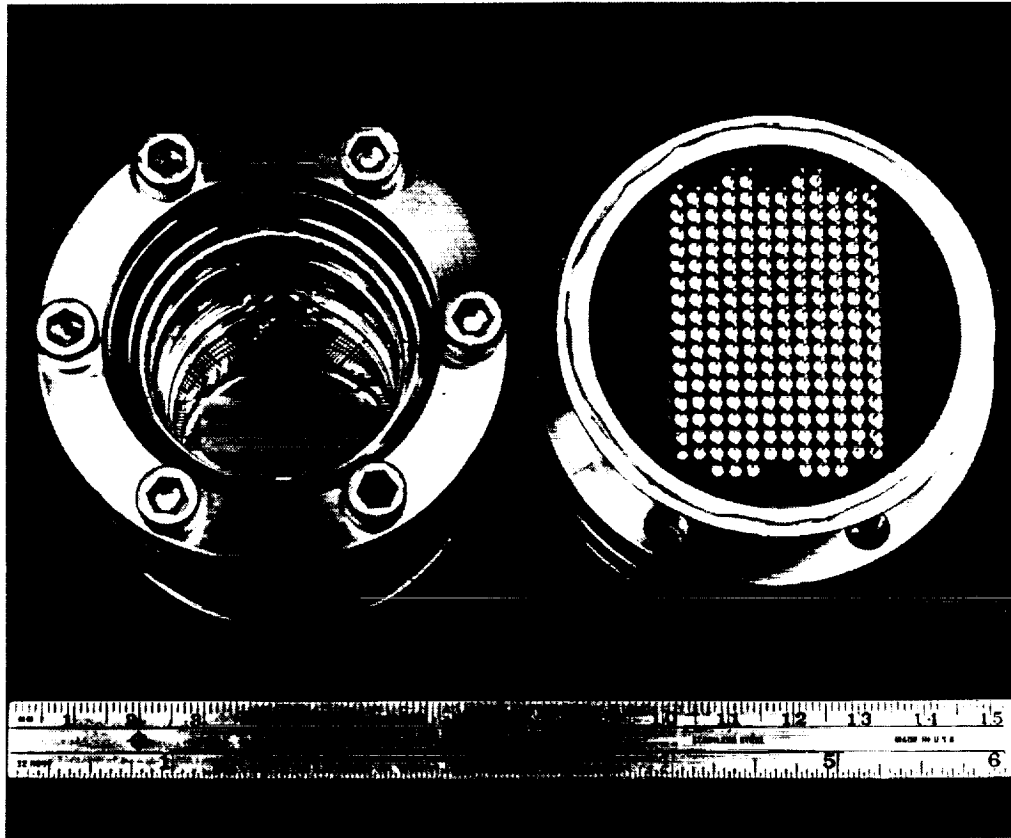


Figure 21. (360 x 1024)-pixel MAMA detector for SOHO.
 Left: anode array mounted in the 25-mm-format demountable tube.
 Right: rear view of tube body showing electrical outputs from the multi-layer ceramic header.

A major effort is underway at Stanford and at BASG to miniaturize the MAMA electronics through the development of custom chips for the amplifier and discriminator and address-decode circuits. The hybrid MAMA electronics systems will be used on both the SOHO and STIS programs. The requirements for SOHO are for a detector head assembly incorporating the amplifier, discriminator and address-decode circuits, together with the detector high-voltage power supplies, with dimensions no greater than 130 x 85 x 180 mm³ and a mass no greater than 4.0 kg. This low volume and mass must be achieved without compromising the requirements of high system speed (~175 ns pulse-pair resolution) and low power (<7 W), coupled with the ability to operate for several years in the radiation environment in low earth orbit and at the L1 libration point. Details of the technologies being employed for the custom chips are given in the papers by David Kastle²⁷ and Ed Cole.³⁰

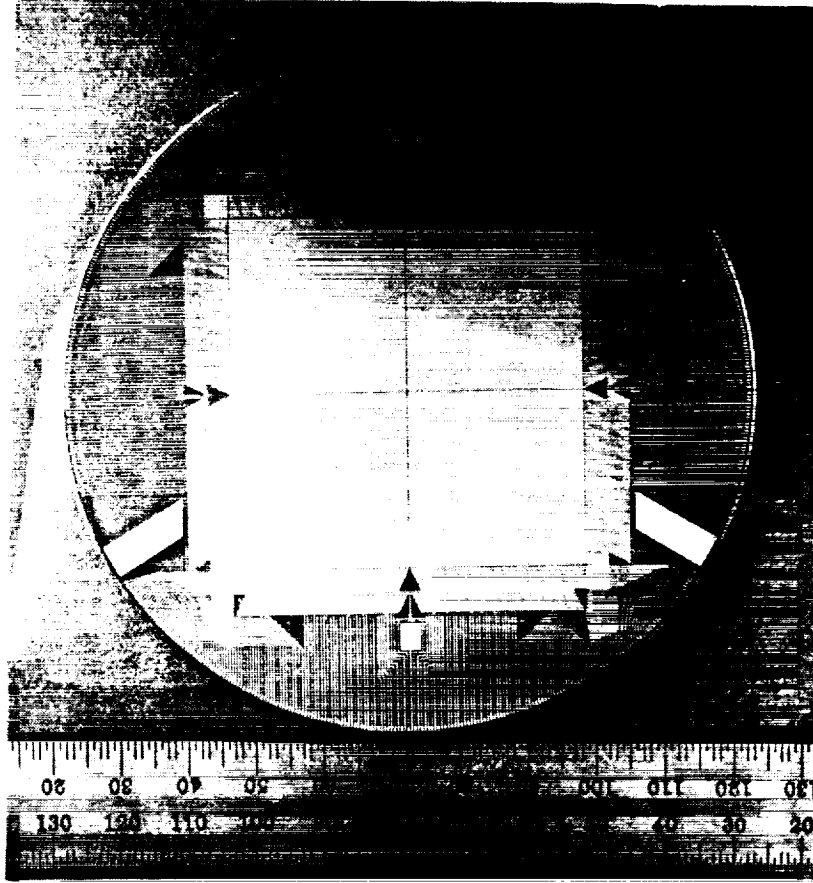


Figure 22. (2048 nx 2048)-pixel fine-fine MAMA array with 25 x 25 microns² pixels for STIS.

ORIGINAL PAGE
BLACK AND WHITE PHOTOGRAPH

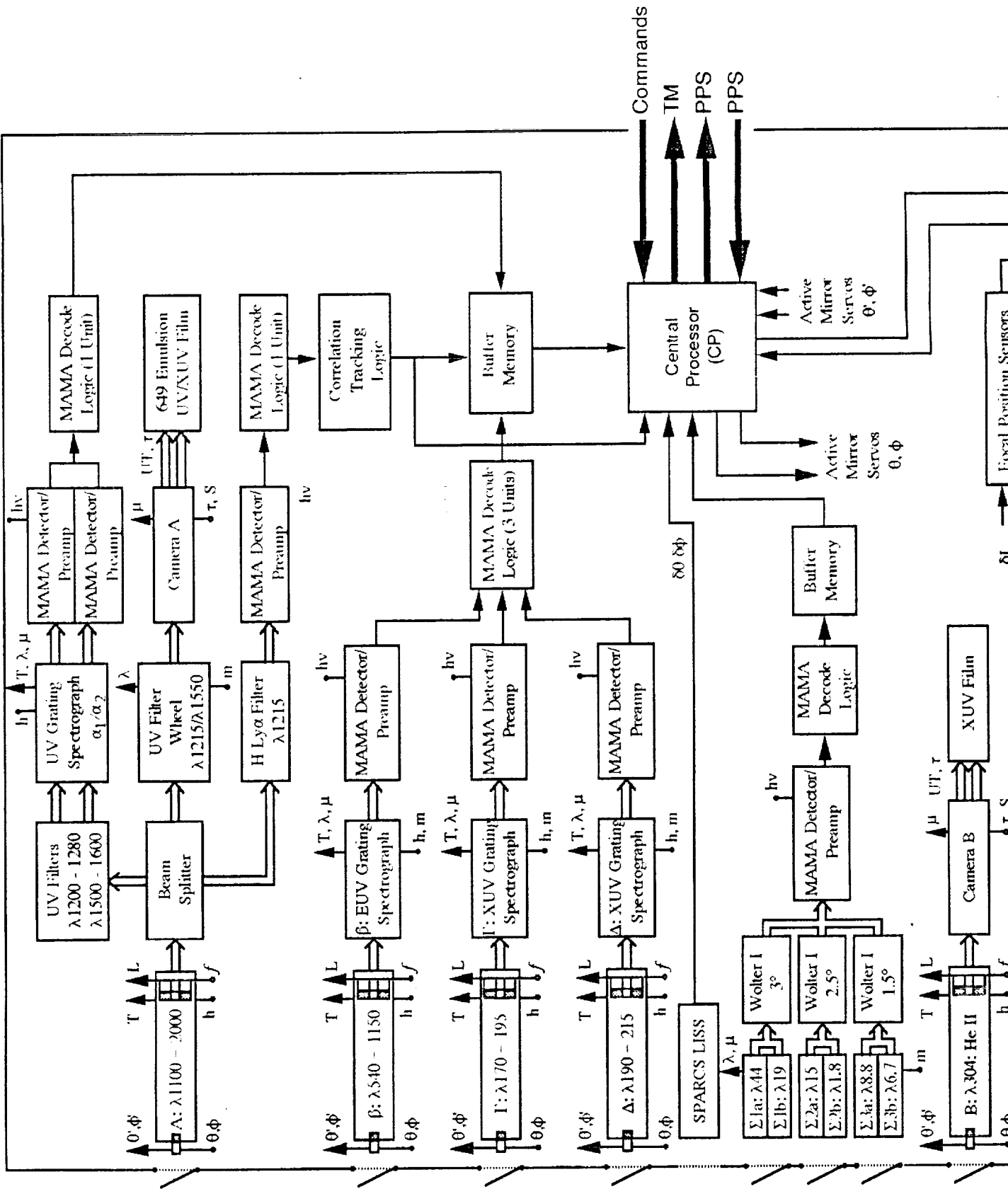
ORIGINAL PAGE IS
OF POOR QUALITY

7.0 Experiment Electronics Logic and Data Formats: The electronic block diagram for the *UHRXS* instrument is presented in Figure 23.

7.1 Experiment Control: Control of the *UHRXS* observations will be exercised by an in-flight microprocessor which will carry out the following functions: (i) distribution of the LISS error signal to the AMS control circuits, (ii) development and distribution of the correlation tracking error signal, (iii) control of exposure time and exposure sequence for all cameras, (iv) control of format and integration time of all MAMA images, (v) selection of FUV filters, (vi) control of wavelength selection and secondary mirror rastering for all spectrographs, (vii) monitoring of MAMA detector gain and adjustment of the programmable high voltage power supplies to keep gain stable, (viii) thermal control, (ix) control of all mechanisms, and (x) formatting of data and transmittal of data to the Space Station telemetry system. Real time control of the pointing of the *UHRXS* can be achieved by using the slit jaw H Ly- α (or C IV) images from the FUV telescope, which covers an area 4' x 4' on the sun and also shows the precise position of the spectrograph slit. Alternatively, the images from the EUV and XUV grating spectrographs may be used. This image will be available to astronauts on the Space Station control panel and to the experimenters on the ground, allowing pointing commands to be sent to *UHRXS*.

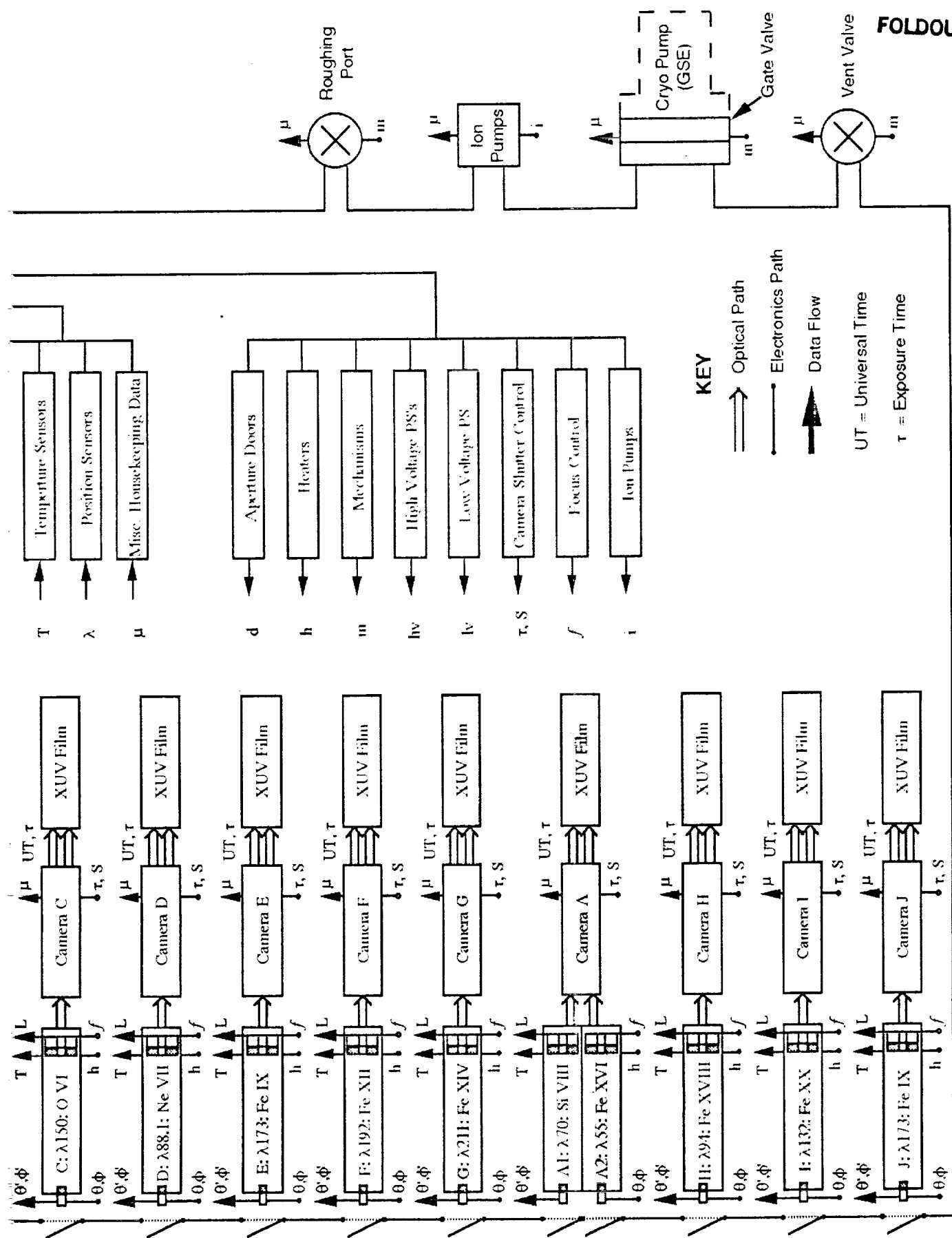
7.2 Data Formats and Data Handling: Telemetry rate is not a constraining commodity for the observations of the *UHRXS* since the majority of our data is recorded photographically. For the photoelectrically recorded images, a typical uncompressed spectroheliogram will have $1000 \times 1000 \times 10 = 10^7$ bits (assuming 0.1% precision). At a TM rate 10^7 bits/sec, it would require 1 second to transfer a single image from image memory to telemetry. During our definition phase, we will address the question of on board data compression in depth. For the present discussion, we will make the conservative assumption that our images can be compressed by a factor of 10. We can, under this assumption, transmit 10 images every second to telemetry. (Note that this does not constrain the rate at which images can be accumulated and placed in memory.) This rate is adequate for most of the solar objectives we have identified. For flares, however, greater time resolution is desirable. The MAMA detector allows the size of the image array read out to be varied so that if x_1 , x_2 , y_1 , and y_2 are addresses within the MAMA array ($x_1, x_2, y_1, y_2 < 1000$), then an array $x_2 - x_1 \times y_2 - y_1$, may be selected. Flare images may, therefore, be further compressed by the following approach: If analysis of flare images by the central processor determines that $x_1 + (x_2 - x_1)/2$ and $y_1 + (y_2 - y_1)/2$ are the central coordinates of a flare enhancement, then we can select an image which includes pixels $x_1 \dots x_2, y_1 \dots y_2$ for formatting, reducing the array size by a factor $(x_2 - x_1)(y_2 - y_1)/10^6$. When observing line profiles, $y_2 - y_1$ may be made only wide enough to accommodate a single line profile, resulting in a pixel array $\sim 1000 \times 50$.

FOLDOUT FRAME



29





FOLDOUT FRAME 2

Figure 23. UHRXS Electronics Logic Diagram.

292



8.0 Film Cameras: The placement of the film cameras for the eight XUV imaging telescope, B-I, is shown in Figures 1b and c. The eight cameras will be configured in four dual camera modules. Figure 24a is a sketch of a dual camera design. We have assumed a film reel size of 10 inches, which should permit a role containing ~2,500 feet of film, corresponding to ~10,000 exposures. It may also be possible to develop a design which incorporates two reels, mounted side by side for each telescope, with a mechanism to select the reel that is in active use. This would permit a storage capacity of 5,000 feet of film per telescope. Details such as the number and type of drive motors, shutter mechanisms, and method of providing identifying information for each exposure remains to be worked out.

The cameras for the coronagraph (N) and the Herschellians ($\Lambda 1$, $\Lambda 2$) are placed back to back in a single dual camera module. The camera for the ultraviolet telescope, A, is a single module.

Access to the film camera modules for the coronagraph/Herschellians and for the FUV telescope present a formidable problem. Some preliminary ideas concerning the configuration of these cameras, and access to them, are shown in Figure 24b.

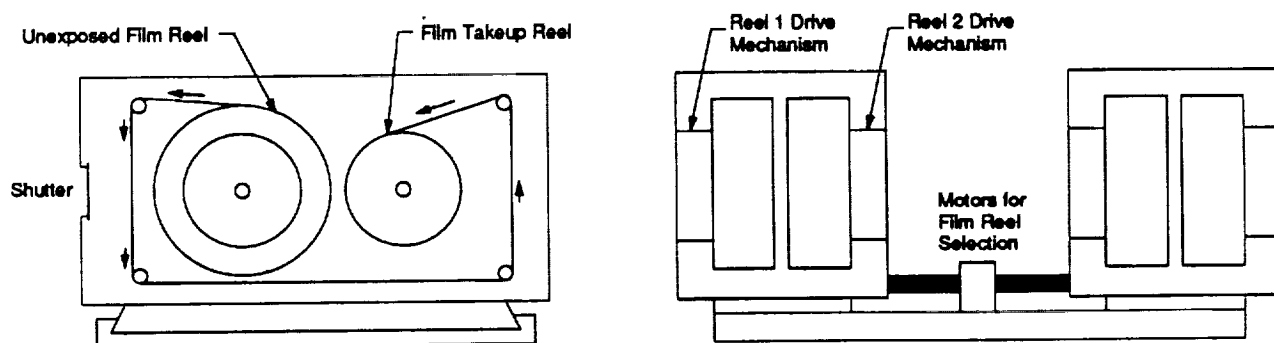


Figure 24a. Configuration of the dual camera module for the XUV imaging telescopes.

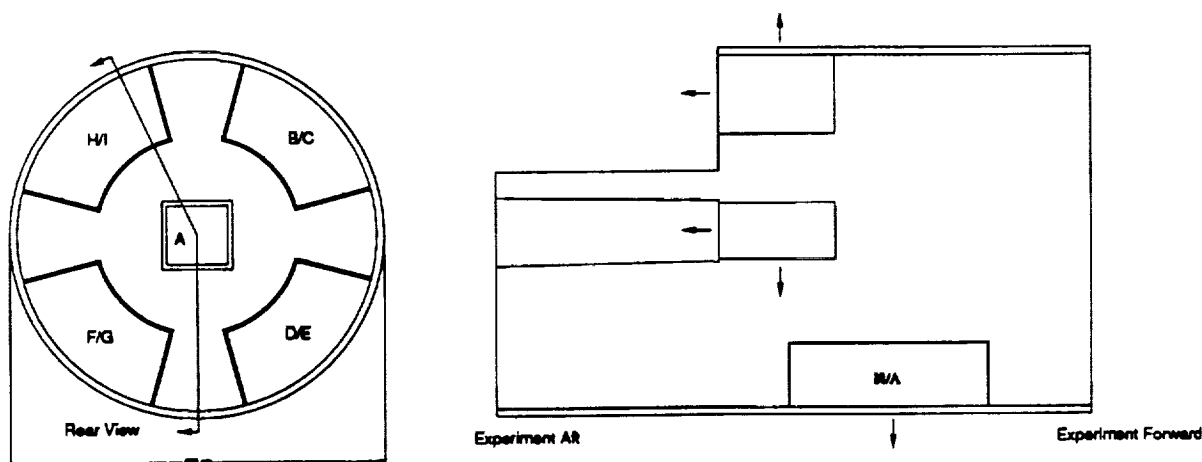


Figure 24b. Placement and access of the film cameras. For an end-mounted pointer, all cameras would be removed orthogonal to the experiment axis. For a center-mounted pointer, cameras A-I would be removed from the rear, while cameras N/ Λ would be removed orthogonal to the axis.

9.0 Expected Performance

9.1 **Imaging Telescopes:** The *UHRXS* imaging telescope focal plane energy densities, D , are given by

$$D_n(x,y) = \frac{1}{4\pi(F.L.)^2} (\pi/4) (A^2 - a^2) V(x,y) a_H \int_{-\infty}^{\infty} dT_e K_n(T_e) n_e^2(T_e, x, y), \quad (1)$$

where A and a are the diameters of the primary and secondary mirrors, $F.L.$ is the focal length of the telescope, and $V(x,y)$ is the vignetting function of the telescope. The solar plasma is described by a_H , the number of electrons per hydrogen atom (assumed constant), and $n_e^2(T_e)$, the emission measure at electron temperature T_e and density n_e which is characteristic of the solar structure under study. The "kernel" of the integral equation, $K_n(T_e)$, which is the convolution of the telescope efficiency and the solar emissivity, is given by

$$K_n(T_e) = \sum_{Zzj} (hc/\lambda_{ij}) A_Z \epsilon(\lambda_{ij}) a_{Zz}(T_e) \alpha_{Zzj}(T_e), \quad (2)$$

A_Z is the abundance of element Z , a_{Zz} is the fractional population of ionization stage z , and α_{Zzj} is the excitation function for transition ($i \rightarrow j$) including all population processes for the upper level i , and branching ratios to the lower level j . The function $\epsilon(\lambda) = \epsilon_p(\lambda) \epsilon_s(\lambda) \epsilon_b(\lambda) \epsilon_f(\lambda)$ [ϵ_p and ϵ_s are the reflection efficiency of the primary and secondary mirrors, $\epsilon_b(\lambda)$ is the efficiency of the beam splitter where appropriate, and ϵ_f is the transmission of the filter (including supporting mesh)] represents telescope throughput. The functions $A_Z a_{Zz}(T_e) \alpha_{Zzj}(T_e)$ are taken from Mewe, Gronenschild, and Van den Oord³¹ and Landini and Fossi³². The functions $K_n(T_e)$ for the *UHRXS* imaging Telescopes are given in Figure 25. The energy density in the focal plane of the *UHRXS* imaging telescopes for typical solar features is given in Table 9. These energy densities significantly exceed those which were achieved for the image of Figure 6. Clearly, images of sufficient sensitivity to address our objectives can be obtained with exposure times from ~ 0.3 second to 10 seconds for the "quiet sun", and in shorter times for flares.

9.2 **The Soft X-Ray Spectroheliographs:** The soft x-ray spectroheliograph count rates are given by

$$C_n(x,y) = \frac{1}{4\pi(F.L.)^2} (A^2 - a^2) (\Phi/8) V(x,y) a_H \int_{-\infty}^{\infty} dT_e K_n(T_e) n_e^2(T_e, x, y), \quad (3)$$

the symbols are the same as in Equation 1; Φ is the angle of the Wolter sector in radians. The kernel $K_n(T_e)$ is given by

$$K_n(T_e) = \sum_{Zzj} A_Z R^2(\theta) \epsilon(\lambda_{ij}) \epsilon_D(\lambda_{ij}) a_{Zz}(T_e) \alpha_{Zzj}(T_e), \quad (4)$$

$R(\theta)$ is the crystal reflectivity, $\epsilon(\lambda)$ is the telescope efficiency as defined for equation 2, and ϵ_D is the detector efficiency. The counting rates expected for post flare coronal loops are given in Table 13. The normalized functions $K_n(T_e)$ for the soft x-ray spectroheliographs are plotted in Figures 26a and b for the principal lines imaged.

9.3 **Spectroscopic Systems:** The count rates for the grating spectrographs are calculated from Equations 1 and 2 by multiplying $K_n(T_e)$ by $\epsilon_g(\lambda) \epsilon_D(\lambda) \lambda/hc$ where ϵ_g is the grating efficiency, and ϵ_D is the efficiency of the MAMA detector. The normalized temperature response $K_n(T_e)$ of the grating spectrometers for the strongest lines within the various bandpasses is given in Figures 26c-f. The anticipated count rates for the *UHRXS* spectrographs are presented in Table 10. For spectrographs α , β , and Γ , rates are given for the "chromospheric network," and for active regions. For spectrograph Δ , the rates are for active regions.

Table 13. Soft X-Ray Spectroheliograph Performance

	λ (\AA)	I ion	Plate Scales		Resolution		Solar Intensity		Count Rate	References
			μ/arcsec	milli \AA / arc-sec	$\Delta\theta$ (arc-sec)	$\Delta\lambda$ (\AA)	Post Flare Loop (a)	Post flare Loop (b)	Post flare Loop (c)	
Σ 1a	40.27	C V	12.5	0.2	2.0"	.20	700	.10	6	Doeschek and Cowan ³⁷
	44.02	Si XII					230	.05	1.5	Doeschek and Cowan ³⁷
Σ 1b	21.6	O VII	12.5	0.1	2.0"	.05	1,550	.05	3	Walker, <i>et al.</i> ³⁹
	18.97	O VIII					7,000	.02	17	Walker, <i>et al.</i> ³⁹
Σ 2a	13.44	Ne IX	12.5	0.7	2.0"	.02	1,150	.01	4	Walker, <i>et al.</i> ³⁹
	15.01	Fe XVII					8,250	.01	4	Walker, <i>et al.</i> ³⁹
Σ 3a	9.17	Mg XI	12.5	.04	2.0"	.001	780	.01	9	Walker, <i>et al.</i> ³⁹
	8.42	Mg XII					10,350	.0025	200	Walker, <i>et al.</i> ³⁹
Σ 3b	6.65	Si XIII	12.5	.03	2.0"	.0008	12,300	.0025	260	Walker, <i>et al.</i> ³⁹
	6.18	Si XIV					6,500	.0010	140	Walker, <i>et al.</i> ³⁹
Σ 2b	1.85	Fe XXV	12.5	.01	2.0"	.0002	1,500	.0002	120/600*	Feldman, <i>et al.</i> ³⁸
	1.79	Fe XXVI					300	.0002	10/500*	Mewe, <i>et al.</i> ³¹

(a) $\text{ergs/cm}^2\text{-sec-str}$; (b) fraction of disk containing emission; (c) $\text{photons/sec-(arc-sec)}^2$; * peak of Class X-1 flare.

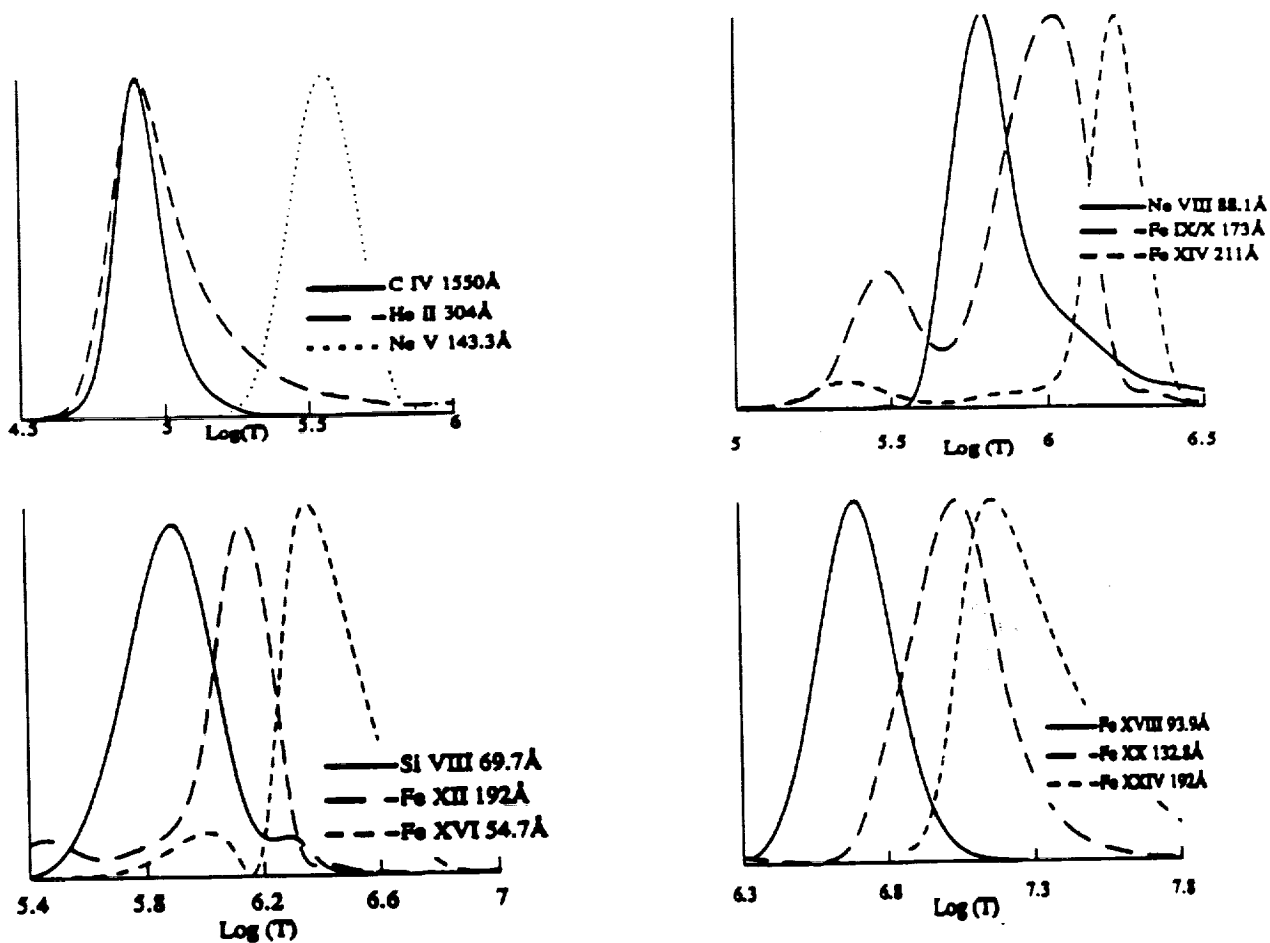


Figure 25. Calculated response of the UHRXS "Freedom" observatory imaging telescopes to the solar emissivity.

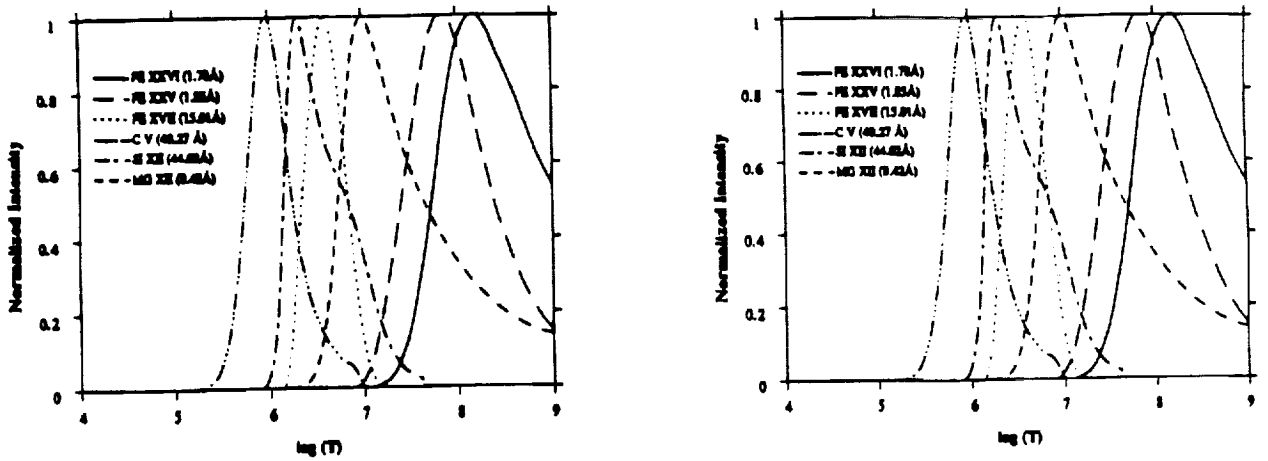


Figure 26. Temperature response of the soft x-ray spectroheliographs to the solar plasma; (a) left O VII, O VIII, Ne IX, Mg XI, Mg XII, Si XIII, Si XIV; (b) right C V, Si XII, Mg XII, Fe XVII, Fe XXV, Fe XXVI.

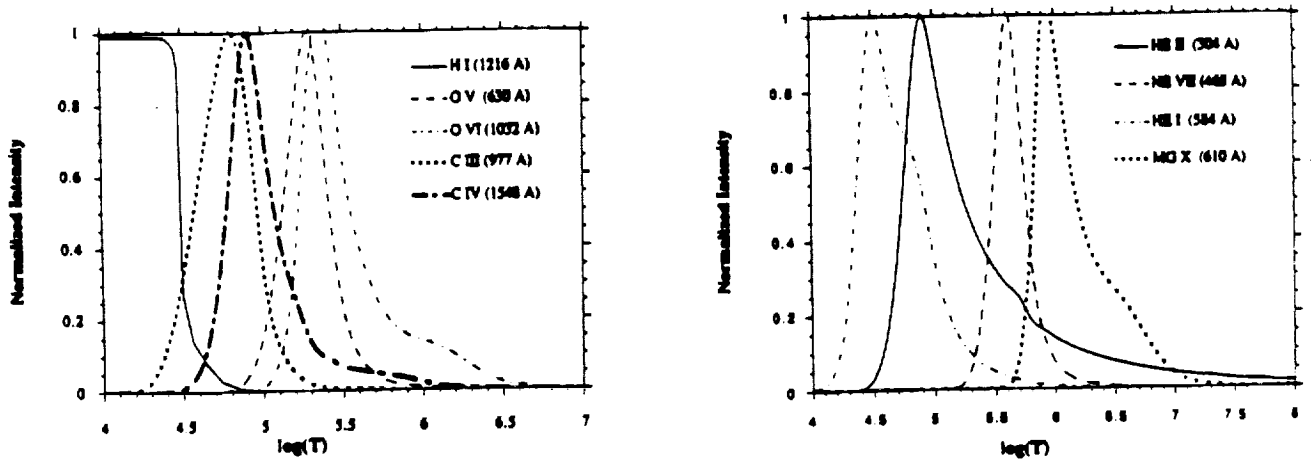


Figure 26 (cont.). Temperature response of the EUV and FUV spectrographs to the solar plasma; (c) left H I, C III, C IV, O V and O VI; (d) right He I, He II, Ne VII, and Mg X.

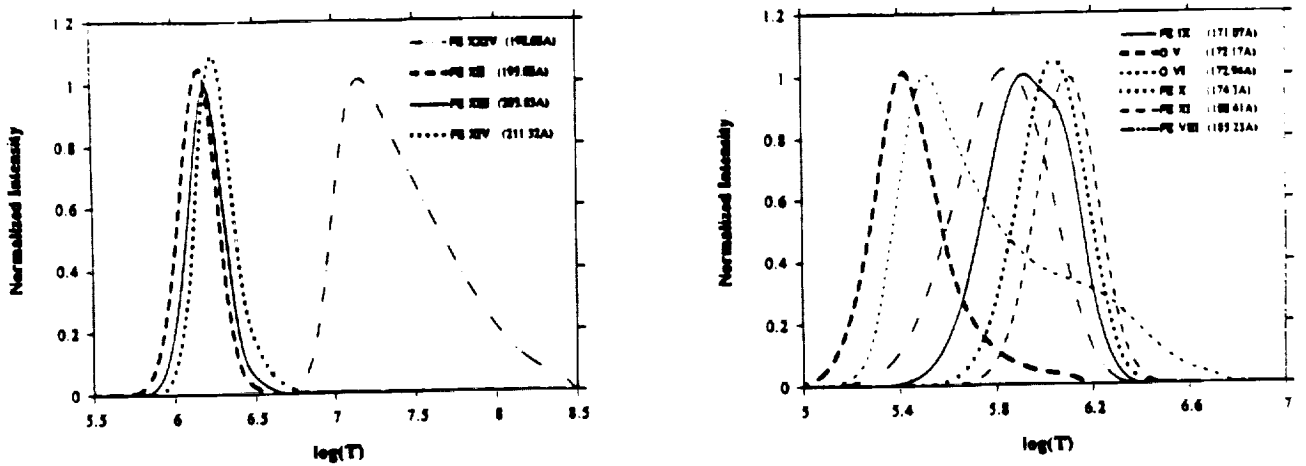


Figure 26 (cont.). Temperature response of the XUV spectrographs to the solar plasma; (e) left Fe XII, Fe XIII, Fe XIV, Fe XXIV; (f) right O V, O VI, Fe VIII, Fe IX, Fe X, Fe XI.

10.0 Environmental Effects

10.1 Thermal Control: If we are able to use thin aluminum or beryllium pre-filters for each telescope, the control of the thermal environment of the optical bench and mirrors will be greatly simplified. We plan to incorporate thermal sensors and heaters to control the temperature of each telescope. The telescopes will utilize Carbon fiber epoxy metering structures which will have a very low coefficient of thermal expansion. We anticipate that only limited use of the thermal control systems will be required to achieve our objectives.

10.2 External Environment: We are concerned about the external contamination environment. The presence of atomic oxygen, and of organic molecules are the most serious problems. *Knowledge of the external environment is a critical experiment requirement.*

10.3 Internal Environment: Prior to launch, the interior of the experiment will be maintained at a high vacuum. We plan to use thin aluminum prefilters for each of the XUV telescopes, which should limit the influx of contaminants to the vicinity of the primary and secondary mirrors. A blocking filter (Section 3.1) will provide protection for the FUV telescope. However, no prefilter design has as yet been identified for the EUV spectroscopic telescope. Each UHRXS telescope will also have a door which can be closed to protect the optical surfaces when venting or other Space Station activities that pose a contamination hazard occur. During observations, the thermal control system will maintain each telescope at elevated temperature compared to surrounding surfaces to further limit deposition of volatile contaminants. *Control of internal contamination by the careful selection of materials is a critical requirement for UHRXS.*

11.0 Preflight and Inflight Calibration: We plan to carry out a very careful pre-flight calibration program using the NIST and Stanford Synchrotron Radiation Laboratory (SSRL) photon light sources. Our calibration procedure will involve use of NIST Calibrated photodiode standard sensors. Our goal is to achieve a photometric accuracy for the photoelectrically recorded spectra over the full wavelength range of ~3%, and ~15% photometric accuracy for the photographically recorded images. Achieving these levels of accuracy is important to many of our scientific objectives. We plan to study the use of one or more of the following techniques to maintain our knowledge of instrument calibration after launch: (i) comparison of UHRXS solar data with periodic flights of our MSSTA solar rocket observatory, which has virtually identical XUV and FUV telescopes, (ii) periodic observation of a series of nearby sources such as hot white dwarfs or the Local Interstellar medium which can be assumed to have constant luminosity over periods of several years, and (iii) the inclusion of radioactive alpha sources (such as Po^{210}) which can excite fluorescent lines [such as $\text{Al L } \alpha$ (λ 171A)] within the band pass of selected telescopes.

12.0 Pointing Accuracy and Stability: The pointing accuracy and stability required for the UHRXS observations will be provided by a control loop consisting of the Lockheed SPARCS solar sensor, and the Active Mirror Servo of each Ritchey-Chrétien secondary (or deep parabolic primary) mirror. This system has already demonstrated a stability of 0.08 arc-second. We also plan to develop a correlation tracking signal based on the H Ly- α image from the Far Ultraviolet Telescope. The resolution of this image is limited to 0.5 arc-sec by the pixel size of the MAMA detector, which corresponds to an image element of 0.25 arc-seconds. However, Morgan, *et al.*⁴⁰ have shown that if the centroid of a pattern is sought, the resolution of the MAMA detector is at least 0.04 pixel. Therefore, we may, by comparison of successive images, determine the motion of the image to an accuracy of 0.01-0.02 arc-seconds. We plan to utilize the correlation error signal derived to further improve the stability of our images.

13.0 Ground Operations: Ball Aerospace will develop a GSE unit, which will be used to operate the UHRXS during testing and calibration. The GSE will be controlled by a sophisticated microprocessor such as the Micro-Vax or Sun 3. After launch, the GSE will be transferred to CSSA/Stanford, and used as the central element in the UHRXS Operations Control and Data Analysis Facility. We will fabricate a shipping container which will have several functions in addition to transportation, including vacuum storage or storage in an ultra clean atmosphere.

14.0 Launch Enclosure: We will develop a launch enclosure for the UHRXS which will interface with the Shuttle.

15.0 Flight Operations: We will establish flight operations centers at both CSSA/Stanford and SSL/MSFC. Commands will be generated and transmitted to GSFC from the MSFC Operations Center, and Data received from GSFC at MSFC. Data will be distributed to the PI, Co I's, and Associated Scientists from the MSFC Operations Center. It is highly desirable that the H Ly α image which is displayed in the Space Station Console be available in real time on the ground, so that real time control of observations is possible. The command structure requirements of the UHRXS are quite modest; consisting of commands to (i) select the UV spectrograph to be read out by the decode unit, (ii) specify the

MAMA array size to be read out, (iii) select the location (on the sun) to which the PPS is to be pointed, (iv) command AMS rasters to obtain 4' x 4' Grating Spectroheliograms, and (v) select exposure times and command image recording for the 11 *UHRXS* cameras.

An integral component of the *UHRXS* investigation is a program of collaborative ground based observations and analysis which will provide critical magnetic field and coronal data. The magnetic field observations will be carried out by Dr. Mona Hagyard with the MSFC Vector Magnetograph, and analyzed using the computer codes developed by Professor S. T. Wu of the University of Alabama, Huntsville. The coronal observations will be carried out by Dr. David Sime using the High Altitude Observatory's Coronal Station on Mauna Loa.

16.0 Observing Programs, Data Reduction and Analysis

The *UHRXS* Science Team: The team that will develop the observing program, carry out observations, and analyze these observations, will consist of the PI and Co-I's, the Project Scientist, the Associated Scientists, and post-doctoral scholars and students who will work with them. Dr. E. Tandberg-Hanssen will chair the meetings of the Associated Scientists and Investigators, and will insure that the Associated Scientists are prepared to utilize the *UHRXS* observations. The Associated Scientists, and Investigators will form teams to address each of the major scientific objectives that we have identified for the *UHRXS* program. Each team will be led by one of the Investigators or Associated Scientists; members of the *UHRXS* Consortium will work with the various teams according to their specific interests and scientific objectives. Each team will develop an observing plan, and a plan for the analysis of the resulting observations. The teams that we have identified, and the team leaders are:

- | | | |
|---------------------------------|---------------------|-----------------------------------|
| • Chromospheric Fine Structure: | R.L. Moore | SSL/MSFC |
| • Solar Prominences: | E. Tandberg-Hanssen | SSL/MSFC |
| • Solar Flares: | P.A. Sturrock | CSSA/Stanford University |
| • Solar Active Regions: | S.K. Antiochos | Naval Research Laboratory |
| • Solar Magnetic Fields: | M.J. Hagyard | SSL/MSFC |
| • Large Scale Solar Structure: | S.T. Wu | University of Alabama, Huntsville |
| • Solar Wind/Corona Interface | D. Sime | High Altitude Observatory |

Data Handling and Archiving: Assuming a modest data rate of 300 photographic images per telescope per day we can anticipate ~1,000,000 high resolution images in a year of operation. We can also anticipate ~10⁷ or more photoelectrically recorded images. These observations will constitute a unique resource for solar physics. We plan to establish data archives for the *UHRXS* observations at both Stanford and MSFC, which will be made available to interested scientists.

Guest Investigations with *UHRXS*: Scientists who are not part of the *UHRXS* team will be invited to become Guest Observers by joining with one or more of the Science Teams defined above.

Analysis of *UHRXS* Observations: The *UHRXS* provides unprecedented tools for the analytical study of the solar atmosphere. The power of the *UHRXS* imaging telescopes is due to a unique combination of ultra-high angular resolution (~ 0.10 arc-second), spectral resolution sufficient to isolate a single line multiplet, and complete thermal coverage (10,000 K - 30,000,000 K). This capability is complemented by high resolution spectra which in most cases permit the observation of line profiles, and which have angular resolution sufficiently high (0.5 arc-sec - 2.0 arc-sec) to isolate very small structures on the sun. The coverage of the isoelectronic sequences of the most abundant elements (Figure 27), is quite complete. We summarize the powerful analytical techniques which can be used to address fundamental problems using *UHRXS* observations, below.

Analysis of Thermal Structure and Abundances: The broad temperature coverage of the *UHRXS*, coupled with full coverage of the isoelectronic sequences of C, O, and Fe in particular suggests that *UHRXS* will allow the analysis of thermal structure and abundances with unprecedented clarity and precision. Walker⁴¹, Walker *et al.*,³⁹ and Allen *et al.*⁴² describe the techniques used in these analyses.

Density Sensitive Line Ratios: Walker⁴¹ has discussed density sensitive line ratios in the wavelength interval ~ 1.5 - 100 Å in He-like, Be-like and Ne-like ions, and Munro *et al.*⁴³ have described density sensitive line ratios between 100 and 2000 Å. An example of a line ratio accessible to *UHRXS* which should prove especially useful is the

C V ($2^3S - 1^1S/2^1P - 1^1S$) ratio which is sensitive to densities in the range $5 \times 10^8 - 2 \times 10^{11} \text{ cm}^{-3}$. Density sensitive line ratios in O VII, Ne IX, Mg XI, Si XIII, Fe XXV, C III, O V and Ne VII will be accessible to UHRXS.

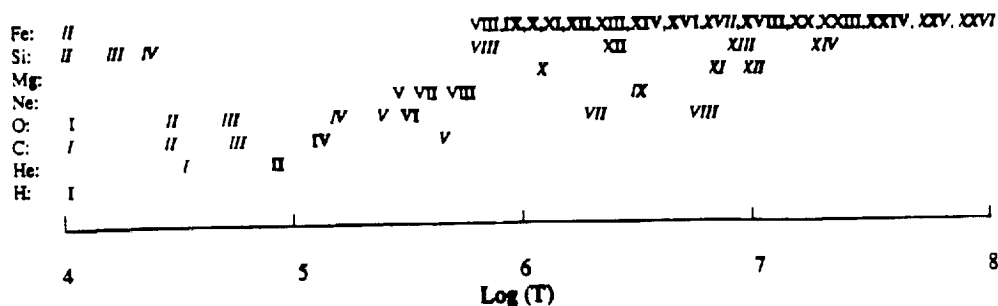


Figure 27. Coverage of the isoelectronic sequences of H, He, C, O, Ne, Mg, Si and Fe. An entry in roman type indicates high resolution images only, *italics indicate spectroheliograms only*, and bold face indicates both.

Temperature Sensitive Line Ratios: Malinovsky and Heroux³⁴ have shown that the intensity ratio of lines of a single ion which differ significantly in the excitation potential of the upper level, such as O VI $2s^1S - 2p^1P$ (λ 1032 Å) and $2p^1P - 3d^1D$ (λ 172.9 Å) are sensitive to temperature. Gabriel⁴⁴ has pointed out that the relative intensity of certain dielectronic recombination satellite lines and their nearby resonance lines varies as T^{-1} , providing a powerful temperature diagnostic for ions such as Mg XI, Si XIII, and Fe XXV, which are accessible to UHRXS.

Lines Sensitive to Non-Equilibrium Conditions: Gabriel⁴⁴ describes the effect of departures from equilibrium between electron and ionization temperature on the ratios of non-autoionizing satellite lines and their nearby resonance lines. Such line ratios in Si XIII and Fe XXV will be important for the analysis of flare generated plasmas.

Line Profiles: The UHRXS grating spectrographs and the soft x-ray spectroheliographs have resolution, $\lambda/\Delta\lambda$ in the range $\sim 8000 - 30,000$, sufficient to measure the profiles of chromospheric and coronal lines. This capability will allow the study of macroscopic motions which have been observed in the chromosphere⁴⁵ and during flares.⁴⁶

Summary: The UHRXS represents a uniquely powerful combination of high angular resolution imaging and diagnostic capability which can address directly the physical processes which control the generation and transport of energy and the flow of mass in the solar atmosphere.

17.0 Utilization of the UHRXS on Space Station: Because of its comprehensive nature, the UHRXS will provide a unique resource for solar observations from space, which cannot be duplicated by any presently approved solar mission, including SOHO and OSL. Indeed, UHRXS will be highly complementary to OSL. Accordingly, we hope that UHRXS can be utilized at as high a duty cycle as possible. The central goal of the long range plan for solar observing facilities is the development of an Advanced Solar Observatory (Walker *et al.*⁴⁷) which is planned as a long duration comprehensive space station based solar observatory with capabilities which will extend beyond those of UHRXS. We hope that UHRXS will be able to make observations from "Freedom" until the ASO can be deployed.

18.0 Future Evolution of UHRXS: The UHRXS instrument can be improved in three specific areas:

- replacement of the baselined MAMA $1000 \times 1000 - 12\mu$ pixel arrays with arrays which have higher resolution and a larger format (see, for example, Figure 22).
- the addition of the capability to measure the polarization of H Ly α radiation in the corona, which will allow the direct measurement of coronal magnetic fields.⁴⁸
- development of a far-ultraviolet Michelson interferometer to allow high resolution wide field spectroheliograms to be obtained at H Ly α and C IV.
- incorporation of an improved soft x-ray spectrograph which will allow six simultaneous channels of spectroscopic data rather than six channels time multiplexed on a single channel.

III. PRELIMINARY WORK BREAKDOWN STRUCTURE

A preliminary Work Breakdown Structure for *UHRXS*, with the anticipated responsibilities designated by organization, is given below. Prime responsibility is indicated by boldface type.

- | | | |
|------------|---|--------------------------------|
| 1.0 | Program Development and Control | <i>Stanford/Ball/MSFC/LLNL</i> |
| 1.1 | Program Management | |
| 1.2 | Fiscal Management | |
| 1.3 | Planning and Scheduling | |
| 1.4 | Project Meetings & Reviews | |
| 1.5 | Travel | |
| 1.6 | Configuration and Data Management | |
| 1.7 | Documentation | |
| 1.8 | Subcontract Administration | |
| 2.0 | Systems Engineering | |
| 2.1 | Image Quality Assessment | |
| 2.1.1 | Error Budgets | <i>Stanford/MSFC/Ball</i> |
| i. | Optical Aberrations | |
| ii. | Thermal and Structural Distortions | |
| iii. | Spacecraft Jitter | |
| iv. | Film and Detector Resolution | |
| v. | Target Motion | |
| vi. | Tracking Errors | |
| 2.1.2 | Experiment Pointing and Aspect | <i>Ball/Stanford/MSFC</i> |
| i. | Solar Aspect Sensors | |
| ii. | Correlation Tracking | |
| iii. | Active Mirror Servo Control | |
| iv. | Roll Stability | |
| v. | Non-Solar Aspect Sensors | |
| 2.2 | Optical Design | <i>MSFC/Stanford</i> |
| 2.2.1 | Ray Trace Analysis | |
| 2.2.2 | Error Assessment | |
| i. | Focus | |
| ii. | Mirror Tilt | |
| 2.3 | Electronic System Analysis | |
| 2.3.1 | Electronic Top Level Configuration Design | <i>Ball/Stanford</i> |
| 2.3.2 | Software Analysis | <i>Ball/Stanford</i> |
| i. | Data Compression and T/M Formatting | |
| 2.3.3 | Electronic GSE | <i>Ball/Stanford</i> |
| 2.4 | Mechanical Systems Analysis | <i>Stanford/MSFC</i> |
| 2.4.1 | Mechanical Top Level Configuration Design | |
| i. | External Architecture | |
| ii. | Internal Architecture | |
| 2.4.2 | Mechanisms | |

- 2.5 Film Analysis *MSFC*
 - 2.5.1 Film Type Selection
 - 2.5.2 Film Storage and Handling Procedures
 - 2.5.3 Film Testing and Calibration
 - 2.5.4 Film Development Procedures

- 2.6 Electronic Detector Analysis *Ball/Stanford*
 - 2.6.1 MAMA Array and Pixel Format Specification
 - 2.6.2 MAMA Multi-channel Plates Specification
 - 2.6.3 MAMA Anode Specification

- 2.7 Modeling and Analysis
 - 2.7.1 Thermal *Ball*
 - 2.7.2 Structural *Ball*
 - 2.7.3 Dynamic *Ball*
 - 2.7.4 Environmental (contamination) modeling *MSFC*

- 2.8 Calibration Analysis
 - 2.8.1 Pre-launch *MSFC*
 - 2.8.2 Post-launch *Stanford*

- 2.9 Interface Control
 - 2.9.1 Robotics Interface, Film Supply and Retrieval *MSFC/Contractor TBD*
 - i. Film Cassette Design
 - ii. Film Transport Enclosure
 - 2.9.2 Experiment/Pointer Interface *Ball/Stanford*
 - i. Electrical
 - ii. Mechanical/Thermal

- 2.10 Performance Assurance *Ball/MSFC*
 - 2.10.1 Performance, Verification and Test Plan
 - 2.10.2 Stress Analysis
 - 2.10.3 Hazardous Materials
 - i. Chemicals
 - ii. Radioactive Sources
 - iii. Pyrotechnics
 - 2.10.4 Failure Model and Effects Analysis
 - 2.10.5 Traceability of Materials
 - 2.10.6 Reliability

- 2.11 Transportation *MSFC*

- 3.0 Engineering Model
 - 3.1 Mechanical Envelope and Optical Bench *Stanford/MSFC/Ball*
 - 3.1.1 External architecture
 - i. Vacuum enclosure
 - ii. Number and control of aperture doors
 - 3.1.2 Internal Architecture
 - i. Placement of telescopes and spectrographs
 - ii. Placement and access to cameras
 - iii. Placement of electronics
 - 3.1.3 Control of internal environment
 - i. Material selection and outgassing
 - ii. Control of gas exchange between experiment interior and exterior
 - iii. Definitions of external environment

- iv. Effect of environment on critical components
 - α. mirrors
 - β. filters
 - v. Control of contamination during manufacture, processing and shipment
 - 3.1.4 Thermal control
 - 3.1.5 Interface with Shuttle Launch Enclosure
 - 3.1.6 Interface with pointer and Space Station
 - i. Mechanical
 - ii. Thermal
 - 3.1.7 Fabrication
 - 3.2 Optical Systems
 - 3.2.1 XUV Ritchey-Chrétien Telescopes
 - i. Optical design *MSFC*
 - α. Ray trace analysis and error budget
 - β. Effects of variations in mirror separation
 - γ. Effects of tilt of secondary mirror
 - ii. Telescope mirror blanks *MSFC/Stanford*
 - α. Material selection
 - β. Specification of figure and finish
 - γ. Measurement of figure and finish
 - δ. Blank thickness and internal structure
 - ε. Handling procedures for mirror blanks
 - iii. Multilayer coatings *LLNL/Stanford*
 - α. Analytical design
 - β. Analysis of response to solar spectrum
 - γ. Fabrication
 - δ. Handling procedures
 - ε. Performance testing
 - ζ. Assessment of contamination and aging problems
 - iv. Optical bench and mirror cells *Stanford/MSFC/Ball*
 - α. Material selection
 - β. Design
 - γ. Metrology
 - δ. Thermal control
 - ε. Fabrication
 - v. Filters *Stanford*
 - α. Placement of filters
 - β. Use of pre-filters
 - γ. Design of filters
 - δ. Thermal analyses
 - a. sunlight rejection
 - b. effect of particulate and gas environments
 - ε. Analysis of response to solar spectrum
 - ζ. Fabrication of filters
 - η. Handling of filters
 - θ. Mounting of filters
 - vi. Active mirror servo *Ball/Stanford*
 - α. Design
 - β. Control
 - γ. Assembly
 - δ. Integration into secondary mirror cell
 - vii. Active focus measurement and control *Stanford/MSFC*
 - α. Selection of actuators
 - β. Mounting of actuators
 - viii. Telescope assembly and testing *MSFC/Stanford*
 - α. Telescope assembly procedure
 - β. Handling of assembled telescopes

- γ. Optical testing
 - δ. X ray/ XUV/ FUV testing
 - ε. Thermal testing
 - ζ. Analyses of response of telescopes to solar spectrum
 - η. Vacuum testing
- 3.2.2 Soft X-Ray Herschellian Telescopes
 - i. Optical design *MSFC*
 - α. Ray trace analysis and error budget
 - β. Effects of variations in minor focal plane separation
 - ii. Telescope mirror blanks *MSFC/Stanford*
 - α. Material selection
 - β. Specification of figure and finish
 - γ. Measurement of figure and finish
 - δ. Blank thickness and interval structure
 - ε. Handling procedures for mirror blanks
 - iii. Multilayer coating *LLNL/Stanford*
 - α. Analytical design
 - β. Analysis of response to solar spectrum
 - γ. Fabrication
 - δ. Handling procedures
 - ε. Performance testing
 - ζ. Assessment of contamination and aging problems
 - iv. Optical bench and mirror cells *Stanford/MSFC/Ball*
 - α. Material selection
 - β. Design
 - γ. Metrology
 - δ. Thermal control
 - ε. Fabrication
 - v. Filters *Stanford*
 - α. Placement of filters
 - β. Use of prefilters
 - γ. Design of filters
 - δ. Thermal analyses
 - a. sunlight rejection
 - b. effect of particulate and gas environments
 - ε. Analysis of response to solar spectrum
 - ζ. Fabrication of filters
 - η. Handling of filters
 - θ. Mounting of filters
 - vi. Active mirror servo *Ball/Stanford*
 - α. Design
 - β. Control
 - γ. Assembly
 - δ. Integration into secondary mirror cell
 - vii. Active focus measurement and control *Stanford/MSFC/Ball*
 - α. Selection of actuators
 - β. Mounting of actuators
 - viii. Telescope assembly and testing *MSFC/Stanford*
 - α. Telescope assembly procedure
 - β. Handling of assembled telescopes
 - γ. Optical testing
 - δ. X-ray/XUV/FUV testing
 - ε. Thermal testing
 - ζ. Analyses of response of telescopes to solar spectrum
- 3.3 Spectroscopic Systems
 - 3.3.1 XUV Grating Spectrographs
 - i. Richey-Chréien telescopes *MSFC/Stanford/LLNL/Ball*

- α. Optical design
 - β. Mirror blanks
 - γ. Reflective coating
 - δ. Optical bench and mirror cells
 - ε. Filters
 - ζ. Active mirror servo
 - η. Active focus control
 - θ. Telescope assembly and testing
 - ii. Grating spectrograph *Stanford/MSFC/Ball*
 - α. Optical design
 - β. Mechanical design
 - γ. Fabrication
 - iii. Slits *Stanford/MSFC*
 - iv. Gratings *LLNL/Stanford/MSFC*
 - α. Material selection
 - β. Specification of figure and finish
 - γ. Grating blank fabrication technology
 - δ. Grating ruling
 - ε. Multilayer coating for gratings
- 3.3.2 EUV Grating Spectrograph
 - i. Ritchey-Chrétien telescope *MSFC/Stanford/LLNL*
 - α. Optical design
 - β. Mirror design
 - γ. Reflective coating
 - δ. Optical bench and mirror cells
 - ε. Filters
 - ζ. Active mirror servo?
 - η. Active focus control
 - θ. Telescope assembly and testing
 - ii. Grating spectrograph *Stanford/MSFC/Ball*
 - α. Optical design
 - β. Mechanical design
 - γ. Fabrication
 - iii. Slits *Stanford/MSFC*
 - iv. Gratings *Stanford/LLNL/MSFC*
 - α. Material selection
 - β. Specification of figure and finish
 - γ. Grating blank fabrication technology
 - δ. Grating ruling
 - ε. Reflective coating
- 3.3.3 FUV Telescope and Spectrograph
 - i. Ritchey-Chrétien telescope *MSFC/Stanford/LLNL/Ball*
 - α. Optical design
 - β. Mirror blanks
 - γ. Reflective coating
 - δ. Optical bench and mirror cells
 - ε. Ultraviolet filters
 - ζ. Active mirror servo
 - η. Active focus control
 - θ. FUV beam splitter
 - ι. Telescope assembly and testing
 - ii. FUV filters *MSFC*
 - iii. Grating spectrograph *Stanford/MSFC/Ball*
 - α. Optical design
 - β. Mechanical design
 - γ. Fabrication
 - iv. Slits *Stanford/MSFC*

- v. Gratings *Stanford/MSFC/LLNL*
 - α. Material selection
 - β. Specification of figure and finish
 - γ. Grating blank fabrication technology
 - δ. Grating ruling
 - ε. Reflective coating

- 3.3.4 Soft X-Ray Spectrograph *Stanford/MSFC/LLNL*
 - i. Wolter Telescope *Stanford/MSFC/LLNL*
 - α. Optical design
 - β. Mirror blanks
 - γ. Reflective coating
 - δ. Optical bench and mirror cells
 - ε. X-ray filters
 - ζ. Active focus control
 - η. Telescope assembly and testing
 - ii. Objective double crystal spectrograph *Stanford/MSFC/Ball*
 - α. Crystal selection
 - β. Crystal preparation and testing
 - γ. Mechanical design
 - δ. Bragg scan drive
 - ε. Fabrication
 - iii. Wolter Cassegrain multilayer mirrors *Stanford/LLNL/MSFC*
 - α. Optical design
 - β. Mirror blanks
 - γ. Multilayer coatings
 - δ. Mechanical design

- 3.4 Film Cameras *MSFC*
 - 3.4.1 Camera Design *MSFC*
 - i. Shutter
 - ii. Film transport
 - iii. Film capacity
 - 3.4.2 Image identification system *MSFC*
 - 3.4.3 Sensing of focal plane *MSFC/Stanford*
 - 3.4.4 Camera fabrication *MSFC/Contractor TBD*
 - i. Selection of materials
 - ii. Selection of film advance motors
 - 3.4.5 Camera handling procedures *MSFC*
 - 3.4.6 Camera testing *MSFC*

- 3.5 MAMA Detectors *Ball/Stanford*
 - 3.5.1 Specification of array and pixel formats
 - 3.5.2 Selection of multi-channel plates
 - 3.5.3 Specification and design of anodes
 - 3.5.4 Fabrication of detector arrays
 - 3.5.5 Testing of detector arrays
 - 3.5.6 Detector vacuum enclosures
 - 3.5.7 Detector calibration

- 3.6 Electronics *Ball/Stanford*
 - 3.6.1 Central processor
 - i. Microprocessor
 - ii. Memory
 - 3.6.2 Experiment control
 - i. Telescope focus

- ii. Active mirror servos
- iii. Spectrometers
- iv. Camera shutter
- v. Mechanisms
- vi. Position sensors
- vii. Heaters
- viii. Temperature sensors
- ix. High Voltage
- x. Low Voltage
- xi. Vacuum enclosures
- xii. Doors
- 3.6.3 MAMA decode logic
- 3.6.4 MAMA tracking logic
- 3.6.5 Data storage and retrieval
- 3.6.6 Experiment/pointer interface
- 3.6.7 Command interface
- 3.6.8 Telemetry interface
- 3.6.9 Experiment mode and observational sequence control
- 3.6.10 Power system interface
- 3.7 Software
 - 3.7.1 Data Compression and T/M Formatting *Stanford/Ball/MSFC*
 - 3.7.2 Experiment Microprocessor
 - 3.7.3 Observing Mode Control
 - 3.7.4 Housekeeping
- 3.8 Experiment Mechanisms *Stanford/Ball/MSFC*
 - 3.8.1 External Doors
 - 3.8.2 MAMA vacuum doors
 - 3.8.3 EUV, FUV, XUV and soft x-ray spectrometer wavelength scans
 - 3.8.4 Objective Bragg crystal wavelength scan
 - 3.8.5 Active mirror servos
 - 3.8.6 Telescope focus sensing and control
- 3.9 Experiment Calibration
 - 3.9.1 Pre-launch Calibration
 - 3.9.2 In-flight calibration
 - 3.9.3 Calibration Rocket Flights
- 3.10 Experiment Launch Enclosure *Stanford/MSFC/Ball*
- 4.0 Flight Unit
 - 4.1 Mechanical Envelope and Optical Bench *Stanford/MSFC/Ball*
 - 4.1.1 External architecture
 - i. Vacuum enclosure
 - ii. Number and control of aperture doors
 - 4.1.2 Internal Architecture
 - i. Placement of telescopes and spectrographs
 - ii. Placement and access to cameras
 - iii. Placement of electronics
 - 4.1.3 Control of internal environment
 - i. Material selection and outgassing
 - ii. Control of gas exchange between experiment interior and exterior
 - iii. Definitions of external environment
 - iv. Effect of environment on critical components
 - α. mirrors
 - β. filters
 - v. Control of contamination during manufacture, processing and shipment

- 4.1.4 Thermal control
- 4.1.5 Interface with Shuttle Launch Enclosure
- 4.1.6 Interface with pointer and Space Station
 - i. Mechanical
 - ii. Thermal
- 4.1.7 Fabrication
- 4.2 Optical Systems
 - 4.2.1 XUV Ritchey-Chrétien Telescopes
 - i. Optical design *MSFC*
 - α. Ray trace analysis and error budget
 - β. Effects of variations in mirror separation
 - γ. Effects of tilt of secondary mirror
 - ii. Telescope mirror blanks *MSFC/Stanford*
 - α. Material selection
 - β. Specification of figure and finish
 - γ. Measurement of figure and finish
 - δ. Blank thickness and internal structure
 - ε. Handling procedures for mirror blanks
 - iii. Multilayer coatings *LLNL/Stanford*
 - α. Analytical design
 - β. Analysis of response to solar spectrum
 - γ. Fabrication
 - δ. Handling procedures
 - ε. Performance testing
 - ζ. Assessment of contamination and aging problems
 - iv. Optical bench and mirror cells *Stanford/MSFC/Ball*
 - α. Material selection
 - β. Design
 - γ. Metrology
 - δ. Thermal control
 - ε. Fabrication
 - v. Filters *Stanford*
 - α. Placement of filters
 - β. Use of pre-filters
 - γ. Design of filters
 - δ. Thermal analyses
 - a. sunlight rejection
 - b. effect of particulate and gas environments
 - ε. Analysis of response to solar spectrum
 - ζ. Fabrication of filters
 - η. Handling of filters
 - θ. Mounting of filters
 - vi. Active mirror servo *Ball/Stanford*
 - α. Design
 - β. Control
 - γ. Assembly
 - δ. Integration into secondary mirror cell
 - vii. Active focus measurement and control *Stanford/MSFC*
 - α. Selection of actuators
 - β. Mounting of actuators
 - viii. Telescope assembly and testing *MSFC/Stanford*
 - α. Telescope assembly procedure
 - β. Handling of assembled telescopes
 - γ. Optical testing
 - δ. X ray/ XUV/ FUV testing
 - ε. Thermal testing
 - ζ. Analyses of response of telescopes to solar spectrum

- η. Vacuum testing
 - 4.2.2 Soft X-Ray Herschelien Telescopes
 - i. Optical design *MSFC*
 - α. Ray trace analysis and error budget
 - β. Effects of variations in minor focal plane separation
 - ii. Telescope mirror blanks *MSFC/Stanford*
 - α. Material selection
 - β. Specification of figure and finish
 - γ. Measurement of figure and finish
 - δ. Blank thickness and interval structure
 - ε. Handling procedures for mirror blanks
 - iii. Multilayer coating *LLNL/Stanford*
 - α. Analytical design
 - β. Analysis of response to solar spectrum
 - γ. Fabrication
 - δ. Handling procedures
 - ε. Performance testing
 - ζ. Assessment of contamination and aging problems
 - iv. Optical bench and mirror cells *Stanford/MSFC/Ball*
 - α. Material selection
 - β. Design
 - γ. Metrology
 - δ. Thermal control
 - ε. Fabrication
 - v. Filters *Stanford*
 - α. Placement of filters
 - β. Use of prefilters
 - γ. Design of filters
 - δ. Thermal analyses
 - α. sunlight rejection
 - β. effect of particulate and gas environments
 - ε. Analysis of response to solar spectrum
 - ζ. Fabrication of filters
 - η. Handling of filters
 - θ. Mounting of filters
 - vi. Active mirror servo *Ball/Stanford*
 - α. Design
 - β. Control
 - γ. Assembly
 - δ. Integration into secondary mirror cell
 - vii. Active focus measurement and control *Stanford/MSFC/Ball*
 - α. Selection of actuators
 - β. Mounting of actuators
 - viii. Telescope assembly and testing *MSFC/Stanford*
 - α. Telescope assembly procedure
 - β. Handling of assembled telescopes
 - γ. Optical testing
 - δ. X-ray/XUV/FUV testing
 - ε. Thermal testing
 - ζ. Analyses of response of telescopes to solar spectrum
- 4.3 Spectroscopic Systems
 - 4.3.1 XUV Grating Spectrographs
 - i. Ritchey-Chrétien telescopes *MSFC/Stanford/LLNL/Ball*
 - α. Optical design
 - β. Mirror blanks
 - γ. Reflective coating
 - δ. Optical bench and mirror cells

- ε. Filters
 - ζ. Active mirror servo
 - η. Active focus control
 - θ. Telescope assembly and testing
 - ii. Grating spectrograph *Stanford/MSFC/Ball*
 - α. Optical design
 - β. Mechanical design
 - γ. Fabrication
 - iii. Slits *Stanford/MSFC*
 - iv. Gratings *LLNL/Stanford/MSFC*
 - α. Material selection
 - β. Specification of figure and finish
 - γ. Grating blank fabrication technology
 - δ. Grating ruling
 - ε. Multilayer coating for gratings
- 4.3.2 EUV Grating Spectrograph
 - i. Ritchey-Chrétien telescope *MSFC/Stanford/LLNL*
 - α. Optical design
 - β. Mirror design
 - γ. Reflective coating
 - δ. Optical bench and mirror cells
 - ε. Filters
 - ζ. Active mirror servo?
 - η. Active focus control
 - θ. Telescope assembly and testing
 - ii. Grating spectrograph *Stanford/MSFC/Ball*
 - α. Optical design
 - β. Mechanical design
 - γ. Fabrication
 - iii. Slits *Stanford/MSFC*
 - iv. Gratings *Stanford/LLNL/MSFC*
 - α. Material selection
 - β. Specification of figure and finish
 - γ. Grating blank fabrication technology
 - δ. Grating ruling
 - ε. Reflective coating
- 4.3.3 FUV Telescope and Spectrograph
 - i. Ritchey-Chrétien telescope *MSFC/Stanford/LLNL/Ball*
 - α. Optical design
 - β. Mirror blanks
 - γ. Reflective coating
 - δ. Optical bench and mirror cells
 - ε. Ultraviolet filters
 - ζ. Active mirror servo
 - η. Active focus control
 - θ. FUV beam splitter
 - ι. Telescope assembly and testing
 - ii. FUV filters *MSFC*
 - iii. Grating spectrograph *Stanford/MSFC/Ball*
 - α. Optical design
 - β. Mechanical design
 - γ. Fabrication
 - iv. Slits *Stanford/MSFC*
 - v. Gratings *Stanford/MSFC/LLNL*
 - α. Material selection
 - β. Specification of figure and finish
 - γ. Grating blank fabrication technology

- viii. Temperature sensors
 - ix. High Voltage
 - x. Low Voltage
 - xi. Vacuum enclosures
 - xii. Doors
- 4.6.3 MAMA decode logic
- 4.6.4 MAMA tracking logic
- 4.6.5 Data storage and retrieval
- 4.6.6 Experiment/pointer interface
- 4.6.7 Command interface
- 4.6.8 Telemetry interface
- 4.6.9 Experiment mode and observational sequence control
- 4.6.10 Power system interface
- 4.7 Software
 - 4.7.1 Data Compression and T/M Formatting *Stanford/Ball/MSFC*
 - 4.7.2 Experiment Microprocessor
 - 4.7.3 Observing Mode Control
 - 4.7.4 Housekeeping
- 4.8 Experiment Mechanisms *Stanford/Ball/MSFC*
 - 4.8.1 External Doors
 - 4.8.2 MAMA vacuum doors
 - 4.8.3 EUV, FUV, XUV and soft x-ray spectrometer wavelength scans
 - 4.8.4 Objective Bragg crystal wavelength scan
 - 4.8.5 Active mirror servos
 - 4.8.6 Telescope focus sensing and control
- 4.9 Experiment Calibration *Stanford/MSFC*
 - 4.9.1 Pre-launch Calibration
 - 4.9.2 In-flight calibration
 - 4.9.3 Calibration Rocket Flights
- 4.10 Experiment Launch Enclosure *Stanford/MSFC/Ball*
- 5.0 Ground Support Equipment (GSE) *Ball/Stanford/MSFC*
 - 5.1 Bench Checkout Unit
 - 5.2 Space Station Simulator
 - 5.3 Instrument Simulator
 - 5.4 Electrical
 - 5.5 Mechanical
 - 5.6 Optical
 - 5.7 Software
 - 5.8 Characterization/Calibration Equipment
 - 5.9 Shipping Container
- 6.0 Flight Operations *Stanford/MSFC*
 - 6.1 Inflight Calibration

6.2 Calibration Rocket Flights

6.3 Observational Programs

7.0 Data Handling and Analysis

Stanford/MSFC

7.1 Microdensitometer analysis of film data

7.2 Analysis of digital data

7.3 Data archiving

7.3.1 Film data archive

7.3.2 Electronic data archive

8.0 Science Programs

Stanford/MSFC

8.1 Chromospheric Fine Structure

8.2 Solar Prominences

8.3 Solar Flares

8.4 Solar Active Regions

8.5 Solar Magnetic Fields

8.6 Large Scale Solar Structure

8.7 Corona/Solar Wind Interface

9.0 The UHRXS Organization and the Work Breakdown Structure: The key to the effective utilization of the Work Breakdown Structure described in sections III:1.0 - 8.0 is the control and coordination of the activities of the 4 organizations which will have primary responsibility for the development of the UHRXS instrument; CSSA/Stanford, MSFC, LLNL, and Ball Aerospace. The organizational structure, and the responsibilities of the various organizations are described in section IV.

IV. The *UHRXS* Program

1.0 *UHRXS* Development Approach: The Ultra High Resolution Soft X-Ray/XUV/UV Spectroheliograph (*UHRXS*) will be developed for flight on the Space Station by a small team of investigators, led by Professor A.B.C. Walker, Jr., who will serve as Principal Investigator (PI) and Mr. Richard B. Hoover, who will serve as Co-Investigator (Co-I) and Principal Scientist (PS). The science team will include three senior Co-Investigators, (T.W. Barbee, Jr., E. Tandberg-Hanssen, and J.G. Timothy), and Project Scientists at MSFC and Stanford. The design of the *UHRXS* instrument is based on the successful rocket instruments developed by the Principal Investigator, the Principal Scientist, one of the senior co-investigators (Troy W. Barbee, Jr.) and the Stanford Project Scientist (Joakim F. Lindblom). The *UHRXS* Grating Spectrographs will utilize the MAMA (Multinode multichannel array) detector developed by a second senior Co-Investigator (J. Gethyn Timothy) in collaboration with R. Bybee of Ball Aerospace. A third senior Co-Investigator (Einar Tandberg-Hanssen) will be responsible for coordinating the activities of a distinguished group of Associated Scientists, who will participate in the analysis of the *UHRXS* data. During the development of the *UHRXS* instrument, the Associated Scientists will meet periodically to follow the progress of the instrument development, to discuss strategies for the operation of the *UHRXS* after launch, and will offer advice as appropriate, but will have no direct role in the Instrument Development.

The expertise necessary to develop the *UHRXS* instrument is available within the three institutions of the PI, PS, and Co-I's (SSL; MSFC; CSSA; Stanford University; LLNL) and the major subcontractor, the Electro-Optical Subsystems Division of Ball Aerospace, of Boulder, Colorado. The contractual responsibility for the development of the film cameras is not yet assigned, due to the requirement for robotics compatibility which has developed subsequent to the original proposal guidelines. The multilayer and ultraviolet telescopes and spectrographs will be fabricated, assembled, tested and calibrated by the PI and Co-I's at their institutions. The film cameras will use technology developed for the S-056 SKYLAB x-ray telescope, modified to accept 70 mm format film, and for compatibility with replacement by robots. These components will be integrated into the *UHRXS* Optical Bench structure which will be fabricated by the MSFC Test Laboratory

Ball Aerospace will develop the *UHRXS* electronics package, including the MAMA detectors, the aspect sensors, and the Active Mirror Servos (AMS), and other mechanisms. Ball Aerospace will also develop the Electronic Ground System Equipment (GSE). The integrated *UHRXS* Optical Bench structure and optical systems will be delivered to Ball Aerospace, where the electronics, aspect sensors, and detectors will be integrated, and appropriate engineering tests will be carried out. Final engineering tests and scientific acceptance tests will be carried out at MSFC. Calibration will be carried out in the EUVE calibration chamber at the Space Sciences Laboratory, U.C. Berkeley, and/or at the Stanford Synchrotron Radiation Laboratory (SSRL) and the SURF II synchrotron at NIST.

2.0 Organization of the *UHRXS* Team: The proposed management structure for the *UHRXS* development is shown in Figure 28. The *UHRXS* team is organized into two parts to efficiently carry out the two phases of the program, (i) definition, design, development, testing, calibration, integration and launch, and (ii) operations, data reduction, and analysis. The first (pre-launch) part of our task will be carried out by the Principal Investigator (A.B.C. Walker, Jr.) the Co-Investigators (R.B. Hoover, T.W. Barbee, Jr., E. Tandberg-Hanssen, and J.G. Timothy), their research team, and the major subcontractors, the Ball Aerospace Systems Group and the (to be selected) camera subcontractor. In order to carry out the second part of our task, the PI and Co-I's have formed a group of Associated Scientists who, collectively with the PI and Co-I's, have the expertise necessary to address the broad range of scientific topics on which the *UHRXS* observations will bear.

2.1 The Investigator Team: The Investigator team is based on the Stanford/MSFC/LLNL consortium which has successfully carried out high resolution X-ray/XUV investigations of the sun with rocket borne Cassegrain multilayer telescopes. The team has been expanded from this base as described below and in Figure 28, which illustrates our planned management structure.

- A.B.C. Walker, Jr., the Principal Investigator, will be responsible for the *UHRXS* activities at CSSA/Stanford. He will hire a Program Manager and a Project Scientist to assist in the implementation of these tasks. Four major tasks will be carried out at Stanford, (i) procurement of the electronics package and Active Mirror Servos (AMS) from Ball Aerospace, the electronic systems subcontractor, (ii) procurement of major components of the XUV, EUV, and UV telescopes and spectrographs (mirror blanks, XUV and UV filters), and testing of the

completed mirrors, gratings and filters, (iii) design of the experiment logic and programming of the flight computer, and the GSE computer, and iv) development of the Flight Operations and Data Analysis Plans.

- R.B. Hoover, the Principal Scientist, will be responsible for the *UHRXS* activities at MSFC. He will secure the services of a Project Engineer and Project Scientist within MSFC to assist him in the development of the instrument. He will be responsible for the assembly of the XUV, EUV, and UV telescopes and spectrographs, and their testing and calibration. Mr. Hoover will be assisted by the Materials and Processes Laboratory and the Test Laboratory at MSFC who will fabricate the fiber epoxy telescope tube structures for the UV, EUV, and XUV telescopes and spectrographs, and the *UHRXS* truss structure (Optical Bench). He will be responsible for the procurement of the film cameras and flight film. He will supervise the development of the flight film.
- T.W. Barbee, a senior Co-Investigator, will be responsible for the ruling of the grating blanks and the fabrication of the multilayer coatings for the XUV telescope mirrors and gratings. (Dr. Barbee is one of the two co-inventors of multilayer technology).
- J.G. Timothy, a senior Co-Investigator, will be responsible for insuring that the MAMA detector fabrication and testing (which will be carried out by Ball Aerospace) is successfully completed. (Dr. Timothy developed the MAMA detector in collaboration with R. Bybee of Ball Aerospace).
- E. Tandberg-Hanssen, a senior Co-Investigator, will chair the meetings of the Associated Scientists, and insure that their views on instrument capabilities, flight operations, and the data analysis and observing plans are made available to the Program Manager and Project Scientists, who are responsible for implementing these capabilities and plans.
- We have arranged that senior engineering personnel from the Chief Engineer's Office, and the Quality Assurance Office at MSFC, will participate in all major *UHRXS* reviews, and will be available to provide advice and guidance to the Program Manager in evaluating and guiding the planning and execution of the *UHRXS* program, including all hardware tasks carried out at Ball Aerospace and the camera subcontractor. A MSFC Project Engineer will be appointed to insure that these responsibilities are implemented and the work to be done within the MSFC laboratories is completed in a timely manner.

2.2 The Organization of the *UHRXS* Team: The organization of the *UHRXS* project team is presented in Figure 28. The PI, Co-I's and Program Manager will form a Senior Council, which will establish policies, plans, and objectives for the program. The Senior Council will meet regularly at either MSFC or Stanford. The PI will implement these policies, plans and objectives, with the help of the Program Manager (PM) and Senior Co-I's, each of whom has specific responsibilities as indicated in Figure 28, and Section 2.1 above. The Program Manager will be directly responsible to the PI for the *UHRXS* activities at Stanford. The Project Manager at Ball Aerospace will report directly to the PM. R.B. Hoover will secure the assistance of a Project Scientist to direct *UHRXS* activities within SSL at MSFC, a Project Engineer to oversee *UHRXS* activities within the Engineering Laboratories at MSFC, and a Project Administrator within SSL. The Ball Aerospace Project Manager, the MSFC Project Engineer, and the Project Scientists at MSFC and Stanford will meet with the Senior Council as necessary, and will have specific responsibilities as indicated. The Program Manager will be responsible for the day to day implementation of the policies, plans and objectives established by the Senior Council at Stanford and Ball Aerospace, and, through the senior MSFC Co-Investigator and the Senior LLNL Co-Investigator, the activities at MSFC and LLNL; he (or she) will report directly to the PI. The Program Manager will be assisted by a Program Administrator at CSSA/Stanford. The Ball Aerospace Project Manager and the Stanford Project Scientist will report directly to the Project Manager, and will be responsible for the tasks indicated in Figure 28, *i.e.*, electronics (including detectors) and Mirror Servo design, documentation, fabrication and testing (Ball Aerospace, P.M.), and the design and testing of the XUV and EUV mirrors and gratings, the MAMA detectors, XUV and EUV filters, and the various other tasks indicated (Stanford P.S.). The MSFC Project Scientist will be responsible for all experimental work at MSFC; specifically telescope structure fabrication, telescope assembly, telescope testing and telescope calibration, and procurement of the film cameras. The MSFC and Stanford Project Scientists will be responsible for bringing instrument design changes, problems, or other matters which may affect the scientific performance of the *UHRXS* instrument to the Senior Council.

The Program Manager will be responsible for insuring that the XUV and EUV telescopes and *UHRXS* Optical Bench are designed, fabricated, assembled, tested, and delivered to Ball Aerospace in a timely manner. The tasks necessary

to achieve this will be carried out by the Stanford Project Scientist, the MSFC Project Scientist and T.W. Barbee, Jr., (who will fabricate the XUV multilayer mirror coatings), and the MSFC Project Engineer (who is responsible for the work to be performed in the MSFC Engineering Laboratories).

The Program Manager will also be responsible for insuring that the major procurements necessary to develop the XUV and UV telescopes are carried out efficiently, although the development of the specifications necessary for these procurements will be the responsibility of the Project Scientists. The most challenging task of the Program Manager will be to manage and administrate the activities of the development team at Ball Aerospace. He will be assisted in this task by the Ball Aerospace Program Manager, by a Project Administrator who will be hired within CSSA/Stanford, and by the MSFC Project Engineer, who will be able to draw on the expertise of senior MSFC electronic, mechanical, quality assurance and reliability engineers.

2.3 The UHRXS Electronics Subcontractor: The Electro-Optics Subsystems Division (EOD) of Ball Aerospace Systems Group will be the primary UHRXS subcontractor.

2.4 The UHRXS Scientific and Data Analysis Team: The team that will develop the observing program, carry out observations, and analyze these observations, will consist of the PI, PS and Co-I's, the Project Scientists and Deputy Project Scientist, the Associated Scientists, and post-doctoral scholars and students who will work with them. Dr. E. Tandberg-Hanssen will chair the meetings of the Associated Scientists and Investigators, and will insure that the Associated Scientists are prepared to utilize the UHRXS observations.

The Associated Scientists and Investigators will form teams to address each of the major scientific objectives that we have identified for the UHRXS program. Each team will be led by one of the Co-Investigators or Associated Scientists; members of the UHRXS Consortium will work with the various teams according to their specific interests and scientific objectives. Each team will develop an observing plan, and a plan for the analysis of the resulting observations. The Principal Scientist will develop the overall UHRXS Observing and Data Analysis Plans, based on these individual team plans. The teams that we have identified, and the team leaders are:

- | | | | |
|---|-------------------------------|---------------------|-----------------------------------|
| • | Chromospheric Fine Structure: | R.L. Moore | SSL/MSFC |
| • | Solar Prominences: | E. Tandberg-Hanssen | SSL/MSFC |
| • | Solar Flares: | P.A. Strurrock | CSSA/Stanford University |
| • | Solar Active Regions: | S.K. Antiochos | Naval Research Laboratory |
| • | Solar Magnetic Fields: | M.J. Hagyard | SSL/MSFC |
| • | Large Scale Solar Structure: | S.T. Wu | University of Alabama, Huntsville |
| • | Coronal/Solar Wind Interface: | D.G. Sime | High Altitude Observatory |

3.0 Instrument Procurement Strategy: We have developed a detailed plan for the procurement of the UHRXS instrument. This plan establishes a very definite and simple interface between the optical systems and the Optical Bench structure, and film cameras, which will be fabricated and tested or procured by the Investigative Team, and the detectors, experiment electronics and mechanisms, aspect sensors, and Active Mirror Servos and GSE which will be developed by Ball Aerospace. This instrument procurement strategy is based on the unique capabilities of the investigative Team and their institutions, and on the capabilities of the major Instrument Subcontractor, Ball Aerospace. The parallel development of the optical systems and Optical Bench by the Investigator Team and of the UHRXS electronics systems by Ball Aerospace is an efficient and cost effective approach, allowing the instrument to be developed and launched in accordance with the Space Station Schedule.

3.1 Development of the UHRXS Instrument: We plan to cost the development of two complete UHRXS Instruments; an Engineering Model and a Flight Unit.

3.1.1 The Optical Systems: The UHRXS optical systems will be developed by the Investigative Team (Stanford, MSFC, LLNL). The technologies and techniques necessary for the UHRXS telescopes have already been successfully implemented in our solar rocket program. Our development approach, and the division of responsibilities among the institutions (Stanford, MSFC, LLNL) will be the same as those used in our successful rocket program. The completed XUV, EUV and UV telescopes will be delivered to the MSFC Test Laboratory for integration into the UHRXS Optical

Bench once completed. We plan to fabricate two complete sets of XUV, EUV and UV telescopes. One set will constitute the flight instruments, the second set will be backups and will also be used during testing and calibration to provide parallel beams which can be used to verify telescope resolving power and sensitivity. A spare policy for other components of the *UHRXS* will be developed during the definition phase. (In our original costing, we have assumed a conservative spare policy.)

3.1.2 The Grating Spectrographs: The grating spectrographs will be designed by the Principal Investigator. The gratings will be fabricated by T. Barbee, at LLL, and tested at CSSA/Stanford. The grating spectrograph structural elements will be fabricated within the Engineering Laboratories at MSFC, and the instrument assembled and tested within SSL/MSFC.

3.1.3 Optical Bench: The optical bench design will be developed by the Principal Scientist, with the participation of the MSFC Engineering Laboratories. The optical bench will be fabricated by the MSFC Test Laboratory.

3.1.4 Cameras: An important objective of the present study will be to identify a contractor for the *UHRXS* cameras. The cameras will be procured by the Principal Scientist.

3.1.5 The Electronics, Detectors and GSE: The *UHRXS* electronics, detectors and GSE will be procured from EOD/Ball Aerospace by the Principal Investigator, with the assistance of J.G. Timothy, Senior Co-Investigator.

3.1.6 Mechanisms: The mechanisms required for *UHRXS* include (i) the aperture door, (ii) a filter wheel for the ultraviolet telescope, and (iii) a motor to rotate the EUV grating to scan wavelength. These are all standard devices and will require no significant development. Ball Aerospace will fabricate these mechanisms. We plan to study the feasibility of a scanning slit for the grating spectrographs during our definition phase. Thermal sensors, and heaters, if required, will be provided by Ball Aerospace.

3.1.7 Active Mirror Servos: The Active Mirror Servos, including the mirror cells, will be developed by EOD/Ball Aerospace. The soft x-ray, XUV, EUV and ultraviolet mirrors will be fabricated by Stanford and LLNL, and shipped to Ball Aerospace for installation into the mirror cells. The LISS Aspect sensor will be procured from Lockheed by Ball Aerospace.

3.1.8 Experiment Shuttle Interface Equipment: The mechanical interface equipment necessary to provide an interface between *UHRXS* and the Shuttle will be designed by Stanford and Ball Aerospace, and fabricated by the MSFC Test Laboratory.

3.2 Subcontracts and Facilities at Other Institutions: We anticipate 6 major subcontracts for the purchase of the following flight components. These are listed below, with the anticipated subcontractors.

- Mirror and grating blanks for the XUV and UV telescopes: *Baker Consulting*
- XUV Filters: *Luxel*
- UV Filters and Coating of the UV mirrors: *Acton Research and the University of Alabama at Huntsville are potential subcontractors.*
- The LISS Solar Aspect sensor and electronics: *Lockheed*
- Film Cameras: *TBD*
- Film: *Eastman Kodak*

In addition, we plan to purchase Laboratory XUV Sources, a Laboratory XUV Monochromator, a Laboratory Interferometer, a Data Analysis Computer and Image Processing Equipment. The XUV monochromator will probably be the Hettrick Scientific HIREFS - 164- 4m-M/F. The XUV sources may be purchased from Hettrick Scientific, or

fabricated at Stanford, based on the design developed by R. Byer and J. Trail of the Applied Physics Department at Stanford.

We have, so far, identified the EUVE calibration facility at the University of California at Berkeley as a potential calibration facility necessary for *UHRXS*. Use of the NIST synchrotron may also be required.

4.0 Instrument Procurement and Operations Plans: We comment on specific *UHRXS* plans below.

4.1 Instrument Specifications: We plan to develop detailed instrument specifications during the Definition Phase of our program, starting in FY1993. We have already prepared preliminary specifications (Appendix B). During the Conceptual Design Study phase we will carry out a detailed ray trace analysis at MSFC, to specify the optical configuration. A detailed design for the Optical system will then be carried out at MSFC. Based on these detailed telescope specifications, we will develop detailed specifications for the entire *UHRXS* instrument. Ball Aerospace will be responsible for developing detailed specifications for the electronics, detectors, active mirror servos, experiment mechanisms, and GSE, during the definition phase. These processes will be reviewed on a monthly basis, utilizing the management structure given in Figure 28. A final specification review will be held with the MSFC Project Manager and mechanical, electronic and quality assurance experts from MSFC before the definition phase report is finalized.

4.2.0 Review Procedures and Documentation

4.2.1 Review Procedures: The Program Manager (PM) will hold monthly reviews of the development program (at Stanford or MSFC) to monitor the status of the Optical system development occurring at Stanford, MSFC, and LLNL, and the major procurements. Following the reviews of the status of the Investigator development program, the PM will hold an overall *UHRXS* review at Ball Aerospace on a bimonthly basis. The MSFC Project Engineer and the MSFC mechanical, electrical, and Q & RA engineers will participate in these reviews as necessary.

4.2.2 Documentation: The Program Manager will be responsible for the overall documentation requirements of the *UHRXS* program. Each element (Co-Investigators, Ball Aerospace, etc.) will develop its own documentation (drawings, change orders, financial records, etc.) as necessary, and will report on a regular basis to the PM, and the Program Administrators at MSFC and Stanford.

4.3.0 Performance Assurance: The overall performance assurance program guidelines will be developed by the Program Manager, with the advice of the Q & RA experts from the MSFC Quality Assurance Office and Ball Aerospace. These procedures will then be carried out by each element (Co-I's, Ball Aerospace, MSFC Labs, etc.) and monitored by the PM, with the assistance of the MSFC Project Manager and the Q & RA experts. A Preliminary Performance Assurance Implementation Plan was presented in Appendix D of our original proposal. [2]

4.4.0 Test Program: The major test responsibility for each component of the *UHRXS* instrument will rest with the element (Co-I's, Ball Aerospace, etc.) responsible for its development. For example, testing of the Optical systems will be carried out by R. Hoover at MSFC, electronic testing of the MAMA detectors will be carried out by Ball Aerospace, etc. In the case of the MAMA detector, extensive XUV tests on a prototype unit will be carried out at CSSA Stanford.

Once the *UHRXS* is fully assembled, testing of the integrated instrument will be carried out by Ball Aerospace (see Appendix A), to qualify the electronics, detectors, and active mirror sensors, and at MSFC (vibration, thermal vacuum) for the overall *UHRXS* package.

4.5.0 Hardware Fabrication Policy: We will cost the fabrication of two complete *UHRXS* units, an engineering model and a flight unit.

4.6.0 Calibration: Calibration tests of the XUV and UV optical systems will be carried out at CSSA Stanford at the level of the individual components and assembled telescopes. Detailed scientific acceptance tests and calibrations of the integrated *UHRXS* instrument will be carried out at MSFC in a SSL XUV calibration facility to be developed as discussed in Section II 4 of Ref [2] and at the U.C. Berkeley SSL, Stanford SRL, and Surf II at NIST.

4.7.0 Integration of the Instrument: The integration of the *UHRXS* instrument will be supported by the PI, Co-I's and the development contractor, Ball Aerospace, to verify electronics operation, and by the MSFC Engineering Laboratories to verify thermal and mechanical properties.

4.8.0 Flight Operations: During the Definition Phase, we will prepare a preliminary Flight Operations Plan. Flight operations will be under the direction of the Principal Investigator. He will be assisted by the Principal Scientist, the Project Scientists, and by the Program Administrators. The PI, Co-I's, Associated Scientists, and the Post-Doctoral Scholars and graduate students working with them will be active in carrying out the various observational programs that are the objective of the *UHRXS*. We plan to have operations centers at both CSSA Stanford and SSL/MSFC. The Associated Scientists will utilize the operations center most convenient to them.

4.9 Data Analysis: During the Definition Phase, we will prepare a preliminary Data Analysis Plan. During the Development Phase, a detailed Data Analysis Plan will be prepared by the Project Scientist. The major data analysis tasks will be carried out in the SSL/MSFC Data Analysis and Computation Facility and the HEPL Data Facility at Stanford. Data formats with the appropriate calibration and with ancillary information will be generated to meet the needs of the PI, Co-I's, Associated Scientists, and Guest Investigators. Microdensitometry of the photographic data will be carried out within SSL/MSFC and at HAO.

REFERENCES

1. A.B.C. Walker, Jr., J.F. Lindblom, J.G. Timothy, T.W. Barbee Jr., R.B. Hoover and E. Tandberg-Hanssen, "The ultra high resolution XUV spectroheliograph," *Optical Engineering* 29, 698, 1990. *ibid*, "The ultra high resolution XUV spectrograph. II. Predicted performance," *Proc. SPIE* 1238, 1990.
2. T.W. Barbee, Jr., "Overview paper: advances in multilayer x-ray/EUV optics - synthesis, performance and instrumentation," *Optical Engineering* 29, 711, 1990.
3. A.B.C. Walker, Jr., J.F. Lindblom, R.H. O'Neal, R.B. Hoover and T.W. Barbee, Jr., "Astronomical observations with normal incidence multilayer optics: recent results and future prospects," to be published in *Physics Scripta* 41, 1053, 1990.
4. H. Brueggerman, *Conic Mirrors*, Focal Press, New York, 1969.
5. A.B.C. Walker, Jr., T.W. Barbee, Jr., R.B. Hoover, and J.F. Lindblom, "Soft x-ray images of the solar corona with a normal incidence Cassegrain multilayer telescope," *Science* 241, 1781-1787, 1988; R.B. Hoover, T.W. Barbee, Jr., J.F. Lindblom and A.B.C. Walker, Jr., "Solar x-ray/XUV imagery with an experimental Kodak T-Max 100 Professional film," *Kodak Techbits*, Summer 1988.
6. L. Golub, M. Herant, K. Kalata, I. Lovos, G. Nystrom, F. Prado, E. Spiller, and J. Wilczynski, "Sub-arc second observations of the solar x-ray corona," *Nature* 344, 842, 1990.
7. A.B.C. Walker, Jr., J.F. Lindblom, R.H. O'Neal, M.J. Allen, T.W. Barbee, Jr., and R.B. Hoover, "Multi-spectral solar telescope array," *Optical Engineering* 29, 581, 1990.
8. R.B. Hoover, T.W. Barbee, Jr., P.C. Baker, J.F. Lindblom, M.J. Allen, C.E. DeForest, C. Kankelborg, R.H. O'Neal, E. Paris, and A.B.C. Walker, Jr., "Performance of compact multilayer coated telescopes at soft x-ray, EUV, and far-ultraviolet wavelengths," *Optical Engineering* 29, 1281, 1990.
9. T.W. Barbee, Jr., "Overview paper: multilayer optics: current status and fundamental limits," to be published in *Proc. SPIE* 1343, 1990.
10. T.W. Barbee, Jr., J.W. Weed, R.B. Hoover, R.H. O'Neal, J.F. Lindblom, C. Kankelborg, M.J. Allen, C.E. DeForest, A.B.C. Walker, Jr., and E. Gluskin, "Performance of the multi-spectral solar telescope array II: The multilayer mirrors," *ibid*.
11. P. Boher, P. Hauder, L. Hennem, J.P. Delabowdiniere and M. Kuhne, "Silicon/silicon nitride multilayers for X-UV optics applications," *ibid*.
12. J.F. Lindblom, R.H. O'Neal, S.F. Powell, A.B.C. Walker, Jr., F.R. Powell, T.W. Barbee, Jr., and R.B. Hoover, "Performance of the multi-spectral solar telescope array IV: filters," *ibid*.
13. R.B. Hoover, P.C. Baker, J.B. Hadaway, R.B. Johnson, A.B.C. Walker, Jr., J.F. Lindblom, and R.H. O'Neal, "Performance of the multi-spectral solar telescope array III: Optical characteristics of the Ritchey-Chrétien telescopes," *ibid*.
14. J.E. Harvey, W.P. Zmek and C. Ftacilas, "Imaging capabilities of normal incidence x-ray telescopes," *Optical Engineering* 29, 603-608, 1990.
15. P. Baker, "Advanced flow polishing of optical surfaces," in *X-Ray/EUV Optics for Astronomy and Microscopy*, R.B. Hoover, ed., *Proc. SPIE* 1160, 263-270, 1989.
16. R.B. Hoover, C.E. DeForest, J.F. Lindblom, R.H. O'Neal, A.B.C. Walker, Jr., and A. DeWan, "Performance of the multi-spectral solar telescope array VI: performance and analysis of photographic film," to be published in *Proc. SPIE* 1343, 1990.

17. A.G. Millikan and C.E. Coykendall, "Some aspects of extreme ultraviolet photography: then and now," *"American Astronomy Society Photo Bulletin"* 1 (3), 11-14, 1977.
18. J.B. Hadaway, R.B. Johnson, R.B. Hoover, J.F. Lindblom, and A.B.C. Walker, Jr., "Design and analysis of optical systems for the multi-spectral solar telescope array," *Proc. SPIE* 1160, 195-208, 1989.
19. J.A.R. Sampson, *Techniques of Vacuum Ultraviolet Spectroscopy*, (John Wiley & Sons; New York, 1967); T.M. Namioka, *Opt. Soc. Am.* 47, 139 (1959); H. Haber, *J. Opt. Soc. Am* 40, 153 (1950), H. Greiner and W. Schaffer, *Optik* 16, 139 (1959)
20. Barbee, *et al.*, "Multilayer diffraction gratings," to be published in *Proc. SPIE* 1343, 1990.
21. M.C. Hutley, "Blazed interference diffraction grating for the ultraviolet," *Optica Acta* 22, 1-13, 1975; M. C. E. Huber, J.G. Timothy, J.S. Morgan, G. Lemaitre, G. Tondello, E. Jannitti and P. Scarin, "Imaging extreme-ultraviolet spectrometer employing a single toroidal diffraction grating: the initial evaluation," *Applied Optics* 27, 3503, 1988. J.S. Morgan, *et al.*, "A high efficiency extreme-ultraviolet spectrometer," to be published in *Extreme Ultraviolet Astronomy*, R. Malina, ed., Space Science Lab, Univ. of Calif., Berkeley, 1990.
22. T. Burek, "Crystals for astronomical x-ray spectroscopy," *Space Sci. Instr.* 2, 53, 1976.
23. R. Giacconi, W.P. Reidy, G.S. Vaiana, L.P. VanSpeybroeck, and T. Zehnpfennig, "Graying-incidence telescopes for x-ray astronomy," *Space Sci. Rev.* 9, 3, 1969.
24. R.M.E. Illing, N.H. Zaun and R.L. Bybee, "Image motion compensation using a photon counting UV/visible detector," *Proc. SPIE* 932, 246, 1988.
25. J.G. Timothy, J.S. Morgan, D.C. Slater, D.B. Kastle, R.L. Bybee, and H.E. Culver, "MAMA detector systems: a status report," *Proc. SPIE* 1158, 104, 1989.
26. J. S. Morgan, D.C. Slater, J. G. Timothy and E.B. Jenkins, "Centroid position measurements and sub-pixel sensitivity variations with the MAMA detector," *Applied Optics* 28, 1178-92, 1989.
27. D.B. Kastle, "High resolution decoding techniques and single-chip decoders for multi-anode microchannel arrays," *Proc. SPIE* 1158, 311, 1989
28. R.C. Taylor, M.C. Hettrick and R.F. Malina, "Maximizing the quantum efficiency of microchannel plate detectors: the collection of photoelectrons from the interchannel web using an electric field," *Rev. Sci. Instrum.* 54, 171-6, 1983.
29. O.H.W. Siegmund, E. Everman, J. Vallerger and M. Lampton, "Extreme ultraviolet quantum efficiency of opaque alkali halide photocathodes on microchannel plates" *Proc. SPIE* 868, 18-24, 1988.
30. E. Cole, Ball Aerospace Company, private communication.
31. R. Mewe, E.H.B. Gronenschild, and G.H.J. Van den Oord, "Calculated x-radiation from optically thin plasmas V," *Astron. Astrophys. Suppl. Ser.* 67, 197-254, 1985.
32. M. Landini and B.C. Monsignori Fossi, "The X-UV spectrum of thin plasmas," *Astron. Astrophys. Suppl. Ser.* 82, 229-60, 1990.
33. J.E. Vernazza and E.M. Reeves, "Extreme ultraviolet composite spectra of representative solar features," *Astrophys. Journal Suppl. Ser.* 37, 485-513, 1978.
34. M. Malinovsky and L. Heroux, "An analysis of the solar extreme ultraviolet spectrum between 50 and 300 Å," *Astrophysics Journal* 181, 1009-30, 1973.

35. L. Cohen, "An atlas of solar spectra between 1175 and 1950 Å, recorded on *Skylab* with the NRL's telescope mount experiment," *NASA Ref. Publ.* 1069, 1981.
36. F.F. Freeman and B.B. Jones, "Grazing incidence spectra of the sun," *Solar Physics* 15, 288-308, 1970.
37. G.A. Doschek and R.D. Cowan, "A solar spectral line filter between 10 and 200 Å modified for application to high spectral resolution x-ray astronomy," *Astrophys. J. Suppl. Ser.* 56, 67-89, 1984.
38. U. Feldman, G.A. Doschek and R.W. Kreplin, "High resolution x-ray spectra of the 1979 March 29 solar flare," *Astrophys. J.* 238, 315-74, 1980.
39. (a.) A.B.C. Walker, Jr., H.R. Rugge and K. Weiss, "Relative coronal abundances derived from x-ray observations. I. Na, Mg, Al, Si, S, and A," *Astrophys. J.* 188, 423-40, 1974; (b.) II N, O, Ne, Mg, and Fe; *ibid* 192, 169-80, 1974; (c.) III. "The effect of cascades on the relative intensity of Fe XVII line fluxes, and a revised iron abundance," *ibid* 194, 471-82, 1974.
40. J.S. Morgan, P.C. Slater, J.G. Timothy and E.B. Jenkins "Centroid position measurements and subpixel sensitivity variations with the MAMA Detector," *Applied Optics* 28, pp 1178-92, 1989.
41. A.B.C. Walker, Jr., "Spectroscopic analysis of solar and cosmic x-ray spectra I," *Space Sci. Instr.* 2, 9, 1976.
42. M.J. Allen *et al.*, "Performance of the multi-spectral solar telescope array V: temperature diagnostic response to the optically thin solar plasma," *this proceeding*.
43. R.H. Munro, A.K. Dupree and G.L. Withbroe, "Electron densities derived from line intensity ratios: beryllium isoelectronic sequence," *Solar Physics* 19, 347, 1971.
44. A.H. Gabriel, "Dielectronic satellite spectra for highly-charged helium-like ion lines," *Mon. Not. Roy. Astron. Soc.* 160, 99, 1972.
45. K.P. Dere, J.D.F. Bartoe and G. E. Bruckner, "Outflows and ejections in the solar transition zone," *Astrophys. J.* 310, 456, 1986.
46. A.B.C. Walker, Jr., "Multi-spectral observations of high energy solar phenomena," *Solar Phys.* 118, 209-29, 1988.
47. A.B.C. Walker, Jr., *et al.*, "The Advanced Solar Observatory," *Optical Eng.* 29, 802, 1990.
48. S. Fineschi, R.B. Hoover, J. Fontenla and A.B.C. Walker, Jr., "Solar soft x-ray/EUV polarimetry I: observational parameters and theoretical considerations," to be published in *Proc. SPIE* 1343, 1990; R.B. Hoover, S. Fineschi, J. Fontenla and A.B.C. Walker, Jr., "II: Instruments and methods," *ibid*.

1